UNIVERSITEIT VAN PRETORIA
UNIVERSITY OF PRETORIA
YUNIBESITHI YA PRETORIA

OPTIMAL CONTROL OF RENEWABLE ENERGY/GRID HYBRID SYSTEMS WITH HEAT PUMP LOAD

by

Sam M. Sichilalu

Submitted in partial fulfillment of the requirements for the degree
Philosophiae Doctor (Electrical Engineering)

in the

Department of Electrical, Electronic and Computer Engineering
Faculty of Engineering, Built Environment and Information Technology

UNIVERSITY OF PRETORIA

February 2016

SUMMARY

OPTIMAL CONTROL OF RENEWABLE ENERGY/GRID HYBRID SYSTEMS WITH HEAT PUMP LOAD

by

Sam M. Sichilalu

Promoter	Prof. Xiaohua Xia
Department:	Electrical, Electronic and Computer Engineering
University:	University of Pretoria
Degree:	Philosophiae Doctor (Electrical Engineering)
Keywords:	Energy management, optimal control, heat pump water heater, photovoltaics, net zero-energy building, diesel generator, mixed integer linear/nonlinear program, time-of-use tariff, battery, feed-in tariff, dispatch strategy, electrolyzer, fuel cell, demand side management

The rising costs, power deficit and environmental concerns about fossil fuel-based energy resources have led to significant research effort in renewable and cleaner energy resources. Globally, governments are adopting policies to promote the development and application of various renewable energy (RE) technologies for generating electricity. The main challenge associated with RE technologies such as solar and wind generation is their intermittent nature, which affects their ability to provide 100% supply reliability. Combining these RE sources with energy storage systems such as battery storage and hydrogen can be cost-effective. Currently there are limitations to the fraction of RE that can be incorporated in the grid system because of their intermittency and base load considerations. The major challenge is the escalating power demand, far above the installed capacity in most countries. This requires urgent mitigation of demand side management(DSM), in order to stabilize the imbalance in the short, medium and long term. Energy efficiency and optimal integration could provide one of the most effective technological solutions, with the usage of energy-efficient devices such as heat pump water heaters (HPWH).

These collective efforts at energy saving should involve proper selection of an appropriate technology, application of optimal control (OC) in RE, usage of energy-efficient equipment, green building materials and an effective energy policy. The proper integration of these sources and the use of HPWH could reduce the power utility's maximum demand and improve the security of the supply. Most countries at policy level are beginning to introduce attractive feed-in tariffs, dynamic energy pricing (time-of-use) and rebate systems for using greener energy and energy-efficient load such as HPWHs. Hence, this thesis provides the first practical attempt to integrate various distributed energy resources (DRE) effectively into the grid, using HPWHs for the generation of the required thermal energy. This multi-directional approach in this work has proven that OC strategy could significantly reduce the cost of energy and provide an opportunity for power trade-off/feed-in in the electricity market.

This thesis developed four main models that meet both the technical and operational constraints of DSM and optimal integration of DREs. Solar energy is abundant in Africa, its exploitation in addition to other REs is a priority in this work. The first model is an optimal scheduling strategy of a grid-tied/battery/PV system supplying HPWH. Secondly, an optimal energy management model with a diesel generator back-up system is developed that minimizes the fuel cost, while maximizing the utilization of renewable energy with a HPWH. Thirdly, in OC model of a HPWH, the thermal output is state variable. It is supplied by the second abundant wind energy hybrid resources. An economic analysis is done in this model to assess the break-even period, which is important to every investor. Finally, the future green energy hydrogen fuel cell hybrid system is modeled. Hydrogen has attracted attention in modern research owing to its ability to reduce carbon dioxide emissions, thus helping to mitigate climate change, improve local air quality, improve energy security by reducing energy imports, increase energy supply options and reduce dependence on fossil fuels.

These models are suitable for application in both urban and rural areas where the electrical power power supply is intermittent. These models have several advantages for building owners intending to turn their dwelling into zero/positive energy buildings and enter electricity market. However, engineering solutions alone cannot yield much success on DSM, sensitization and education on energy savings at individual level and how these are intertwined with climate change are of the utmost importance.

OPSOMMING

OPTIMALE BEHEER VAN HERNUBARE ENERGIE/NETWERK-HIBRIEDE SISTEME MET HITTEPOMP AANVRAAG

deur

Sam M. Sichilalu

Promotor(s):	Prof. Xiaohua Xia
Departement:	Elektriese, Elektroniese en Rekenaar-Ingenieurswese
Universiteit:	Universiteit van Pretoria
Graad:	Philosophiae Doctor (Elektriese Ingenieurswese)
Sleutelwoorde:	Energiebestuur, optimale kontrole, hittepompwaterverhitter, foto-voltaïes, netto- zero-energiegebou, dieselgenerator, gemengdeheelgetal-lineëre/nie-lineëre program, tyd-van-gebruik, windgenetator, battery, in-voertarief, verspreidingstrategie, elektroliseerder, aanvraagkantbestuur

Die stygende koste, kragtekort en besorgdheid oor die uitwerking van fossielgebaseerde energie op die omgewing het tot beduidende navorsingspogings rakende hernubare en skoner energiebronne gelei. Wëreldwyd aanvaar regerings beleid om die ontwikkeling en aanwending van verskeie hernubare energietegnologieë vir die opwekking van elektrisiteit te bevorder. Die hoofuitdaging in verband met hiedie tegnologieë, soos sonkrag- en windopwekking, is hulle wisselvallige aard, wat ’n invloed het op hulle vermoë om volledige betroubaarheid van voorsiening te verseker. ’n Kombinasie van hierdie hernubare energiebronne met energiebergingsisteme soos batteryberging en waterstof kan koste-effektief wees. Daar is tans beperkings op die gedeelte van die hernubare energie wat in die netwerk ingesluit kan word, omrede hulle wisselvalligheid en basisladingoorwegings. Die hoofuitdaging is die groeiende aanvraag vir krag, ver meer as die geïnstalleerde kapasiteit in die meeste lande. Gevolglik is dringende ingryping deur aanvraagkantbestuur nodig om die wanbalans in die kort, medium en lang termyn te stabiliseer. Energiedoeltreffendheid en optimale integrasie kan een van die mees effektiewe tegnologiese oplossings verskaf, deur die gebruik van energie-effektiewe toestelle soos hittepompwaterverhitters.

Hierdie kollektiewe pogings om energie te bespaar behoort 'n toepaslike keuse van geskikte tenologie, aanwending van optimale kontrole in hernubare energie, gebruik van energie-doeltreffende toerusting, groen boumateriale en 'n effektiewe energiebeleid in te sluit. Die behoorlike integrasie van hierdie bronne en die gebruik van hittepompwaterverwarmers mag die maksimunaanvraag van die energievoorsiener verminder en die sekuriteit van voorsiening verbeter. Op beleidsvlak begin die meeste lande aanloklike invoertariewe, dimamiese energieprysbepaling (tyd-van-gebruik) en kortingsisteme invoer om die gebruik van groener energie en energie-doeltreffende belading soos hittepompwaterverhitters te bewerkstellig. Hierdie tesis bied die eerste praktiese poging om verskeie verspreide energiebronne in die netwerk te integreer deur die gebruik van hittepompwaterverhitters vir die opwekking van die vereiste hitte-energie. Die multi-gerigte benadering in hierdie werk het bewys dat optimale kontrolestrategie die koste van energie beduidend kan verminder en die geleentheid bied vir kragruil/krag-invoer in die elektrisiteitsmark.

Hierdie tesis het vier hoofmodelle ontwikkel wat sowel die tegniese en operasionele beperkings van aanvraagkantbestuur en optimale integrasie van verspreide energiebronne kan hanteer. Sonkrag-energie is oorvloedig beskikbaar in Afrika en die benutting daarvan saam met ander hernubare energiebronne is 'n prioriteit in hierdie werk. Die eerste model is 'n optimale skeduleringstrategie van 'n netwerkgebonde/battery/fotovoltaïese sisteem wat krag voorsien aan 'n hittepompwaterverhitter. Tweedens word 'n optimale energiebestuurmodel met 'n dieselgeneratorrugsteunsisteem ontwikkel wat die brandstofkoste minimeer, terwyl dit die gebruik van hernubare energie met 'n hittepompwaterverhitter maksimeer. Derdens is die hitte-uitset in 'n optimale-kontrolemodel van 'n hittepompwaterverhitter veranderlik volgens toestand. Dit word verskaf deur die tweede oorvloedige hibridiese bron, windenergie. 'n Ekonomiese analise word in hierdie model gedoen om die gelykopuitkomsperiode te bepaal, wat vir alle beleggers belangrik is. Laastens word die toekomstige groen-energie waterstof-brandstofselhibriedsisteem gemodelleer. Waterstof het in moderne navorsing aandag getrek deur sy vermoë om koolstofdioksieduitlatings te verminder en sodoende te help om klimaatverandering te beperk, plaaslike lugkwaliteit te verbeter, energiesekuriteit te verbeter deur energie-invoer te verminder, energievoorsieningopsies te vermeerder en afhanklikheid van fossielbrandstowwe te verminder.

Hierdie modelle is geskik vir aanwending in sowel stedelike as landelike gebiede waar kragvoorsiening ongereeld is. Hulle het verskeie voordele, byvoorbeeld vir eienaars van geboue wat hulle woonplekke wil omskep in zero/positiewe energiegeboue en die elektrisiteitsmark wil betree. Desnieteenstaande kan ingenieursoplossings op hulle eie nie veel sukses behaal met aanvraagkantbestuur nie; sensitering

en opvoeding oor energiebesparing op persoonlike vlak en bewustheid van hoe dit vervleg is met klimaatverandering is van die uiterste belang.

DEDICATION

This thesis is dedicated to my first-born son, Nguzu; you were born in the middle of my studies, denying you the father's guidance and love because of this noble cause. This doctorate degree is yours, even beyond my time on earth, let it be your inspiration to achieve success. To my radiant, lovely wife, Kawama Mfuni Sichilalu, for your love, patience, support and care, this is yours too.

It is also dedicated to my single mother; you sold everything you had and toiled the land with your hands for me to go to school. Mom, it's amazing how you believed in education when you yourself could not read or write. My brother, Collins Sichilalu, for your endless support towards my education, this is your achievement. My sisters, Beatrice and Eunice, this degree is yours too. I thank the almighty God for everything.

ACKNOWLEDGEMENT

I would like to thank the National Research Foundation (NRF) of South Africa grant NRF SFH14080687344 and grant No. 99766, Maastricht University under (MUNDO) NICHE ZMB 037, the University of Zambia and the National Hub for Energy Efficiency and Demand Side Management (EEDSM) for financial and other support for this research.

Special thanks go to my supervisor Prof.X. Xia; you are truly a servant of science, your works are improving the lives of people around the globe. Thanks for your encouragement, help and inspiration. I will always be grateful. My period spent with you has made me realise that the earth has finite resources, hence we should strive to use them optimally and sustainably.

To my colleagues at the EEDSM centre, I will always be grateful for your help and both technical and emotional support throughout this work. To my wife as well, thanks for your love and taking care of the family in my absence.

PUBLICATIONS

1) S. Sichilalu, T. Mathaba, X. Xia, Optimal control of a wind-PV-hybrid powered heat pump water heater, *Applied Energy* 456 (2015) http://dx.doi.org/10.1016/j.apenergy.2015.10.072.

2) S.M. Sichilalu, X. Xia, Optimal energy control of grid tied PV-diesel-battery hybrid system powering heat pump water heater, *Solar Energy* 115 (2015) 243-254.

3) Sichilalu, S. M, Xia, X. Optimal power dispatch of a grid tied-battery-photovoltaic system supplying heat pump water heaters, *Energy Conversion and Management* 102 (2015) 81 - 91

4) Sichilalu, S., Tazvinga, H. and Xia, X., 2016. Optimal control of a fuel cell/wind/PV/grid hybrid system with thermal heat pump load. *Solar Energy* 135 (2016), pp.59-69

5) S. Sichilalu, X. Xia, J. Zhang, Optimal scheduling strategy for a grid-connected photovoltaic system for heat pump water heaters, *Energy Procedia* 61 (2014) 1511-1514.

6) Sichilalu, S. M., and X. Xia. Optimal Power Control of Grid Tied PV-battery-diesel System Powering Heat Pump Water Heaters. *Energy Procedia* 75 (2015): 1514-1521.

7) Sam. M. Sichilalu, X. Xia, Optimal energy scheduling of grid-connected PV-diesel hybrid system to power heat pump water heater, *International Green Energy Conference* (2014), May 25-28, Tianjin, China.

8) Sam. M. Sichilalu, J. Zhang, X. Xia, Optimal scheduling strategy for a grid-connected photovoltaic system for heat pump water heater, *Applied Energy Conference* (ICAE2014), 29th May-3rd June,

Taipei Taiwan.

9) Sam. M. Sichilalu, X. Xia, Optimal power control of grid tied PV-battery-diesel system powering heat pump water heaters, *7th International Conference on Applied Energy* (ICAE2015), March 28-31, 2015, Abu Dhabi, UAE.

10) Evan M. Wanjiru, S.M. Sichilalu, X. Xia, Optimal integrated diesel grid-renewable energy system for hot water devices, *Applied Energy Symposium and Forum, REM2016* , April 19-21, 2016, Bandos Island, Maldives.

11) S.M. Sichilalu, X. Xia, Integrated energy management of Grid-tied-PV-Fuel Cell hybrid system, *Applied Energy Symposium and Forum, REM2016* , April 19-21, 2016, Bandos Island, Maldives.

12) Evan M. Wanjiru, Sam M. Sichilalu, Xiaohua Xia, Optimal operation of integrated heat pump-instant water heaters with renewable energy, *The 8th International Conference on Applied Energy - ICAE2016*, October 8-11.2016, Beijing , China.

13) Fhazhil Wamalwa, Sam M. Sichilalu, Xiaohua Xia, Optimal control of hydrokinetic-powered pumpback system for a hydropower plant in dry season, *The 8th International Conference on Applied Energy - ICAE2016*, October 8-11.2016, Beijing , China.

14) Fhazhil Wamalwa, Sam M. Sichilalu, Xiaohua Xia, Optimal control of conventional hydropower plant retrofitted with a cascaded pumpback system powered by an on-site hydrokinetic, *Energy conversion and management Journal* (Submitted August 2016)

LIST OF ABBREVIATIONS

a, b and c	diesel generator coefficients
A_m	true or accepted value
A_w	wind generator rotor sweeping area (m^2)
$B_c(0)$	initial status of charge of the battery (kW)
$B_c(t)$	battery capacity at every given time t in (kWh)
B_c^{max}	maximum battery rated capacity in ($A-h$)
c	specific heat capacity of water ($J/kg\,^{\circ}$C)
C_f	diesel fuel price (R/l)
C_p	Betz limit
F	diesel generator fuel consumption in (l/h)
h	surface heat transfer coefficient (W/m^2K)
$H_{2,t}$	stored hydrogen energy (kWh)
h_{ref}	anemometer reference height (m)
J	cost function
L	mass of water inside the tank (kg)
m	project life period (years)
N	total number of sampling intervals
p	TOU electricity price (R/kWh)
$P_{dl,t}$	domestic appliances power demand (kW)
$P_{el,t}$	power supply to the electrolyzer (kW)
$P_{FC,t}$	hydrogen power input to the fuel cell (kW)
$P_{FC-IN,t}$	fuel cell power output (kW)
$P_{g,t}$	grid power (kW)
$P_{H2,t}$	eletrolyzer hydrogen power output (kW)
$P_{hp,t}$	heat pump water heater rated power (kW)
P_i	control variable, which is the power in the i-th branch (kW)
$P_{pv,t}$	photovoltaic power output (kW)
$P_{RE-IN,t}$	direct renewable power supply (kW)
P_r	rated wind electrical power (kW)
P_{wr}	rated wind turbine power output (kW)

$P_{w,t}$	wind generator power output (kW)
Q_D	total losses due to water demand
Q_L	total standby (convectional) losses
q_{loss}	conventional loss in (W/m^2)
r	interest rate or discount rate
R	South African rands (ZAR)
T_a	ambient temperature ($^\circ$C)
$T_{in,t}$	inlet cold water temperature ($^\circ$C)
T_{low} and T_{up}	lower and upper hot water temperature set points ($^\circ$C)
T_o	initial hot water temperature ($^\circ$C)
t_s and k	sampling time ($hour$) and k^{th} sampling interval
T_t	hot water temperature inside the tank ($^\circ$C)
$\dot{T}$	derivative of temperature
u_t	heat pump power supply switch control variable (0 or 1)
V	wind speed at the hub height (m/s)
V_c	cut-off wind speed (m/s)
V_i	cut-in wind speed (m/s)
V_N	rated wind speed (m/s)
V_r	wind speed (m/s)
v_{hub}	wind speed at the desired height h_{hub}
v_{ref}	wind speed at the reference height h_{ref}
$W_{D,t}$	flow rate ($liters/hour$)
Z_m	experimental measured values
$\o$	diameter (m)
η_t	turbine coupling gearbox efficiency (%)
χ	Weibull shape parameter
η_c	battery charging efficiency
η_d	battery discharging efficiency
η_g	wind generator efficiency (%)
η_i	inverter efficiency
κ	thermal conductivity ($W/m\ K$)
ω	weighting factor
ρ	air density factor of the wind generator

σ	battery self-discharged factor
$\sigma_{m,meas}$	standard deviation
$\triangle x$	thickness of the insulation (m)
φ	ground surface friction coefficient
n	time in years before the future cash flow occurs
p_c	photovoltaic feed-in tariff (R/kWh)
$P_{\text{Load,t}}$	domestic load (kW)
S_{area}	total surface area (m^2)
COP	coefficient of performance
Eskom	South African power utility company
NERSA	national energy regulator of South Africa
min and *max*	minimum and maximum of the variable
MINLP	mixed integer nonlinear program
NPV	net present value
REFIT	renewable energy feed-in tariff
SOE	battery status of energy (kWh)
TOU	time-of-use electricity tariff

TABLE OF CONTENTS

LIST OF FIGURES

LIST OF TABLES

CHAPTER 1 INTRODUCTION

1.1 RESEARCH BACKGROUND AND MOTIVATION

Demand side management (DSM) has gained wide interest worldwide; this strategy has eased operational constraints of the power utility companies [1]. Torriti [2] defined demand response (DR) as multiple actions taken by energy consumers in response to the particular utility conditions especially the time-of-use tariff (TOU) or incentives. In response to DR, various countries are currently implementing policies that promote DSM [3]. These policies mostly focus on promotion of energy efficiency, dynamic demand response, end-users behavior changes and penetration of distributed energy resources. Incentives and policies have scored their successes and failures, and in most cases the failure to reach full potential lies in technological challenges rather than policy [4].

Demand response programs are mainly classified into three categories, namely: price-based, incentive-based and energy-efficiency [5]. Price-based demand response promotes changes in energy consumption of the end-user customer because of the variation of the energy cost. This mitigation includes the TOU, real time pricing and critical peak pricing electricity tariffs. However, these price-based demand response solutions are mostly voluntary. It is left to the customers' discretion whenever they feel the need to operate appliances during cheaper TOU electricity tariff periods in order to save costs [6]. These factors reduce the success of the strategy. Therefore, an appropriate load control strategy is needed to compensate for insufficient voluntary action if it is to succeed.

Secondly, incentive-based demand response offers customers fixed or time-dependent incentives in addition to the existing energy unit rates. These incentives are usually proposed by utilities, load-serving agencies, or other electricity market operators. These incentives/rebates are either on unit energy saved, maximum demand, carbon emission or end-user installation of green power generation

[7]. In most cases monitoring and verification are strongly dependent on the adherence of the customer and a penalty is effected whenever there is contractual breach.

Finally, the energy efficiency and dynamic demand response has highest overall potential for decreasing energy consumption and cost in the medium/long term. This can be achieved through load-shifting strategies, optimal control (OC) strategies and promotion of usage of energy-efficient devices such as heat pump water heaters (HPWH) [8]. Beyond technological success, energy saving education is cardinal to change the energy usage mindset and behavior. The end-users should be able to appreciate the importance of all this mitigation in saving energy and climate change control. Everyone is concerned about the sustainability of the future source of primary energy input, since the earth has finite resources for power production. The demand for power is increasing in most countries and in the quest to meet this ever increasing deficit, actions that are taken cause huge environmental damage. In response to climate change mitigation/adaptation, most research is focusing on green power production and energy efficiency, which can supplement the power deficit and avoid carbon emission [9]. The optimal integration of energy-efficient devices with renewable energy hybrid systems is the future solution to the ever growing production-demand gap. This is the major motivation for the work presented in this thesis to provide practical technological solutions to achieve OC, DSM and optimal integration of distributed renewable energy (DRE) sources.

The most important step in designing an effective energy efficiency control model and system is firstly to make an accurate estimation of energy consumption, control and state variables. In buildings, for example energy consumption accounts for about 42% of global energy production in developed countries [10]; 60.51% and 23.60% of this energy goes for space and water heating respectively[1]. It shows that most of the energy consumed in buildings is for thermal energy production. This part of energy ought to be minimized on the demand side. Utilization of energy-efficient equipment such as HPWH could greatly reduce energy consumption [11, 12, 13]. HPWHs are devices that drive heat energy from a cooler surrounding medium to a much warmer place using a working fluid (refrigerant) [14, 15, 16, 17, 18, 19, 20, 21]. The refrigerant absorbs the ambient energy of the surrounding medium in the evaporator and passes through the compressor, where it gains extra heat energy through an increase in pressure as a result of compression. This hot working fluid then circulates through the heat exchanger (condenser), where thermal energy is dispatched to the water and the process repeats, using

[1] http://www.dti.gov.uk/energy/inform/

two thirds less energy. HPWHs effect huge energy saving and are slowly gaining wider application in space and water heating [22] .

Energy-efficiency devices alone might not achieve significant energy savings; a multi-directional approach can yield more results. There is need to integrate these energy-efficient devices with DREs such as wind, fuel cells (FCs), diesel generators (DGs), storage batteries and photovoltaic (PV) power in buildings [23, 24]. The integration of on/off-site DREs into buildings and small communities is a promising technology for DSM. Various researchers [25, 26, 27, 28, 29, 30, 31, 21, 32] have developed optimal sized models and long-term life cycle costings. There is an urgent need to develop an optimal strategy and integrate DREs to realize net-zero energy buildings (NZEB), cost-effective billing and positive-energy buildings [33, 34, 35, 36, 33]. Therefore, future optimal energy-mixing will rely on the successful implementation of OC techniques [37, 38, 39, 40, 41].

The OC finds an optimality criterion from set of control laws for the given process or plant. The problem is usually a cost function of the control and state variables. The OC deals with the problem of calculus of variation and consists of differentiation equations depicting the control variables path that minimizes the cost function. The solution of an OC problem is found using Pontryagin's Principle or solution of Hamilton-Jacobi-Bellman sufficient condition [42]. The choice of control strategy can widely influence the efficiency and product quality in many industrial processes and systems [43, 44, 45]. The interest to apply control theories begun during the industrialization age, today most industrial process are controlled by lower and higher level control system. The lower level techniques are mainly the proportional-integral-derivative (PID) controllers, based on minimizing the gain error in relationship to the referral settings [46]. These types of controllers, have their limitations in that the problem of multi-variable dynamic constrained processes can not be handled. Application of lower level PID controllers to a process with uncertainty perturbations can lead to system failure because of inaccurate gain adjustment. However, the higher level control strategy such as; OC and model predictive control (MPC) can effectively handle multi-variable dynamic constrained systems and optimization problem that minimizes the cost function [47]. The OC strategy has many economic advantages on the system, it can handle multi-variable constraints and can control several process having different dynamics. The OC has a superior advantage, therefore, it is considered for application in this thesis.

Despite all the above successes in optimal designs and control, there is no research on HPWHs

integration into DRE-grid hybrid system, making them uneconomical in most developing countries (e.g., South Africa), with only 16% market penetration [48]. Lack of OC and integration of the DRE and HPWHs is the main motivation behind this works. The other motivation is to solve some of the limitations of digital thermostat control systems used in HPWHs and in some tank hot water heaters (geysers) on the market. These conventional control devices depend on the thermostat's dead-zone to control, actuating on/off on the bounds of set-points (bang-bang) strategy. Bang-bang control consumes a lot of energy because each time in the case of a HPWH, water has to repeatedly heat to upper set-point regardless of hot water demand. Though, digital thermostats based control system are coming on market, there operation is still unable to predict demand or load-shifting to avoid operation during peak time-of-use (TOU) electricity tariff periods. Most HPWH and geysers in South Africa are fitted with a digital thermostat control system. Therefore, this work proposes the OC strategy in HPWHs, that can optimize, predict and load-shift over the given control horizon.

Therefore, this work is a first attempt at a multi-directional approach to integration of DRE-grid hybrid systems with HPWHs, that effectively conquer the existing challenges. The work developed a new HPWH hot water state model and OC strategy that meets both technical and operational constraints.

1.2 OBJECTIVES OF THE THESIS

1) to develop an optimal scheduling strategy of a grid-tied/battery/PV system supplying power to a heat pump water heater

2) to develop an optimal energy control strategy of a grid-tied diesel/PV/ battery hybrid system powering HPWHs

3) to develop an OC of a HPWH powered by Wind-PV-hybrid system and economic analysis

4) to develop and model an OC of a FC/wind/PV/grid hybrid system having a thermal heat pump load

5) to carryout the life cycle cost (LCC) analysis of the models to help make the investment choice

An additional contribution is that, unlike many previous works that evaluated the techno-economic benefit [15, 16, 17, 18, 19, 20, 21], where the objective functions are performances of averaged day over a year, or multiple years, this work proposes operational performances that are evaluated over a much shorter period, such as a day, 24 hours. A short 24-h period control horizon gives a better control and prediction, as the variations in weather and other independent variables which easily changes within a day. The prediction is always precise because it is run 365 times, meaning each day using the input parameters such as; wind speed, inlet water temperature, solar irradiance and ambient temperature of each specific day. However, a 24-h control horizon has challenges in that you have to run 365 times, for each day and your input parameter have to be updated on daily basis that is: irradiance, load, wind speed, inlet cold water temperatures and ambient temperature. The daily variation of input parameters could be cumbersome and voluminous for 365 days for each consecutive day. A short time has a better prediction. On the other side, an annual control horizon will be run once, with prediction done on input parameters at once, which in actual sense might vary over time. This annual control horizon will definitely give less accurate optimal solution. All input parameters and independent variables should be predicted in advances, that might lead to inaccuracies especially on open-loop control strategy. This is a major difference in this work.

1.3 LAYOUT OF THE THESIS

This thesis is structured as follows:

Chapter 1 comprises of the thesis research background and motivation as well as the main contributions.

Chapter 2 is the literature review on DSM, DRE sources (PV power, wind power, FC, battery storage and DG) and heat pumps. The optimal DREs-grid integration and control strategies are also included.

While chapter 3 presents an optimal scheduling strategy of a grid-tied/battery/PV system supplying HPWH. This chapter develops the first attempt to design a greener, practical and economically attractive OC model for a grid-tied PV system that considers the TOU electricity tariff. The model presents an OC breakthrough in the integration of renewable energy resources and a potential to turn a dwelling

into an positive energy buildings. The other contribution of this chapter is the application of mixed integer non-linear programming (MINLP) to this complex nonlinear engineering problem.

In chapter 4, a backup DG is added to the chapter 3 model. In order to model the existing challenges of demand leveling and load shedding in South Africa. Though the DG acts as a backup during load shedding, the performance index is to minimize the cost function on fuel and energy costs. In addition, this chapter proposes new battery usage model, which works as storage of cheaper-to-buy off-peak grid energy instead of its conventional usage of storing the excess DRE power.

Chapter 5 presents an OC of a HPWH and calculated the economic analysis. The main power sources are wind, PV and the grid. It proposes a first attempt on OC application in HPWHs that is superior to a digital thermostat control strategy that has no prediction and load shifting capabilities. This chapter's OC can effectively provide the required hot water temperature without necessarily reaching the set-points based on deterministic hot water demand. This in turn minimizes the energy required to raise the hot water temperature to the set-point.

Chapter 6 presents an optimal energy management strategy for a FC hybrid system. The hybrid system meets the load demand consisting of an electrical load and a HPWH which is a source of thermal energy in the case study. The performance of the proposed control strategy is tested by simulating different operating scenarios, with and without renewable energy feed-in and the results confirm its effectiveness, as it increases the supply reliability of the system.

Chapter 7 compares the life cycle cost (LCC) analysis of baseline (existing) and the developed OC models. LCC is important to show the cost benefits of the proposed models and enable investors/homeowners make informed investment choices. In most cases, investment in DREs and energy efficiency devices is viewed as unattractive on short term basis due to lack of a LCC analysis of system over the its life. However, this chapter shows that some of the DREs/HPWH models in fact yields positive net present value (NPV) over their useful life. This chapter summarizes the LCC of each model over the whole system life, unlike the preliminary payback period calculated using few assumptions.

Finally, chapter 8 concludes all the findings of the thesis, points out research gaps and makes recommendations.

CHAPTER 2 LITERATURE STUDY

2.1 INTRODUCTION

This chapter looks at the body of literature on energy efficiency and DSM. In South Africa, the installed power capacity[1] is around 42 090 MW, with a slight marginal operational reserve of just 10%. The operational reserve cannot meet the peak demand, hence the government developed an integrated resource plan (IRP)[2]. This marginal operational reserves demands an urgent solution on supply side management and DSM. Therefore, the South African in addition to energy efficiency measures, it proposes under IRP 2010-2030 new installation of 17 800 MW renewable energy generation across the country. Though these mitigation intended as long-term measures, meanwhile short-term measures on supply and demand side are continue to be taken. Therefore, with the strategic plan in place, the obvious challenges would be operational control and optimal energy mix/feed-in to achieve system stability. The work of this thesis is mainly focused on short-term mitigation on the utilization of energy-efficiency devices such as HPWHs on DSM, as well as long-term integration of DRE sources. So far incentives/rebated-based policies have been put in place to encourage the use of energy-efficiency equipment. The main power utility, Eskom, is implementing DSM as a long-term measure to reduce the demand by 5 000 MW by 2015 [49]. These measures are being implemented to counter the anticipated national demand of 40 GW [50, 51]. DSM challenges and their mitigation are being solved in the short, medium and long term. However, these programs are hampered by the lack of skilled personnel, measurement and verification, energy-inefficient device production and manufacturing incompetence.

[1] http://www.eskom.co.za/IR2015/Documents/Eskom_fact_sheets_2015.pdf
[2] http://www.energy.gov.za/files/Annual%20Reports/DoE-AnnualReport201415.pdf (12.10.2015)

2.2 ENERGY EFFICIENCY UTILIZATION

The expansion of coal-fired power plants is still given priority at the expense of sustainable green energy development. Research into greener energy production is a global agenda, exploring environmentally friendly sources such as: wind, hydrogen, FCs, biomass and solar energy [52]. These research output will in the long term reduce the dependency on fossil fuel in the generation of electricity. There are other effective strategies apart from policies that can greatly improve the stability and energy security in the existing system. These are: management efficiency, carrier efficiency, optimal integration, operational efficiency, information and billing efficiency and control efficiency [53].

Energy management efficiency increases the sustainability and effective utilization of available energy resources. This can provide immediately relief from power demand; the energy saved by effective management can help to supply other loads. Therefore, in order to appreciate the full benefit, energy management should be promoted at industrial, residential and transportation sector levels. This management approach should be applied to both conventional and sustainable energy generation.

Energy efficiency looks at a broader perspective, which is the main focus of this thesis. This includes efficient performance, maintenance, equipment, thermal, fuel, conversion and luminous processes. Energy efficiency is a relationship between output and input energy. It is an important factor for rationalizing and assessing energy usage in any sector. The major contribution of this thesis in terms of conversion efficiency, thermal efficiency and equipment efficiency. The HPWH is one of such energy-efficient items of equipment in the production of thermal energy at domestic and commercial level. On the other hand, DRE power conversion, OC and integration improve the conversion and operational efficiency.

2.3 HEAT PUMP WATER HEATERS

HPWHs are used for space and water heating in domestic and commercial buildings. This equipment can be used for both space and water heating and cooling (air conditioning) in various seasons (i.e primary thermal extractor in chillers). In contrast to the laws of thermodynamics, heat flows in the direction of a lower gradient, the HPWH reverses this process by pumping heat from a colder to a much warmer medium [14]. There are several types and classifications of HPWHs. Their names are mostly

derived from the evaporator's design and its principle of harvesting the ambient/surrounding air energy. These include; ground-source heat pumps, air-source heat pumps and multi-function heat pumps and gas-engine driven heat pumps. Others are integrated with solar thermal namely; solar-assisted heat pumps, integrated solar-assisted heat pumps and direct-expansion solar-assisted [54].

Figure 2.1 shows the schematic components of a typical single-unit heat pump. HPWHs drive heat energy from a cooler surrounding medium to a much warmer place using a working fluid (refrigerant). The refrigerant absorbs the ambient energy of the surrounding medium in the evaporator and passes through the compressor, where it gains extra heat energy through an increase in pressure as a result of compression. This hot working fluid then circulates through the heat exchanger (condenser), where thermal energy is dispatched to the water. This process is continuous in a closed loop system. T_t is the outlet hot water temperature at any given time, while u_{hp} represents the power supply switch.

The past two decades have seen major advances in HPWH technology [55, 8], which has led to its wider application and improved coefficient of performance (COP). Essen and Yuksel [56] extensively investigated both ground-sourced and air-sourced HPWHs and made an economic analysis. Various authors [41, 57, 58, 59, 60, 61] have developed models and investigated ways of improving the COP. Research on optimal sizing and maximization of ambient energy harvesting from the surrounding environment using HPWHs continues. Many researchers [62], [54], [63], [59], [64] have presented models that can efficiently recover the natural surrounding ambient energy through a combination of techniques. However, most of them agree that OC, system design, sizing and renewable energy integration remain technological challenges. These technological challenges in system design and integration [8] contribute to their low implementation. The initial cost remains a major draw-back in the application of HPWHs, especially in developing countries [48]. Their application in developing countries is still uneconomical because of various technological challenges and policies; for example, in South Africa the market penetration of HPWHs is just slightly above 16% [48].

2.4 RENEWABLE ENERGY HYBRID SYSTEMS

Rising costs, an escalating power deficit and environmental concerns about fossil fuel-based energy resources have led to significant research effort in renewable and cleaner energy resources [65, 66, 67, 68, 69, 70]. Globally, governments are adopting policies to promote the development and application of

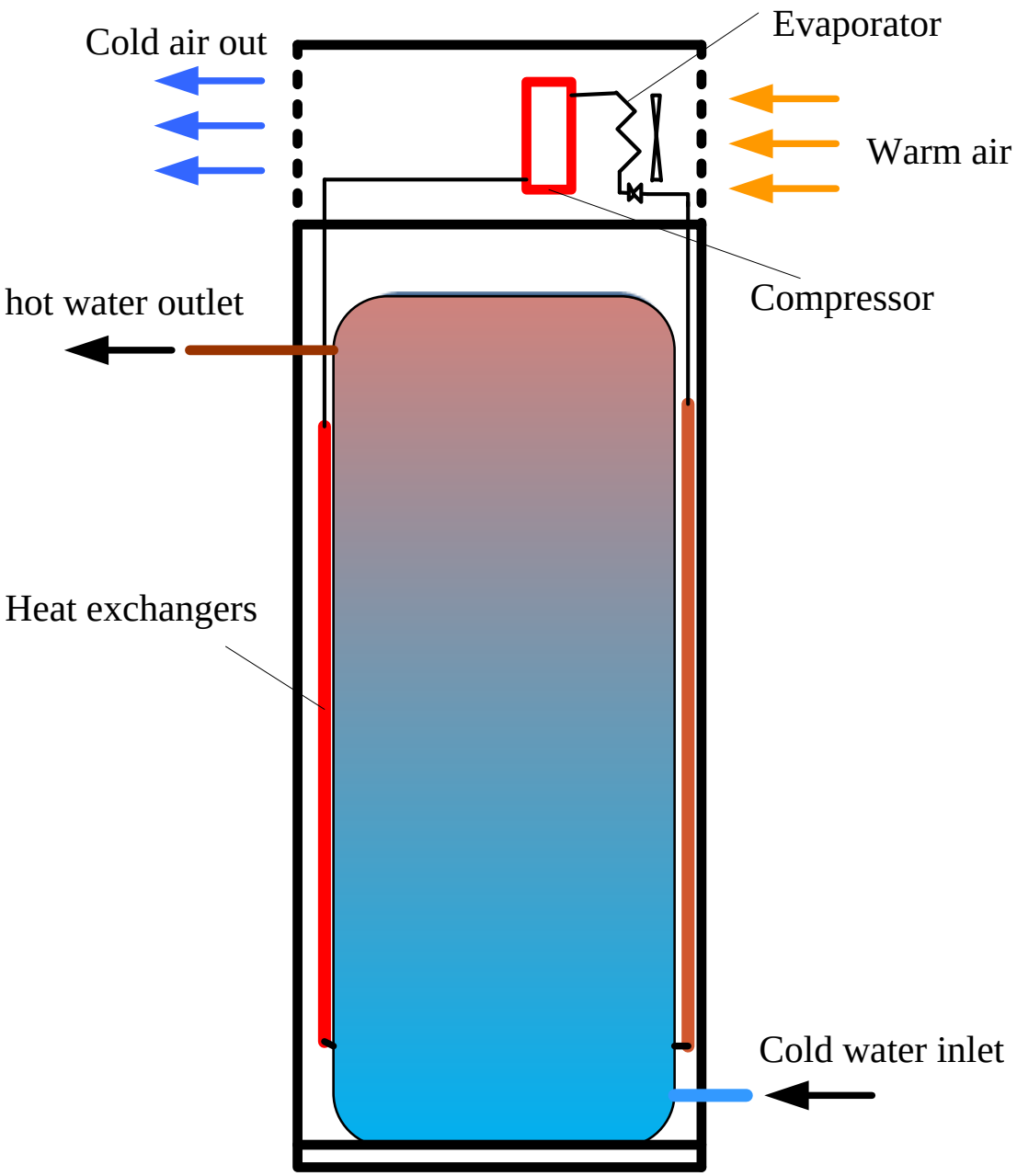

Figure 2.1. Heat pumps layout

various RE technologies for generating electricity. The main challenge associated with RE technologies such as solar and wind generation is their intermittent nature, which affects their ability to provide 100% supply reliability. Various studies have shown that combining these RE sources with battery storage and DG systems is cost-effective [71, 72].

Currently there are limitations on the fraction of RE (wind and solar) that can be incorporated into the grid system because of their intermittency and base load considerations. With the latest developments pointing towards the feasibility of the hydrogen economy, solar and wind power fractions can be safely extended in the grid system by compensating for their intermittent nature with an energy storage medium such as hydrogen and batteries. Interest in green energy sources is mainly driven by their ability to reduce carbon dioxide emissions, thereby helping to mitigate climate change, improve local air quality, improve energy security by reducing energy imports, increase energy supply options and reduce dependence on fossil fuels.

Various DRE hybrid system and energy management control strategies have been proposed with different system configurations [73, 74, 75]. A standalone RE/FC hybrid system that uses at least one RE source and a polymer electrolyte membrane as backup source is analyzed in [76]. Frequency fluctuation analysis of a wind, DG and FC hybrid power system connected to a local utility is presented in [77] and the results show that the system can yield better performance by stabilizing the frequency of the system. Electrochemical energy storage systems such as hydrogen systems offers a better flexibility if integrated with stochastic power sources like wind and PV generators. Local energy storage system helps to increase the penetration of other energy sources [74]. Use of hydrogen as a storage medium for intermittent power sources is gaining momentum owing to its variable application, since it can be used as a clean fuel in the transport sector and for power production in stationary FCs [74, 76].

The expansion and integration of renewable energy into the existing grid system is still a major challenge, although more positive breakthrough are expected [68, 78]. DRE is an important source of energy [79]. The other major drawbacks in the exploitation of RE are: financial incentives, as well as political, fiscal, technological, environmental and legislative measures [67]. Private investment in RE comes at a huge cost in comparison to the conventional power plant in terms of capital per unit output. Moreover, conventional power plants in most cases are heavily subsidized by the state, which lowers the unit cost. In addition to the challenges mentioned, profitable feed-in tariffs and favourable financial accessibility can help increase the potential of the technology. Otherwise, investment in DREs will remain a riskier investment in view of its intermittent nature and lack of incentives.

2.5 OPTIMIZATION AND CONTROL METHODS IN ENERGY SYSTEMS

The development of early control system for commercial application was a result of achieving energy savings and precise process control [80, 81]. In most buildings and other systems, thermostats were widely applied in feedback and control systems (e.g. cylinder water heaters) [82]. Early thermostats had their own limitations; the change of frequency between states was rapid until the introduction of more stable dead-zone thermostats. These haphazard (bang-bang) control strategies are still in application in most domestic and industrial devices, despite the inability to predict the desired output and demand time. Advances in control engineering and plant modeling have seen the birth of more precise control techniques, such as proportional-integrate-derivative (PID) controllers [83, 84]. PIDs have been implemented in various industrial applications and replaced most of the haphazard thermostatic control systems owing to their accuracy and feedback system. However, though the PIDs controller has gained wide application, the major disadvantage its inability to tune the controller's gain value accurately. The gain is an important parameter that helps in the precise control of a plant. In most cases improper adjustment of the gain results in the whole system being unstable [85].

In the past three decades, a new research focus on modern control techniques have been growing fast. The development of predictive, adaptive and optimal control is changing the conventional control strategies [86]. These modern control techniques can achieve optimal output at the same time handle hard plant constraints. The application of an OC strategy at industrial level is still applied as often as the PID because of lack of an accurate plant/process model which is required for it to be implemented [87]. Model predictive control (MPC) has the best capability to handle future disturbances or uncertainty in the controlled process or input parameters [88], while an adaptive controller is able to self-regulate according to the conditions of the controlled building or plant process. The OC strategy minimizes the controlled variables to a global/local minimum of the objective function, thus giving an output of the controlled process with the optimal benefit. The OC strategies can be simulated by various optimization algorithms readily available in software on the market (e.g., in MATLAB) [89].

The application of optimal design and control of an integrated RE hybrid system is important in achieving a practical cost-effective DRE system. Many authors have developed optimal sizing and performance analysis [9, 23, 25, 26, 27, 28, 29, 30, 31]. However, an accurate plant model is necessary before implementation of OC, predictive or adaptive control strategies in NZEB, cost-effective billing or positive-energy buildings [33, 34]. In the same vein, an OC strategy will gradually replace PIDs

controllers in DRE integration in the near future [37, 38, 90]. This is because OC has ability to predict demand, adaptation and load-shifting during peak TOU electricity tariff periods, which saves a lot of energy and cost. Unlike the bang-bang or PID control strategy [41, 23, 13]. The major work in this thesis was the development and application of an OC strategy for practical control of energy-efficient devices and RE hybrid systems, solving one of the main engineering challenges.

The next chapter looks at the optimal power dispatch of a grid-tied-battery-PV system supplying an HPWH.

CHAPTER 3 OPTIMAL POWER DISPATCH OF A GRID TIED-BATTERY-PHOTOVOLTAIC SYSTEM SUPPLYING HEAT PUMP WATER HEATERS

3.1 INTRODUCTION

HPWH have gained wide usage in an offering economical means of heat recovery from the environment for industrial and domestic applications [8]. The predominant usage of the HPWH is for water and space heating [22], [91]. Heat pumps have low energy consumption, approximately two thirds less than resistive element water heaters, owing to their COP [48]. The heat pump is used in DSM as an efficient means of providing the thermal energy requirements of the building; however, usage of energy-efficient equipment alone as DSM without integration of renewable energy sources (e.g., solar power) will not yield significant energy savings. The major challenge is the OC and integration of DREs and HPWH to mitigate the energy deficit.

Therefore, this chapter develops an optimal scheduling strategy model for a grid-tied/battery/PV system to power a HPWH. The objective function of this model is the grid energy cost minimization while taking into consideration the TOU tariff. The OC strategy of this grid-tied PV system can be implemented to reduce energy cost while meeting technical and operational constraints. In this model the battery is not charged by the PV as usual; instead it is being used as a storage of cheaper-to-purchase (off-peak) grid energy to make it available during the peak demand period. The baseline case study shows that OC is a breakthrough in the integration of renewable resources to power the HPWH and has

the possibility of turning a dwelling into an energy/cost-positive building. The content of this chapter has been published in [39]

3.2 MODEL DEVELOPMENT

3.2.1 Schematic model layout

The OC strategy schematic layout in Figure 3.1 consists of five sub-models: the power utility grid 230/400V, PV modules with grid-interactive inverter, battery with inverter/charger, HPWH and the domestic load.

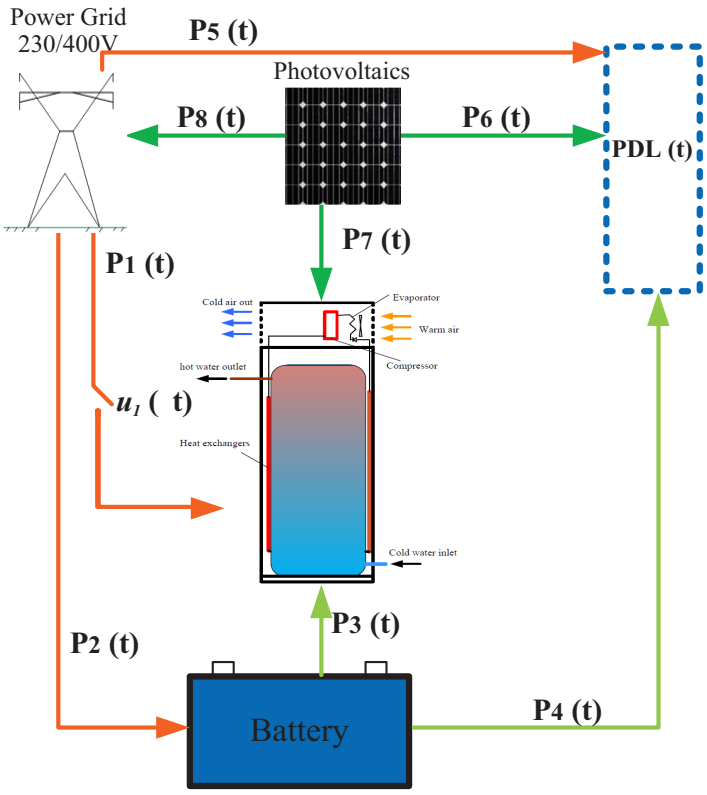

Figure 3.1. Schematic layout of the model

The grid can supply power $P_1(t)$ directly through a switch $u_1(t)$ to the HPWH, while $P_2(t)$ is for charging the battery and $P_5(t)$ supplies the domestic load $P_{DL}(t)$. The battery is used to store off-peak cheaper energy from the grid through $P_2(t)$; this off-peak stored energy is made available during peak demand to supplement the loads. The battery supplies $P_3(t)$ and $P_4(t)$ to the HPWH and domestic load

respectively. The PV modules can supply power to all the loads and at the same time feed into the grid, $P_7(t)$ supplies the HPWH, $P_6(t)$ supplies the domestic load and $P_8(t)$ is the excess power from the PV, which is sold to the grid. The proposed model is controlled by energy management systems, which are not shown in the schematic layout. The power flows $P_1(t)$, $P_2(t)$, $P_3(t)$, $P_4(t)$, $P_5(t)$,$P_6(t)$, $P_7(t)$, $P_8(t)$ and the switch $u_1(t)$ in Figure 3.1 are the control variables in this model.

Here the grid acts as the excess PV power storage system, unlike using the PV power to charge the battery. The sale of PV power to the grid attracts rebates and other incentives in most countries in addition to revenue generation. The battery is charged during the cheapest TOU tariff and makes use of this cheaper-to-buy stored energy during the peak demand period. The weighting factor was incorporated in the objective function as factor for selling excess PV power to the grid, based on the desired effects of each client. The formulation of OC of the HPWH was achieved using the operational constraints and objective function.

3.2.2 Sub-models

3.2.2.1 Heat pump water heater

The heat pump is modeled as a fixed load at a discrete time interval with respect to the power demand. The power demand of the heat pump is taken to be proportional to the thermal load requirements and inversely proportion to its COP. Hawlader [92] extensively formulated a heat pump model; however, in this study the HPWH is modeled as input data based on an annual demand profile taken from a case study in South Africa. The grid can supply $P_1(k)$ to the HPWH directly through a switch $u_1(k)$. This supply route has a continuous and binary variable, which is a nonlinear constraint. The HPWH is mainly supplied by the solar PV $P_7(k)$ and battery $P_3(k)$ whenever available. In this chapter, for simplicity we denoted $P_i(k)t_s = P_i(k)$, with $i = 1,\ldots,9$ being the number of the control variables. The sampling time t_s is one hour and the sampling interval $k = 1,\ldots,N$, where $N = 24$. The HPWH energy balance is given as:

$$P_1(k)u_1(k) + P_3(k) + P_7(k) = P_{hp}(k), \tag{3.1}$$

$$P_{hp}^{min} \leq P_{hp}(k) \leq P_{hp}^{max}, \tag{3.2}$$

3.2.2.2 Photovoltaic

The PV is treated as input data which is a variable power source, varying from zero to maximum rated power as shown in equation (3.4). The PV power acts as the main power source for the HPWH whenever available. The battery is a supplementary source. However, during the period when the HPWH demand is too high for the PV and the battery to meet, the grid supply (P_1) is switched on through switch $u_1(k)$. The generated PV power is connected to the grid interactive inverter to enable selling. The inverter efficiency η_i is taken from the case study. The energy balance of the PV output is shown in equation (3.3).

$$0 \leq P_6(k) + P_7(k) + P_8(k) \leq \eta_i P_{pv}(k), \tag{3.3}$$

$$0 \leq P_{pv}(k) \leq P_{pv}^{max}, \tag{3.4}$$

3.2.2.3 Battery

The battery is charged with $P_2(k)$ from the grid. The stored energy in the battery is made available during peak demand and whenever it is uneconomical to use the PV or the grid power. The battery performance index is its status of energy (SOE), which depends on the initial state of charge $B_c(t-1)$ and the power discharging to the loads. The SOE of the battery at any given time t and the flow of power from $t-1$ to t governed by the battery dynamic given in equation (3.5), where $t = 1, \ldots, 24$.

$$B_c(t) = B_c(t-1) + \eta_i \eta_c P_2(t) - \eta_i \eta_d P_3(t) - \eta_i \eta_d P_4(t), \tag{3.5}$$

where $\eta_c = 0.91$ and $\eta_d = 0.85$ are the battery charging and discharging efficiency respectively. $\eta_i = 0.92$ is the round trip grid-tied inverter efficiency converting alternating current (AC) to direct current (DC) to charge the battery and vice versa to the loads. $\eta_c P_2(t)$ is the charging power accepted by the battery from the grid, whereas $\eta_d P_3(t)$, $\eta_d P_4(t)$ are the discharged power to the HPWH and domestic load respectively. Here $B_c(t)$ is the battery SOE in (kWh) and $\tau = 1, \ldots, k$, therefore, from equation (3.5) the generalised discrete battery dynamics are expressed as:

$$B_c(k) = B_c(0) + \eta_i\eta_c \sum_{\tau=1}^{k} P_2(\tau) - \eta_i\eta_d \sum_{\tau=1}^{k} P_3(\tau) - \eta_i\eta_d \sum_{\tau=1}^{k} P_4(\tau), \tag{3.6}$$

However, utilization of the power from the battery must be within its nominal range B_c^{min} and B_c^{max} in order to maximise the battery life cycle.

$$B_c^{min} \leq B_c(k) \leq B_c^{max}, \tag{3.7}$$

where B_c^{min} and B_c^{max} are the minimum and maximum nominal capacity respectively. In this model, a step-down transformer are avoided since the voltages are at domestic level; rather the grid-interactive inverter/charger with an efficiency of 92% is used.

3.2.2.4 Grid power

The grid is modeled as an infinite busbar at domestic voltage levels of 230/400 V capable of simultaneously supplying and accepting power from the DREs connected through the grid-interactive inverters without transformers. The TOU electricity tariff is factored in the model, which is one of the most important OC parameters. In South Africa, Eskom is the main power supply utility company, which has a dynamic pricing system $p(t)$ or rather TOU tariff, off-peak (p_o), standard (p_s) and peak (p_p). In this study, the recent Eskom [1] Megaflex Active Energy-TOU tariff was used. The DRE feed-in tariff is regulated by the National Energy Regulator of South Africa (NERSA)[2], which commissioned a Renewable Energy Feed-in Tariff (REFIT) for South Africa. NERSA, through the Renewable Energy Purchasing Agency (REPA), which in South Africa's case is the Single Buyer Office (SBO) of the national electricity utility Eskom under phase II (PV systems large ground or roof mounted) pegged REFIT[3] at 3.94 R/kWh. In this model p_c was used to denote the PV feed-in tariff. These regulatory measures and SBO provide the necessary incentive to the DRE developers and private investors. They guarantee the availability of a renewable energy market and provide venture capital at low financial risk. The Eskom TOU electricity tariff is:

$$p(t) = \begin{cases} p_o = 0.3656\text{R/kWh} & \text{if } t \in [0,7] \cup [23,24], \\ p_s = 0.6733\text{R/kWh} & \text{if } t \in [7,8] \cup [11,19] \cup [21,23], \\ p_p = 2.2225\text{R/kWh} & \text{if } t \in [8,11] \cup [19,21], \end{cases} \tag{3.8}$$

[1] http://www.eskom.co.za/

[2] http://www.nersa.org.za/

[3] https://energypedia.info/wiki

where R is the South African Rand and time t is the whole period of the day with $t = 0,\ldots,23$.

3.2.2.5 Domestic loads

The domestic appliances P_{dl} are modeled as the total power demand of all other loads in the building except the HPWH and constitute the input data for that period.

$$P_4(k) + P_5(k) + P_6(k) = P_{dl}(k), \tag{3.9}$$

3.2.3 Objective function

The objective function is expressed in a discrete-time domain at sampling time t_s, to minimize grid energy costs J while maximizing the solar energy sales to the grid. The OC strategy makes use of the cheaper PV and stored battery energy whenever available to power the HPWH and load. The grid's direct supply to the HPWH is restricted by the binary variable $u_1(k)$ switch, $(1$ or $0,$ when On/Off respectively$)$ and can only be *On* if the PV and battery power is uneconomical to use, dependent on the TOU/feed-in tariff, or is completely unavailable. The weighting factor ω_i is adjusted based on the desired effects (e.g savings on energy or maximum rebate) of the customer. The sampling time t_s in this model is one hour and the sampling interval $k = 1,\ldots,N$ where $N = 24$.

Objective function:

$$J = t_s\left(\omega_1 p(t)\sum_{k=1}^{N}(P_1(k) + P_2(k) + P_5(k)) - \omega_2 p_c \sum_{k=1}^{N} P_8(k)\right), \tag{3.10}$$

subject to the following constraints:

$$P_1(k)u_1(k) + P_3(k) + P_7(k) = P_{hp}(k), \tag{3.11}$$

$$0 \leq P_6(k) + P_7(k) + P_8(k) \leq \eta_i P_{pv}(k), \tag{3.12}$$

$$B_c(k) = B_c(0) + \eta_i\eta_c\sum_{\tau=1}^{k} P_2(\tau) - \eta_i\eta_d\sum_{\tau=1}^{k} P_3(\tau) - \eta_i\eta_d\sum_{\tau=1}^{k} P_4(\tau), \tag{3.13}$$

$$P_4(k) + P_5(k) + P_6(k) = P_{dl}(k), \tag{3.14}$$

where $p(t)$ and p_c is the TOU electricity tariff and the PV feed-in tariff (R/kWh).

Control variables and limits

The model is a mixed integer nonlinear problem with continuous and binary control variables. The continuous variables are the power flows $P_1(k)$, $P_2(k)$, $P_3(k)$, $P_4(k)$, $P_6(k)$, $P_7(k)$ and $P_8(k)$, while the switch $u_1(k)$ is a binary variable, which can only assume values (0 or 1). The upper and lower bounds of the continuous variables are given in equation (3.15) for every k^{th} sampling interval. The continuous variables are $P_i(k)$, where $i = 1,2,\ldots,8$.

$$P_{(i)}^{min} \leq P_i(k) \leq P_{(i)}^{max} \tag{3.15}$$

3.2.4 Mixed integer nonlinear programming

The objective function contains linear and nonlinear constraints with a binary variable. The power supply to the HPWH is control by the switch $u_1(k)$ and a continuous variable $P_1(k)$. This makes the problem a mixed integer nonlinear, which is formulated according to [93]. An additional MINLP optimization solver *OPTI toolbox* in MATLAB was used.

The general *OPTI toolbox* algorithm solver is formulated as follows:

$$min_x f^T x \text{ subject to } \begin{cases} A \cdot x \leq b \\ Aeq \cdot x = beq \\ lb \leq x \leq ub \\ c(x) \leq d \\ c_{eq}(x) = d_{eq} \\ x_i \in \mathbb{R} \\ x_j \in \{0,1\} \end{cases} \tag{3.16}$$

f^{T_x} is scalar function to be minimised containing the nonlinear objective function, which is subject to the following constraints:

Linear equalities: *Aeq* is a *k* x *n* sparse matrix, *beq* is a *k* x 1 vector.
Linear inequalities: *A* is a *m* x *n* sparse matrix, *b* is a *m* x 1 vector. *Decision variable bounds*: *lb* and *ub* are *n* x 1 indicating the lower and upper bound respectively.
Nonlinear inequalities: *c* is a *u* x 1 vector of functions containing inequality constraints, *d* is a *u* x 1 vector.
Nonlinear equalities: *ceq* is a *v* x 1 vector of functions containing nonlinear equality constraints, *deq* is a *v* x 1 vector.
Integer constraints: x_i are decision variables which must be an real number $\mathbb{R}$.
Binary constraints: x_j are decision variables which must be a binary number $(0,1)$, where $i \neq j$.

3.2.5 Case study

A case study is done based on 3x16 kW HPWH installed at the Pretoria Hotel in South Africa. The weighting factor is assumed to have equal weights $\omega = 0.5$. The sampling time $t_s = 1$ hour, since most published research has proved that there is only a marginal difference on PV generator when sampled at 15 min or 30 min, therefore, even an hour interval measurements of the PV generator could still give accurate prediction. The choice of sampling time was as well influenced by the HPWH's operational constraints, nothing much at shorter t_s can lead to a noticeable hot water temperature gain.

The power consumption of the HPWH was measured at hourly intervals for a year. The power consumed by the heat pump is directly proportional to the thermal energy flow requirement and inversely proportional to its system COP. The simplified hourly power demand of the HPWH is given as:

$$P = \frac{Q_D}{COP} \tag{3.17}$$

where Q_D is the total thermal demand, which is a function dependent on the mass and energy balance of the system. Figure 3.2 shows the hourly energy consumption of the HPWH on a selected date of the month considered in the case study. The energy consumed by the other domestic load excluding

the HPWH was also measured and treated as input data. The months in the case study were selected from each prevailing season in South Africa. The baseline is the current situation at the hotel where the HPWH and domestic load are supplied by the grid only. The rooms in the hotel are fitted with an occupancy sensing system, a lower level of energy management. The proposed OC strategy is the main intervention that considers the TOU tariff. This model yielded a significant energy and cost reduction presented in section 3.3.

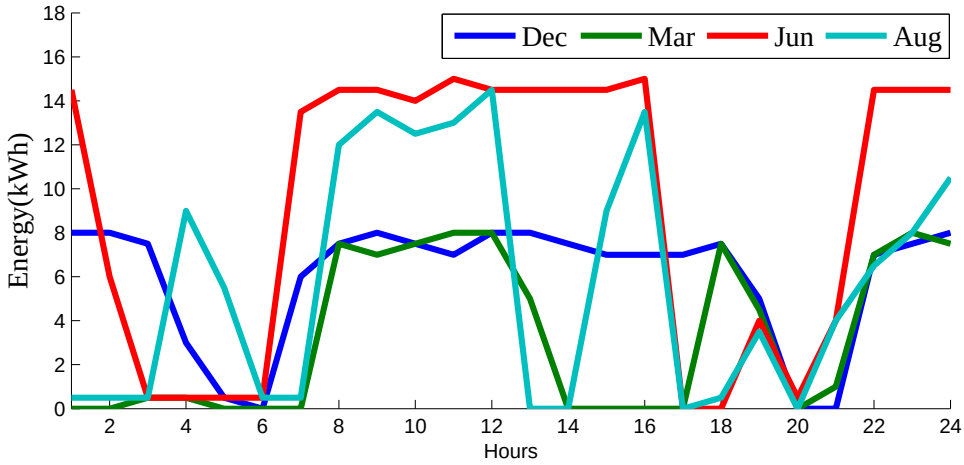

Figure 3.2. HPWH hourly energy consumption(kWh)

The input data on the PV power generation shown Figure 3.3 are adopted from the measured data from our research [75] on tilted roof-top mounted PV modules. The PV arrays are mounted on a 66.2m^2 roof-top area. Erratic PV power generation is observed during the month of December because it is the summer period in South Africa, characterised by heavy cloud and rain.

The deep cycle battery SunXtender[4] type-PVX-2580L is used, with a total capacity of $3x165$A-h. The battery capacity is deliberately undersized to reduce the initial investment cost and to hold only enough power to supplement the grid during peak demand. During the off-peak period the grid charges the battery. This power is released during the peak TOU tariff period to the HPWH and the domestic loads. It is assumed that the initial SOE of the battery is $B_c(0) = 0.55B_c^{max}$. For simplicity of the optimization problem, the battery charging/discharging was assumed to be unconstrained. Therefore, the charging/discharging process could happen simultaneously, this applies to all the battery models in this thesis. Although in practice, charging and discharging should not happen at same time.

[4]http://www.sunxtender.com

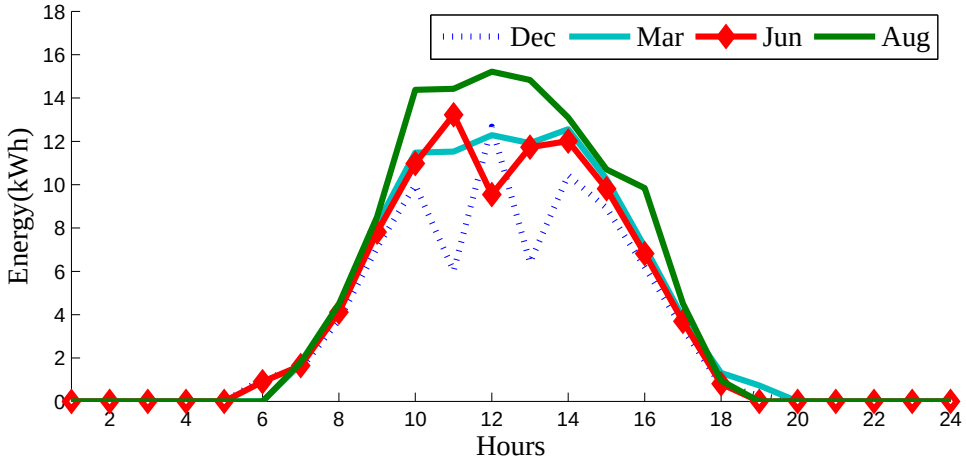

Figure 3.3. PV power output(kW)

3.3 SIMULATION RESULTS AND DISCUSSION

3.3.1 Optimal control strategy of the heat pump water heater and domestic load - December

The optimal schedule in December illustrated in Figure 3.4(a) shows the power from the grid (P_1) and battery (P_3) meeting the HPWH demand (P_{hp}) from midnight till 06:00 in the morning. The OC prioritised the battery to power the HPWH up to the start of the standard TOU tariff period. The grid supply around 04:00 shut down, as shown in Figure 3.4(b). Instead the stored energy was used to supply the HPWH. However, in Figure 3.4(b) the OC switched the grid supply to the HPWH at once again 05:00 and kept it on standby, though no power was flowing. This could be attributed to fact that the OC opted to use the cheaper stored energy, but still kept the grid on standby in case the battery failed to sustain the HPWH. The schedule changed when the tariff entered peak TOU; it shows that PV (P_7) and the battery (P_3) supplying much of the HPWH demand, thereby avoiding the expensive energy from the grid. The battery continued supplying the required demand after the peak period, and the grid just supplemented the supply. The PV dropped supply immediately after the peak demand period and the generated power (P_8) was sold, as illustrated in Figure 3.5(a), to the grid in order to maximise the benefits. The SOE in Figure 3.5(b) was increasing after the peak period, meaning the battery was storing more energy than what was being discharged to the loads. The OC switching frequency was low in the peak period shown inFigure 3.4(b) in order to save energy from the grid. The

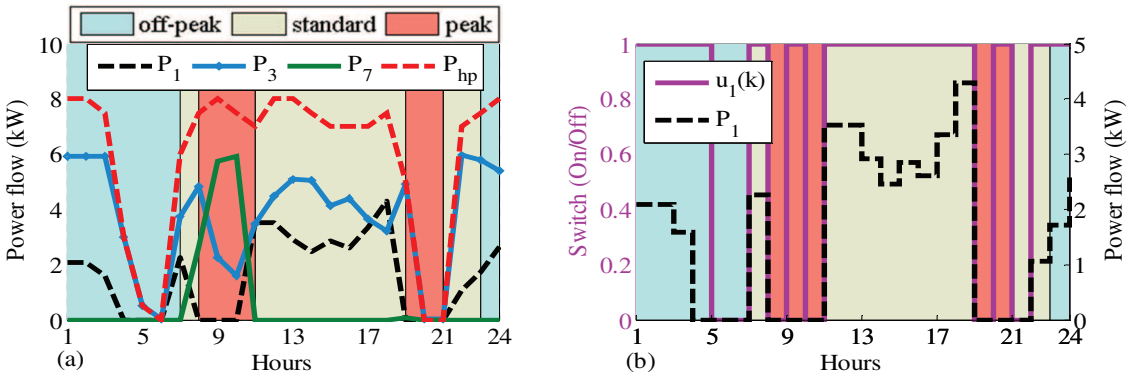

Figure 3.4. (a) Optimal power dispatch to the HPWH; (b) Optimal switching control to the HPWH

OC followed a similar schedule in the evenings. The TOU electricity tariff legend in Figure 3.4 applies to all results in this chapter.

The power dispatched to the domestic load is presented in Figure 3.5(a). The battery (P_4) supplied the entire load from midnight until 07:00 before the grid (P_5) was brought into supply. The PV (P_6) supplied the domestic load only during peak demand, afterwards all the generated power was traded off to the grid.

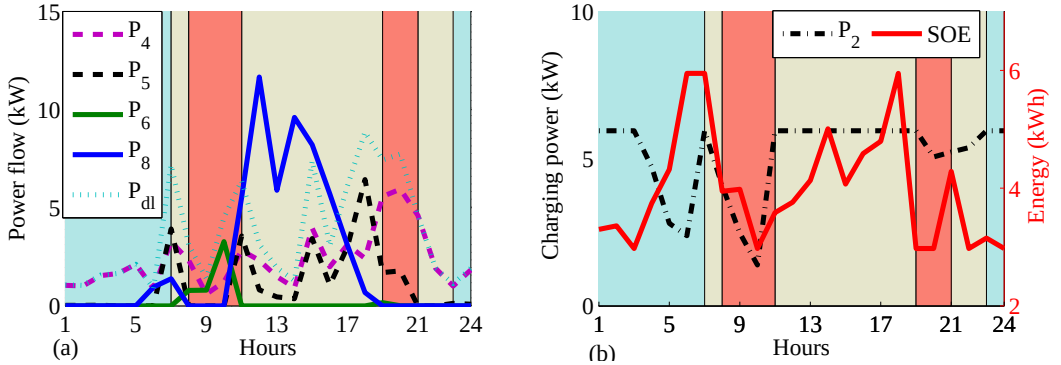

Figure 3.5. (a) Optimal load scheduling and solar sales; (b) Status of charge and battery power dispatch

Figure 3.5(b) shows the battery SOE and the dispatched power to the HPWH (P_3) and domestic load (P_4). The battery was only charged through (P_2) during the off-peak and standard TOU tariff periods. The SOE rose during these periods, meaning the battery was accumulating cheaper energy that would be made available during peak demand. During peak TOU the SOE declined because the battery was

discharging the stored power to the loads. The schedule was observed to drop the grid power supply (P_2) to the battery during peak period to save on energy cost.

3.3.2 Optimal control strategy of the heat pump water heater and domestic load - March

In March, as shown in Figure 3.6(a), the power consumed by the HPWH was relatively lower when compared to December. The PV power (P_7) supplied much of the morning peak demand, with supplement from the battery (P_3). The grid supply (P_1) to the HPWH was off the whole time and came in at the beginning of the standard TOU period. The PV supply gradually dropped and the cheaper battery energy sustained the supply to the HPWH till 14:00. The optimal schedule in the evening followed a similar trend; the battery was charging in this period, as shown by the SOE in Figure 3.7(b). The stored energy, thereafter, supplied most of the HPWH demand up to midnight. The OC in Figure 3.6(b) shows a low switching frequency matching the low load demand. The grid supplied power only during the standard TOU tariff period, which was beneficial for cost saving.

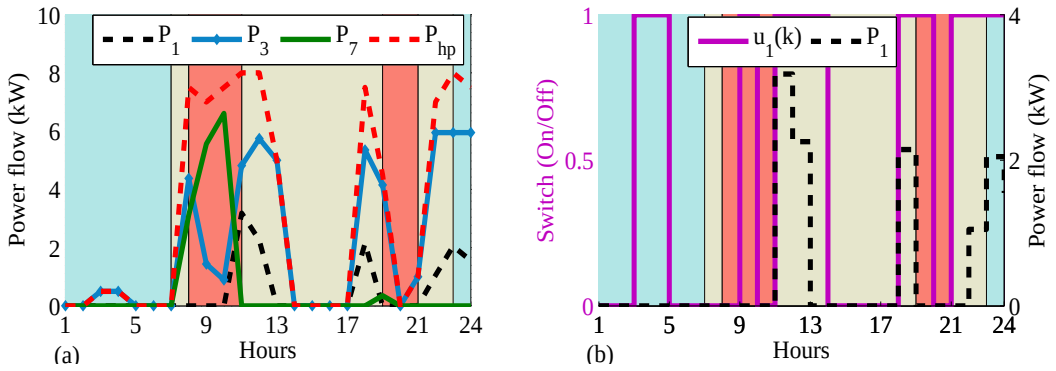

Figure 3.6. (a) Optimal power dispatch to the HPWH; (b) Optimal switching control to the HPWH

The load demand shown in Figure 3.7(a), was met by the battery (P_4) throughout the day except during peak period demand. The PV supplied much of the peak period, thereafter the battery continued. This change of the OC strategy was not as a result of the TOU, but rather to satisfy the load demand using economical energy. However, most of the morning peak demand was met by the PV power. The excess solar power (P_8) was sold to the grid. The grid (P_5) barely supplied the domestic load because the OC always prioritised the stored cheaper energy.

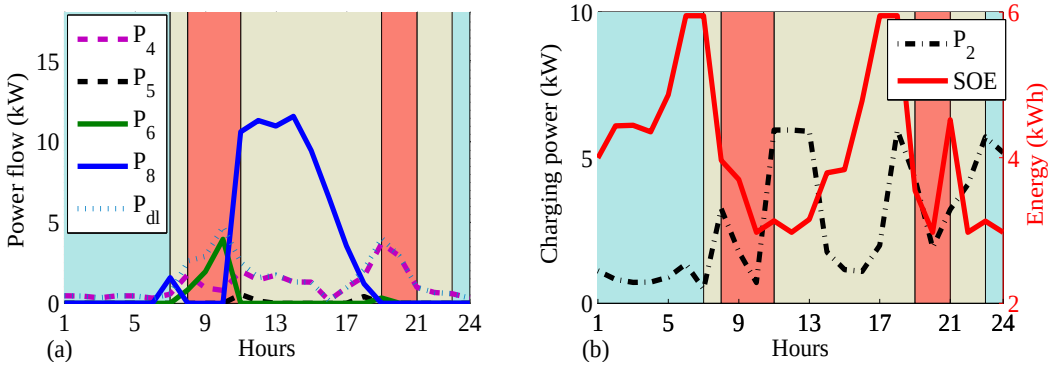

Figure 3.7. (a) Optimal load scheduling and solar sales; (b) Status of charge and battery power dispatch

The SOE in Figure 3.7(b) showed the battery was storing energy from midnight till the beginning of the morning standard TOU tariff. The battery, however, discharged most of the energy during the peak demand period, consequently the SOE in Figure 3.7(b) declined between 07:00 and 11:00, though as the tariff entered standard TOU again the charging resumed.

3.3.3 Optimal control strategy of the heat pump water heater and domestic load - June

Figure 3.8(a) indicates the highest power demand was experienced during June. The HPWH demand was high throughout the day because it was a winter period of the year in this case study, characterised by a higher thermal requirement for bathing and space heating.

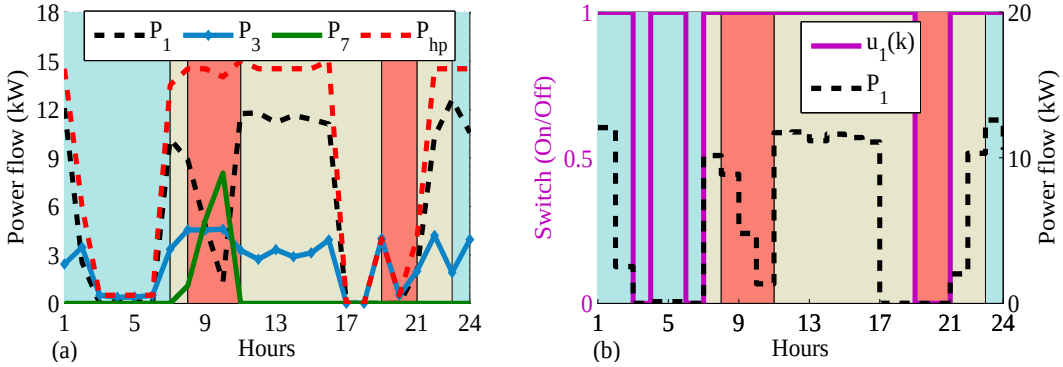

Figure 3.8. (a) Optimal power dispatch to the HPWH; (b) Optimal switching control to the HPWH

The grid (P_1) supplied the HPWH from midnight till morning with minor supplement from the battery (P_3). The switching frequency in Figure 3.8(b) was different from the rest of the year. The OC switch

was *on* throughout morning peak TOU despite having complementary sources. This can also be attributed to the low PV power output, as shown in Figure 3.3; in winter solar irrandiance is low in the southern hemisphere because of the sun's geometrical position.

The power scheduling to the load in Figure 3.9(a) shows that the grid (P_5) supplied most of the domestic demand with the help of the battery. In Figure 3.9(b), the battery SOE showed continuous oscillation for the whole period, charging and discharging. The frequent cycles had a negative effect on the battery life. The grid power (P_2) charging the battery was steady throughout owing to the increased discharge frequency of the battery.

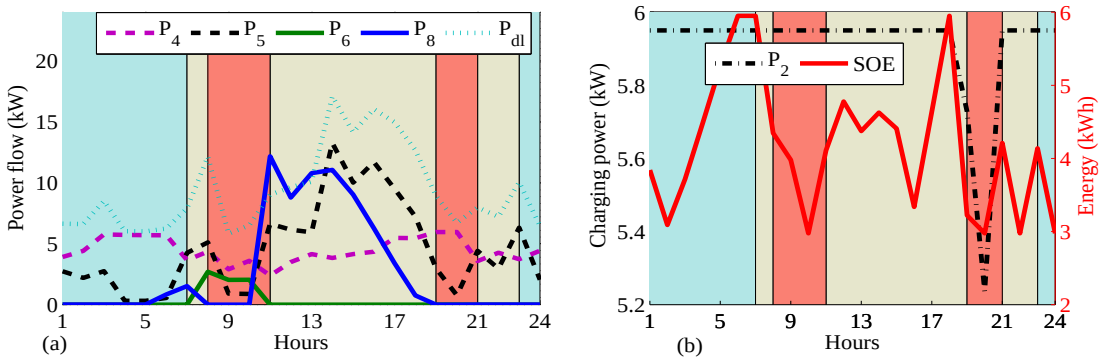

Figure 3.9. (a) Optimal load scheduling and solar sales; (b) Status of charge and battery power dispatch

Notwithstanding the highest demand, solar energy sales were relatively better than in December, as shown in Table 3.1 because of the absence clouds and rain, but June had the lowest cost savings.

3.3.4 Optimal control strategy of the heat pump water heater and domestic load - August

The optimal scheduling strategy in August illustrated in Figure 3.10(a) was similar to that of the previous months discussed above. August had the best solar irradiance which increased the PV power output. In addition, there was an increase in solar power sales (P_8) to the grid as shown in Figure 3.11(a). The generated revenue was more as well during this month, when compared to other months.

The battery SOE Figure 3.11(b) showed that the battery had enough stored capacity, except during the peak demand period. The HPWH load was erratic in Figure 3.10(a), which is depicted by (P_{hp}); however, the OC prioritised usage of the stored energy in the battery.

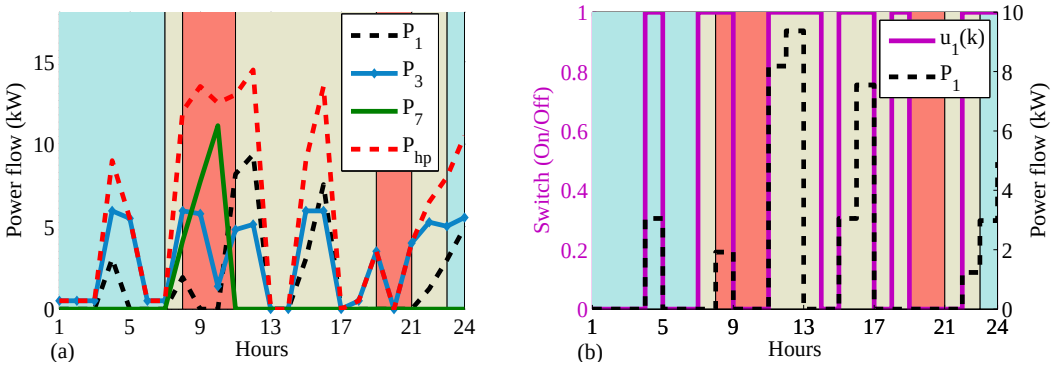

Figure 3.10. (a) Optimal power dispatch to the HPWH; (b) Optimal switching control to the HPWH

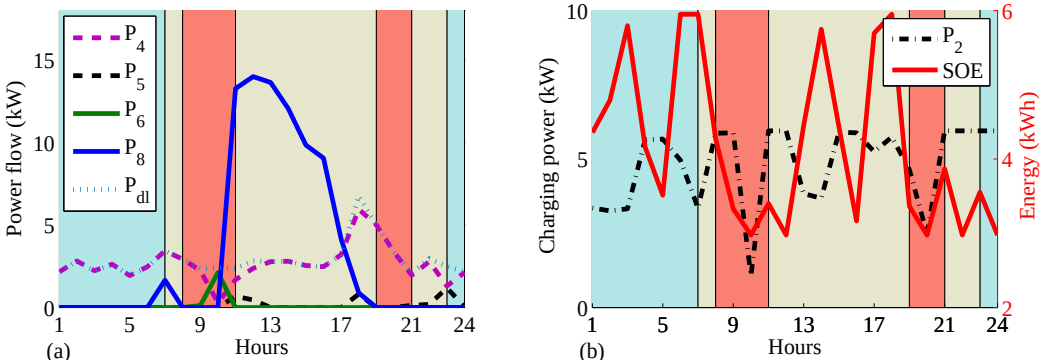

Figure 3.11. (a) Optimal load scheduling and solar sales; (b) Status of charge and battery power dispatch

The OC showed huge savings on the grid side owing to the power that was not delivered. The optimal energy mixing, saving and renewable energy feed-in that were achieved are presented below in Table 3.1. The challenges in achieving NZEBs would be solved by the implementation of this model.

3.3.5 Baseline and optimal energy cost

The baseline energy cost is the current situation in the case study, where the grid meets the total demand of the HPWH and loads. The optimal cost, on the other hand, is the energy cost after employing the OC strategy presented in this chapter. The optimal cost comprises the sum of energy consumed by the domestic load, HPWH and the energy used to charge the battery. The proposed integration of PV energy yields more benefit on cost saving, which is presented in Table 3.1. The PV energy sales are the revenue generated by selling solar energy to the power grid. Not all the PV power produced was

sold; some went to supplement the load demand.

The energy saved represents the power utility (grid) power not delivered to the load, which would have been delivered without the OC intervention of this model. The saved energy is the difference between the baseline and the OC strategy. There is significant energy saving, which is directly translated into a reduction on primary input of utility power generation (e.g., gas, coal and water). The consumption of more primary input in the generation of power has a negative effect on global warming. However, these impacts are not considered in this chapter. The results in Table 3.1 are the energy and cost saving per day, on the selected dates in the case study.

Table 3.1. Daily optimal energy and cost savings

Month	Baseline cost (R/day)	Optimal cost (R/day)	Solar sales (R/day)	Energy saved (kWh)	Cost savings (%)
December	219.03	146.27	207.70	72.11	33.22
March	138.39	65.68	263.03	89.46	52.54
June	400.32	319.29	254.47	85.66	20.24
August	212.06	126.92	309.53	103.75	40.15

The optimal scheduling strategy showed a maximum energy cost saving of 52.54% in March. For example, December had a baseline cost of 219.03 R/day and after optimization the cost reduced to 146.27 R/day, which translated to a cost saving of 33.22%. If monthly energy cost is assumed to be constant daily demand, for December with 31 calender days the costs would be: baseline cost 6789.93 R/month, optimal cost 4534.37 R/month, PV energy sales 6438.7 R/month and energy saving amounting to 2235.41 kWh/month. The optimal schedule presented a huge benefit, especially that the battery acted as storage for the cheaper-to-purchase energy from the grid.

June had the lowest energy cost savings which stood at 20.24% because of higher load demand in winter. On the other hand, August had the highest solar sales at 309.53 R/day mainly because of the better solar irradiance and clear sky in the southern hemisphere. The huge revenue from the PV energy sales is in part attributed to the attractive feed-in tariff in this case study. The hotel is energy cost-positive on some days, though not on others. The main intervention of the optimal schedule achieved energy and cost savings.

3.3.6 Economic analysis

The economic analysis is done, based on the following assumptions: A discount factor or interest rate of 5.9% is used to reflect the time value of money and the 5.9%[5] is indicative of the inflation rate in South Africa. Thus the present value (PV)[6] one cash flow per year future is:

$$PV = \frac{FV}{(1+r)^n} \tag{3.18}$$

where

PV - present value (FV);

FV - nominal value of a cash flow amount in a future period;

r - interest rate or discount rate;

n - time in years before the future cash flow occurs.

Table 3.2 below shows the revenue from solar energy sales and the benefit on cost savings owing to the OC intervention, based on the average of all the months tested in the case study, and then the costs/revenue of that day is annualized to reflect an average amount per annum.

Table 3.2. Annualised benefits

Month	Baseline cost (R/day)	Optimal cost (R/day)	Solar energy sales	Cost savings
December	219.03	146.27	207.7	
March	138.39	65.68	263.03	
June	400.32	319.29	254.47	
August	212.06	126.92	309.53	
Averages	**242.45**	**164.54**	**258.68**	**77.91**
Annualized totals			**94 419.11**	**28437.15**

[5]http://www.resbank.co.za/Pages/default.aspx

[6]https://en.wikipedia.org/wiki/Discounted-cash-flow (date accessed 10.10.2014)

It is assumed that the solar sales, cost savings, operations and maintenance costs will remain constant throughout the period. Though it is expected that there will be an increase in all these factors, it cannot be reliably estimated at this time. Increases in solar sales and costs would reduce the payback period. The detailed economic analysis of payback period is shown in the Table 3.3.

Table 3.3. Economic analysis and pay back period

Years	0	1	2	3	4	5
Solar modules	(160,000.00)					
Deep cycle battery	(28,760.00)					
Energy manager controller	(75,900.00)					
Inverter/charger for the battery	(26,490.00)					
PV grid-interactive inverter	(42,188.00)					
ZigBee load control switches	(15,227.00)					
Installation cost	(25,000.00)					
Operation and maintenance cost		(33,725.00)	(33,725.00)	(33,725.00)	(33,725.00)	(33,725.00)
Solar sales		**94,419.11**	**94,419.11**	**94,419.11**	**94,419.11**	**94,419.11**
Cost Savings		28,437.15	28,437.15	28,437.15	28,437.15	28,437.15
	(373,565.00)	89,131.26	89,131.26	89,131.26	89,131.26	89,131.26
Discount factor @ 5.9%	1	0.944287063	0.891678058	0.842000055	0.795089759	0.750792973
Discounted cash flows	(373,565.00)	84,165.50	79,476.39	75,048.53	70,867.35	66,919.13

Discounted Payback Period	Years	Discounted cash flows	Cumulative cash flows
	0	(373,565.00)	(373,565.00)
	1	84,165.50	(289,399.50)
	2	79,476.39	(209,923.11)
	3	75,048.53	(134,874.58)
	4	**70,867.35**	**(64,007.23)**
	5	66,919.13	2,911.90
Payback is	4 years 11 months		

Table 3.3 clearly shows that the discounted payback period goes up to the fourth year, when the invested capital indicated in brackets in Table 3.3 reaches the break-even point. By exactly 4 years and 11 months this proposed system would have completely paid back the capital investment. Though, as mentioned above assumptions were made about certain factors that may influence the payback period, the cash flows and maintenance costs are treated as constant. These factors, though, have minimal effects on this proposed model, making it economically feasible with a shorter payback period.

3.4 SUMMARY

The optimal scheduling strategy presented in this chapter shows huge energy cost savings. The HPWH's operational constraints were satisfied through the use of the actual performance index in this chapter. The scheduling strategy presented a practical integration of renewable resources to the grid in order to achieve NZEBs. The current rebate system on the usage of HPWH for generation of hot water in place of resistive element heaters (geysers) in South Africa will further increase the market penetration. The application of this model would further reduce initial investment costs. In respect of a global call for climate change awareness , most building owners are now looking for energy-efficient and sustainable technologies. Though this model presents such solutions, future research should look into integration of other renewable energy sources (e.g biomass, wind) to supply specifically the HPWH.

The initial investment payback would be further reduced with a rebate on the usage of HPWHs and DREs in South Africa, which were not considered in this chapter. The case study showed that for part of the period the building was energy cost-positive, meaning the utility bills could be paid from the generated revenue. The model result showed huge revenue from solar energy sales. In addition Eskom gives rebate on HPWH, which is not considered in this chapter. The grid-connected PV optimal scheduling strategy could be applied to realise sustainable energy integration for low demand loads such as HPWHs. This would improve the utility's power reserves and security of supply through optimal integration of DRE sources. In addition, employment of the battery as an off-peak energy storage system was beneficial, as the building could qualify for rebates and incentives on renewable energy trade-off.

This model is suitable for application in both urban and rural areas. There are several advantages of this model, among others that it is suitable for regions with intermittent electrical power supplies.

The battery is the only back-up power supply in this chapter. Depending on the load demand the security of supply might not always be guaranteed, though it has the lowest initial investment cost. However, the next chapter (chapter4) looks into a model with much higher security of power supply that has a DG as the main back-up.

CHAPTER 4 OPTIMAL ENERGY CONTROL OF GRID TIED PV-DIESEL-BATTERY HYBRID SYSTEM POWERING HEAT PUMP WATER HEATER

4.1 INTRODUCTION

Chapter 3 presented the model of the PV-grid-tied-battery with the HPWH. This chapter 4 deals with a model that includes a DG as the main back-up giving more reliability on energy security during power outages. DGs have gained wider application in developing nations with intermittent electricity supply in both urban and rural areas. The major disadvantage of DGs is the high running and maintenance costs. Optimal operation is important, so that the DG only comes into operation at a desirable time, taking into account fuel cost and for the purpose of maintaining the security of power supply.

In this regard, chapter 4 develops an OC strategy for power dispatch of the grid-tied/PV/battery/DG system supplying the HPWH that provides the necessary thermal energy. The model minimizes energy and fuel cost while maximizing PV power feed-in. The power flows from each source are the control variables, while the status of energy of the battery is the state variable. OC shows great potential to realize a practical NZEB and DSM. This chapter in addition proposes a different model of battery usage. It works as storage for cheaper-to-buy off-peak grid energy instead.

The model meets both the technical and operational constraints. Simulations are based on the case study run over a year on selected seasonal dates using the actual measured demand of the HPWH. The work presented in this chapter has been published in [23]

4.2 MODEL DEVELOPMENT

4.2.1 Schematic model layout

The OC strategy schematic diagram shown in Figure 4.1 consists of the utility power grid, PV modules, battery, DG, HPWH and domestic load. The grid can supply power $P_1(t)$ directly through a switch $u_1(t)$ to the HPWH, while $P_2(t)$ is used to charge the battery and $P_3(t)$ supplies the domestic load. This paper presents a new battery connection model; unlike many conventional models found in literature [94],[95], [96], the battery is used to store cheaper-to-buy off-peak grid energy. The stored off-peak energy is then made available during peak TOU tariff hours to supplement the PV and DG supplies to the HPWH. In situations where the battery, DG and PV power are uneconomical or insufficient to meet the demand, the OC switches on $u_1(t)$ enabling direct grid supply to the HPWH. The DG supplies power P_8 to the HPWH only, in periods when it is uneconomical to use grid energy. The PV modules can supply power to all the loads and at the same time feed into the grid, $P_5(t)$ supplies the HPWH, $P_6(t)$ supplies the domestic load and $P_4(t)$ is the excess PV power sold to the grid.

The optimal scheduling decides the amount of excess PV energy to be sold to the grid, mainly based on the weighting factor to maximize the net benefit of the customer. The PV energy trade-off and usage of the HPWH attract incentives in the case study, though these are not considered in this chapter. The DG is a backup power supply in the periods when the PV or grid energy is unavailable or uneconomical, depending on the TOU.

4.2.2 Sub-models

4.2.2.1 Diesel generator

The DG usually attains a maximum fuel efficiency of 3 kWh/l, if operated above 80% and the lowest fuel efficiency when running below 30% of its rated power [97]. The DG fuel consumption F in (l/h) is modeled according to [98], as shown in equation (4.1), where P is the power delivered and C_f is the fuel price (*R/l*).

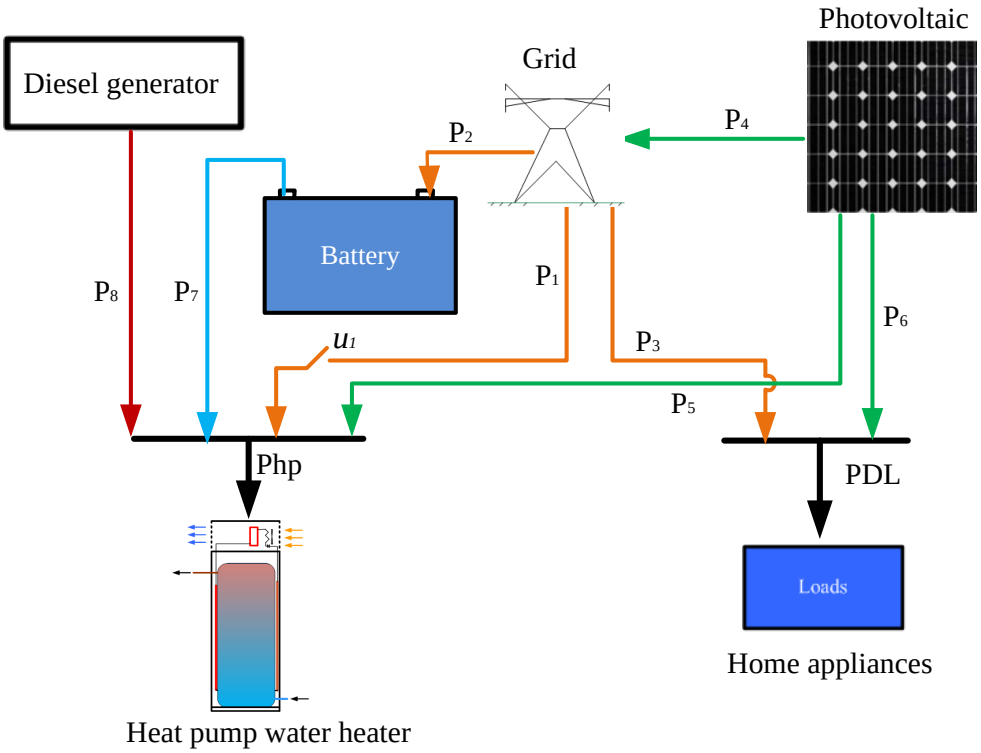

Figure 4.1. Schematic layout of the model.

$$F = C_f \left(aP^2 + bP + c\right), \tag{4.1}$$

The generator coefficients a, b and c are obtained from the manufacturer's data; in this model we adopted the coefficient proposed by Duo-Lopez Rodolfo et al. [99], $a = 0.246\ l/kWh$ and $b = 0.08145\ l/kWh$. The DG fuel efficiency, $\eta_g\ (kWh/l)$, is given in equation (4.2)

$$\eta_g = \frac{P}{F} = \frac{P}{C_f\left(aP^2 + bP + c\right)}, \tag{4.2}$$

The DG power output operates within its lower and upper bounds.

$$0 \leq P \leq P_{dg}^{rated}. \tag{4.3}$$

where P_{dg}^{rated} is the rated power output of the DG.

4.2.2.2 Heat pump water heater

The HPWH is modeled as a fixed load at a discrete time interval with respect to the electrical power consumption. The power demand, $P_{hp}(k)$, of the heat pump in this chapter is taken to be proportional to the thermal load requirements and inversely proportional to its COP. Hawlader [92] presented a detailed model of all major heat pump components. However, this chapter treated the HPWH demand as input data taken from the measured annual profile in the case study in South Africa. The grid supplies $P_1(k)$ directly through switch $u_1(k)$ to the HPWH. The switch and the continuous variable $P_1(k)$ form a mixed integer nonlinear constraint. The grid's direct supply to the HPWH is restricted by the binary variable switch, $u_1(k)$, which can only be 1 or 0, when On/Off respectively. In addition, the HPWH is supplied by the battery, $P_3(k)$, PV $P_5(k)$ and the backup DG, $P_8(k)$. In this chapter, for simplicity we denoted $P_i(k)t_s = P_i(k)$, with $i = 1,\ldots,9$ the total number of control variables inclusive of the switch $u_1(k)$. The sampling time t_s is one hour, while k is the sampling interval $k = 1,\ldots,N$, with $N = 24$. The HPWH power balance is given in equation (4.4) as:

$$P_1(k)u_1(k) + P_5(k) + P_7(k) + P_8(k) = P_{hp}(k), \tag{4.4}$$

$$P_{hp}^{min} \leq P_{hp}(k) \leq P_{hp}^{max}, \tag{4.5}$$

The generalised coefficient of performance of the HPWH is given in equation (4.6) as:

$$COP = \frac{Q_D}{P}. \tag{4.6}$$

where Q_D is the total hot water demand; a function of mass and energy balance of the HPWH's evaporator, condenser and hot water storage system. P is the total electrical power input to the HPWH, mainly consumed by the compressor, fan and controller unit.

4.2.2.3 Photovoltaic

The PV power generation $P_{pv}(k)$ is input data in this model, a variable power source from zero to its maximum rated, as shown in equation (4.8). The PV supplies $P_5(k)$ to the HPWH , $P_6(k)$ to the loads and $P_4(k)$ feed-in to the grid. The PV power output balance is shown in equation (4.7).

$$0 \leq P_4(k) + P_5(k) + P_6(k) \leq P_{pv}(k), \tag{4.7}$$

$$0 \leq P_{pv}(k) \leq P_{pv}^{max}. \tag{4.8}$$

4.2.2.4 Battery

The battery performance index is the SOE [100], which depends on the initial state of energy $B_c(t-1)$, which is dependent on charging/discharging of power. The battery SOE model is adopted from [98] for any given time t. The power flow from $t-1$ to t is given in equation (4.9), where $t = 1, \ldots, 24$.

$$B_c(t) = B_c(t-1)(1-\sigma) + \eta_c P_2(t) - \eta_d P_7(t), \tag{4.9}$$

The battery is charged with $P_2(k)$ from the grid, while $P_7(t)$ is the discharged power to the HPWH. The stored energy is made available during peak demand and whenever it is uneconomical to use the grid, PV or DG energy. The self-discharged factor σ and the inverter efficiency are neglected in this chapter. η_c and η_d are the battery charging (set at 85%) and discharging (100%) efficiency respectively. Here $B_c(t)$ is battery SOE in (kWh) and $\tau = 1, \ldots, k$, therefore, from equation (4.9) the generalised discrete battery dynamics is expressed as:

$$B_c(k) = B_c(0) + \eta_c \sum_{\tau=1}^{k} P_2(\tau) - \eta_d \sum_{\tau=1}^{k} P_7(\tau), \tag{4.10}$$

However, the utilization of the battery must be within its nominal range, the minimum state of energy B_c^{min} is set to 50% and the maximum B_c^{max} is equal to the battery capacity to prolong the battery life.

$$B_c^{min} \leq B_c(k) \leq B_c^{max}. \tag{4.11}$$

4.2.2.5 Power grid

The grid is modeled as an infinite busbar capable of simultaneously supplying and accepting power from the DREs. The TOU electricity tariff is factored in the model, which is one of the most important OC parameters. In South Africa, Eskom is the main power supply utility company, which has a dynamic pricing system $p(t)$ or rather TOU tariff: off-peak (p_o), standard (p_s) and peak (p_p). In this study, the recent Eskom [1] megaflex active energy-TOU tariff was used. In this model p_c is used to denote the PV feed-in tariff at $3.94R/kWh$ [2]. The Eskom TOU electricity tariff is:

$$p(t) = \begin{cases} p_o = 0.3656\text{R/kWh} & \text{if } t \in [0,7] \cup [23,24], \\ p_s = 0.6733\text{R/kWh} & \text{if } t \in [7,8] \cup [11,19] \cup [21,23], \\ p_p = 2.2225\text{R/kWh} & \text{if } t \in [8,11] \cup [19,21], \end{cases} \tag{4.12}$$

where R is the South African rand and time t is the whole period of the day with $t = 0,\ldots,23$.

4.2.2.6 Domestic appliance

The domestic appliances P_{dl} are modeled to be the total energy consumed by all other loads in the building except the HPWH and constitute input data for that period.

$$P_3(k) + P_6(k) = P_{dl}(k). \tag{4.13}$$

4.2.3 Objective function

The objective function is expressed in a discrete-time domain to minimize energy and fuel cost while maximizing the usage of the greener and cheaper energy whenever available. The DG comes on only when the PV and grid energy proves to be uneconomical. The TOU electricity tariff and the feed-in tariff are some of the important control parameters. The weighting factor ω_j is adjusted based on the desired effects (e.g. savings on energy or maximum rebate) of the customer, $j = 1,\ldots,3$. The sampling time t_s is one hour and the sampling interval $k = 1,\ldots,N$ where $N = 24$.

[1] http://www.eskom.co.za/
[2] https://energypedia.info/wiki

Objective function:

$$J = t_s \left(\omega_1 p(t) \sum_{k=1}^{N} (P_1(k) + P_2(k) + P_3(k)) + \omega_2 C_f \sum_{k=1}^{N} \left(aP_8^2(k) + bP_8(k) + c \right) - \omega_3 p_c \sum_{k=1}^{N} P_4(k) \right), \tag{4.14}$$

subject to the following constraints:

$$0 \leq P_8(k) \leq P_{dg}^{rated}, \tag{4.15}$$

$$P_1(k)u_1(k) + P_5(k) + P_7(k) + P_8(k) = P_{hp}(k), \tag{4.16}$$

$$P_{hp}^{min} \leq P_{hp}(k) \leq P_{hp}^{max}, \tag{4.17}$$

$$0 \leq P_4(k) + P_5(k) + P_6(k) \leq P_{pv}(k), \tag{4.18}$$

$$0 \leq P_{pv}(k) \leq P_{pv}^{max}, \tag{4.19}$$

$$B_c(k) = B_c(0) + \eta_c \sum_{\tau=1}^{k} P_2(\tau) - \eta_d \sum_{\tau=1}^{k} P_7(\tau), \tag{4.20}$$

$$B_c^{min} \leq B_c(k) \leq B_c^{max}, \tag{4.21}$$

$$P_3(k) + P_6(k) = P_{dl}(k). \tag{4.22}$$

where $p(t)$ and p_c are the TOU electricity tariff and the PV feed-in tariff (R/kWh) respectively.

4.2.3.1 Control variables

This optimization problem is nonlinear, having binary and continuous variables. The continuous variables are the power flows $P_1(k)$, $P_2(k)$, $P_3(k)$, $P_4(k)$,$P_5(k)$, $P_6(k)$, $P_7(k)$ and $P_8(k)$. The binary variable is the switch $u_1(k)$, which assumes the values of 1 or 0, when On/Off respectively. The SOE is the state variable. The upper and lower bounds of the continuous variables are given in equation (4.23) for every k^{th} sampling interval. The continuous variables are $P_i(k)$, where $i = 1, 2, \ldots, 8$.

$$P_{(i)}^{min} \leq P_i(k) \leq P_{(i)}^{max} \tag{4.23}$$

4.2.4 Mixed Integer Nonlinear Programming

This model contains linear and nonlinear constraints. The binary constraint is the switch $u_1(k)$ that controls the direct power supply $P_1(k)$ to the HPWH. This problem therefore becomes a mixed integer

nonlinear one formulated according to [93]. An additional MINLP optimization solver *OPTI toolbox* in MATLAB was used.

The general *OPTI toolbox* algorithm solver is formulated as follows:

$$min_x f^T x \text{ subject to } \begin{cases} A \cdot x \leq b \\ Aeq \cdot x = beq \\ lb \leq x \leq ub \\ c(x) \leq d \\ c_{eq}(x) = d_{eq} \\ x_i \in \mathbb{R} \\ x_j \in \{0,1\} \end{cases} \tag{4.24}$$

f^{T_x} is the scalar function to be minimized, containing the nonlinear objective function, which is subject to the following constraints:

Linear equalities

Aeq is a *k* x *n* sparse matrix, *beq* is a *k* x 1 vector.

Linear inequalities

A is a *m* x *n* sparse matrix, *b* is an *m* x 1 vector.

Decision variable bounds

lb and *ub* are *n* x 1, indicating the lower and upper bound respectively.

Nonlinear inequalities

c is a *u* x 1 vector of functions containing inequality constraints, *d* is a *u* x 1 vector.

Nonlinear equalities

ceq is a *v* x 1 vector of functions containing nonlinear equality constraints, *deq* is a *v* x 1 vector.

Integer constraints

x_i are decision variables, which must be an real number $\mathbb{R}$.

Binary constraints

x_j are decision variables, which must be a binary number $(0,1)$, where $i \neq j$.

4.2.5 Case study

A case study is done on a 3x16 kW HPWH installed at the Pretoria Hotel in South Africa. The energy consumption of the HPWH was measured at hourly intervals for a year in order to account for seasonal and temperature variations. Figure 4.2 shows the hourly demand of the HPWH in (kW) on the selected date in the case study. The other domestic loads were measured as well. The months in the case study were selected in such a way as to match each season in South Africa. The baseline is the current situation at the hotel, where the grid meets the requirements of both the HPWH and domestic appliances. This model proposes an OC strategy intervention to realize cost and energy savings at this hotel, with a possibility of transforming it into an NZEB. This model yields significant savings, as presented in section 4.3.

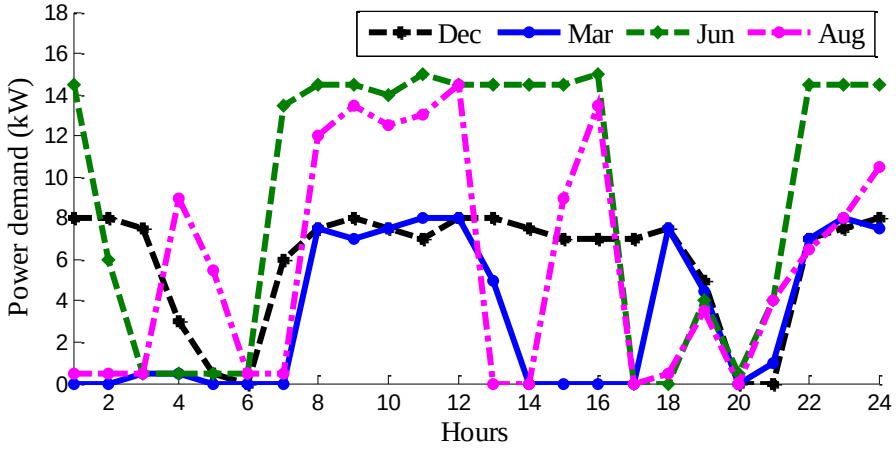

Figure 4.2. HPWH hourly demand (kW)

The input data on the PV power generation shown Figure 4.3 were adopted from the measured data from our on going research [75] on PV models mounted on a tilted rooftop. The month of December is observed to illustrate erratic PV power generation because of of cloud cover and rain in South Africa.

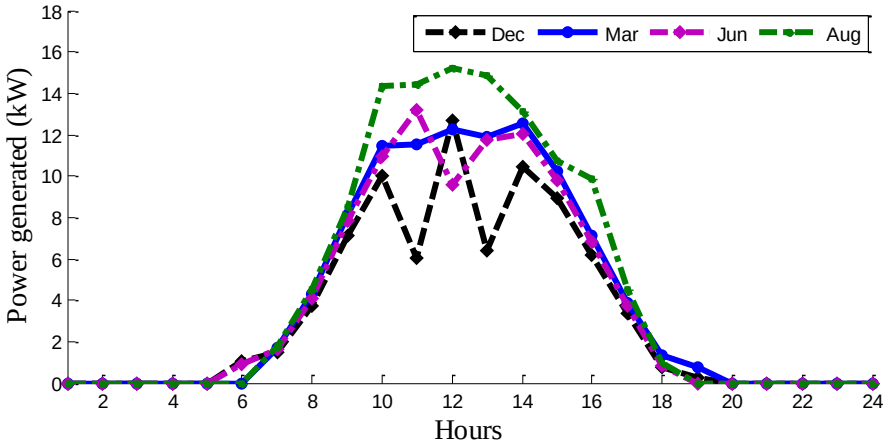

Figure 4.3. PV power output (kW)

The deep cycle battery SunXtender[3] type-PVX-2580L was used, with a total capacity of $3x165$A-h. The battery capacity was specifically undersized to reduce the initial investment cost and to hold only enough power to supplement the grid during peak demand. During the off-peak period the grid charges the battery with cheaper energy and it makes this cheaper stored energy available to the HPWH and load when needed. The initial SOE of the battery was assumed to be $B_c(0) = 0.5B_c^{max}$.

DG BP20S[4] with a maximum power output of 22 kVA, 230V at 1500 rpm. The current diesel fuel pump price in South Africa is 13.3 R/l.

4.2.5.1 Uncertainty analysis of the experimental data

In order to ascertain the confidence level of the measured demand of the heat pump water heater in this case study, the uncertainty error analysis was performed. There is no single method of determining uncertainty error, several techniques exist in assessing uncertainty of the experimental measurement and results. Some methods require knowledge of the system's mathematical model [55] and independent variables. Uncertainty analysis is a vital tool at every planning stage of an experiment; it assesses the viability of the outcomes. However, in this chapter we used the approach presented in [101] to analyze the uncertainty of the experimental data according to equation (4.25). The random error (noise) with an instrument's absolute uncertainty is initialized in the experimental (measured) values. The true

[3]http://www.sunxtender.com
[4]http://www.bundupower.co.za

(accepted) values are then estimated from the measured (corrupted) values. The difference between true values and the measured (corrupted) values is that the corrupted values are assumed to contain noise resulting from systematic errors, especially random errors.

The random errors are generated using Matlab with a distribution mean of 0 and standard deviation equal to 1, which is multiplied by the instrument's absolute uncertainty $\sigma_{m,meas} = \pm 0.01$ given by the manufacturer.

$$Z_m = A_m + RAND_m * \sigma_{m,meas}. \tag{4.25}$$

where: Z_m is the measured (corrupted) or experimental value of mth measurement; A_m is the true value while $RAND_m$ is the random noise; $\sigma_{m,meas}$ is the standard deviation of the mth measurement and $m = 1, \ldots, 24$ the number of measurement.

The month of December was sampled to analyze the uncertainty of the measured data and the results are shown in Table 4.1. A simple visual inspection of the true values show that the results are in close agreement with the measured values with a higher confidence level.

Further analysis is carried out to determine the relative uncertainty of each measurement.

$$\text{Relative uncertainty } (\%) = \frac{\text{Absolute uncertainty}}{\text{Measured value}}. \tag{4.26}$$

The weakest link rule [5] is applied and the measurement with the largest relative uncertainty is picked from Table 4.1. The largest relative uncertainty, which is the weakest link, is used to perform the calculation to determine the final performance index's absolute uncertainty. The performance index in this case is the energy cost.

The performance index of this model is run using the true values A_m to give confidence in the results. The true value simulation results are presented in Table 4.3.

[5] http://www2.fiu.edu/ dbrookes/ExperimentalUncertaintiesCalculus.pdf

Table 4.1. Uncertainty error of the measured demand of the HPWH for the month of December

m	Measured (corrupted) value	Random error	Value(with absolute uncertainty)	True (accepted) value	Relative uncertainty
1	8	0.5688	(8 ± 0.01)	7.421	0.125%
2	8	0.1622	(8 ± 0.01)	7.828	0.125%
3	7.5	0.1656	(7.5 ± 0.01)	7.324	0.133%
4	3	0.6892	(3 ± 0.01)	2.301	0.333%
5	0.5	0.229	(0.5 ± 0.01)	0.261	2.000%
6	0	0.5383	(0 ± 0.01)	-0.548	–
7	6	0.1067	(6 ± 0.01)	5.883	0.167%
8	7.5	0.8173	(7.5 ± 0.01)	6.673	0.133%
9	8	0.2599	(8 ± 0.01)	7.730	0.125%
10	7.5	0.1818	(7.5 ± 0.01)	7.308	0.133%
11	7	0.8693	(7 ± 0.01)	6.121	0.143%
12	8	0.853	(8 ± 0.01)	7.137	0.125%
13	8	0.4018	(8 ± 0.01)	7.588	0.125%
14	7.5	0.1839	(7.5 ± 0.01)	7.306	0.133%
15	7	0.9027	(7 ± 0.01)	6.087	0.143%
16	7	0.3377	(7 ± 0.01)	6.652	0.143%
17	7	0.7803	(7 ± 0.01)	6.210	0.143%
18	7.5	0.0965	(7.5 ± 0.01)	7.394	0.133%
19	5	0.5752	(5 ± 0.01)	4.415	0.200%
20	0	0.8212	(0 ± 0.01)	-0.831	–
21	0	0.6491	(0 ± 0.01)	-0.659	–
22	7	0.547	(7 ± 0.01)	6.443	0.143%
23	7.5	0.6868	(7.5 ± 0.01)	6.803	0.133%
24	8	0.7802	(8 ± 0.01)	7.210	0.125%

4.3 SIMULATION RESULTS AND DISCUSSION

4.3.1 Optimal control strategy of the heat pump water heater and domestic load - December

The OC results in Figure 4.4 show the power scheduling to the HPWH and the domestic loads for December. The TOU electricity tariff legend in Figure 4.4(c) applies to all figures in this chapter. In Figure 4.4(a), the battery P_7 supplied most of the load demand from midnight to the beginning of the morning peak period. The direct grid supply P_1 in Figure 4.4(b) to the HPWH only came in for few hours after midnight and at the end of the evening standard TOU period. The OC during a certain period turned *on* the switch; though very little power was consumed, the schedule opted to keep the grid on standby. The optimal switching avoided the peak period to save on energy cost and instead

used the cheaper-to-buy battery-stored energy.

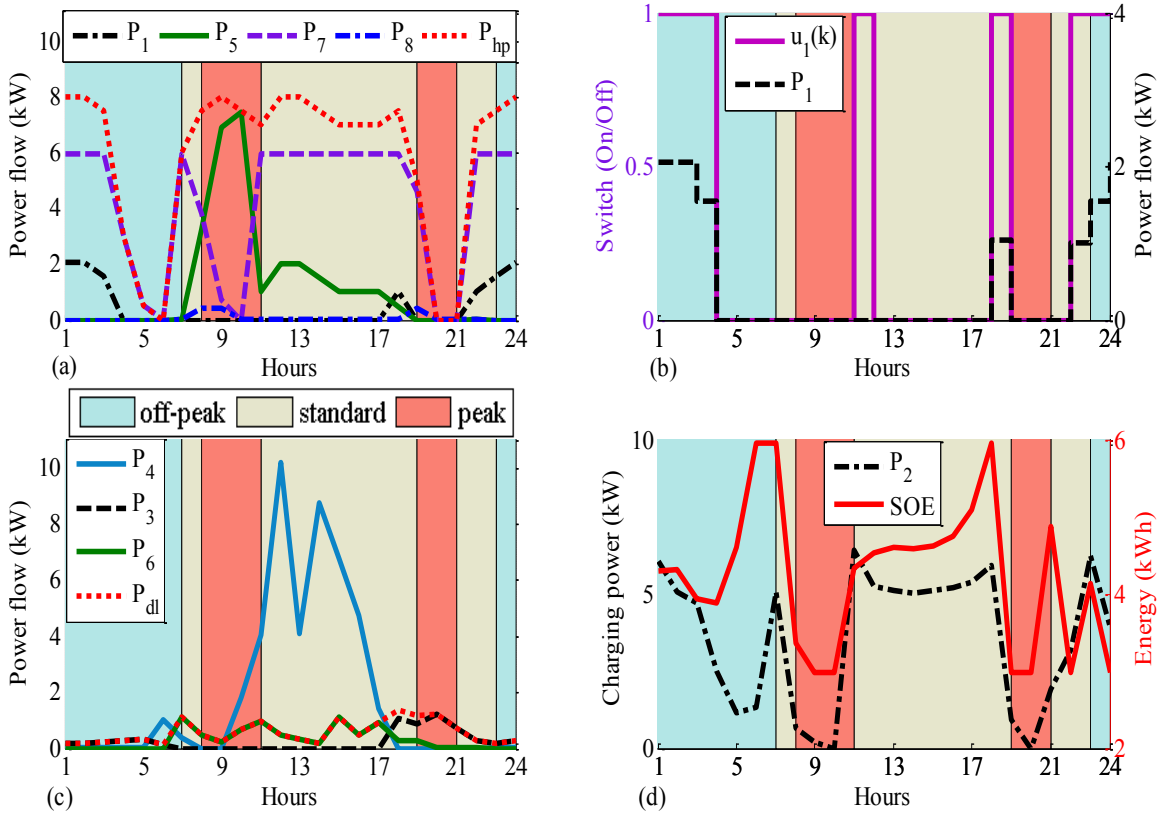

Figure 4.4. (a) OC of power to the HPWH; (b) OC switching to the HPWH; (c) Domestic load and solar sales ;(d) Battery SOE

The DG supply P_8 in Figure 4.4(a) came in to assist the PV P_5 during the morning and evening peak periods. The rest of the day the DG was off. The PV P_5 sustained most of the morning peak demand with supplementary power from the DG. In Figure 4.4(d) the battery SOE is observed to decline owing to the depletion of the stored off-peak energy in the battery. The optimal control could not charge the battery using peak TOU tariff to save on cost. The charging activities resumed immediately after peak demand and the battery SOE increased. The battery resumed supplying P_7 to the HPWH in the standard period, taking over from the PV. The OC in the standard TOU period reduced the usage of the PV power to supply the load. Instead it opted to sell P_4 to the grid, as shown in Figure 4.4(c). This action was more profitable according to the cost function.

4.3.2 Optimal control strategy of the heat pump water heater and domestic load - March

Figure 4.5(a) shows that the power demand of the HPWH was lower when compared to December. The battery P_7 met all the demand from midnight to 08:00, though at the beginning of the standard TOU the DG came in and operated till the end of the morning peak period. During the peak period the PV P_7 became the main source and sustained the supply of power till 13:00. In Figure 4.5(b) the grid P_1 was completely off from midnight till 18:00 when the PV generation started declining. The grid supplied power thereafter for an hour in the evening standard period and avoided the peak period. Th OC brought it in again after 22:00 to complement the battery. March has relatively fair weather conditions with less cloud cover than December.

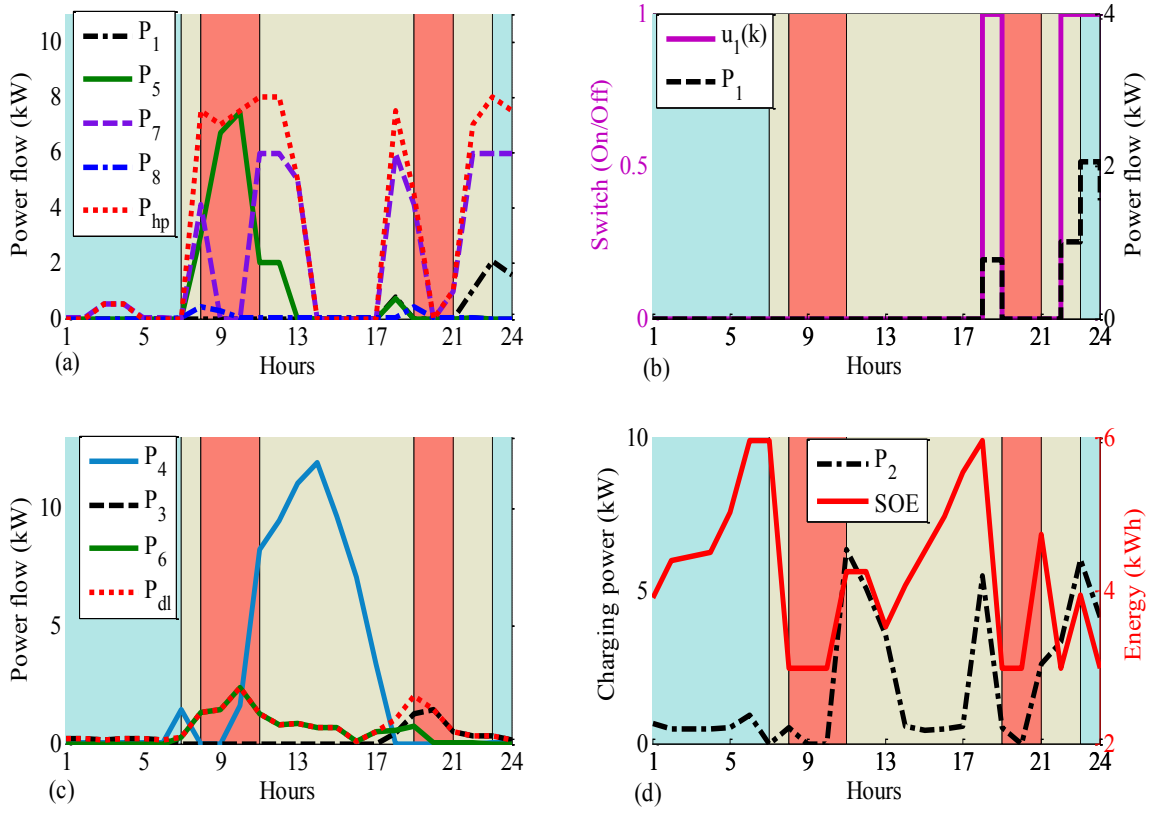

Figure 4.5. (a) OC of power to the HPWH; (b) OC switching to the HPWH; (c) Domestic load and solar sales ;(d) Battery SOE

The domestic load in Figure 4.5(c), was met by the grid P_3 from midnight to 07:00; thereafter the PV P_6 supplied power the rest of the morning and up to the evening. The optimal schedule sold most

excess PV P_4 energy to the grid. This was possible because of low load demand in March. The SOE in Figure 4.5(d) shows the battery storing energy from midnight till the beginning of the morning standard TOU tariff period. There was less charging P_2 activity most of the day.

4.3.3 Optimal control strategy of the heat pump water heater and domestic load - June

June in Figure 4.6(a), unlike all other months, falls in winter in this case study. The thermal requirement is usually high, for bathing and space heating. The battery P_7 supplied the HPWH from midnight till

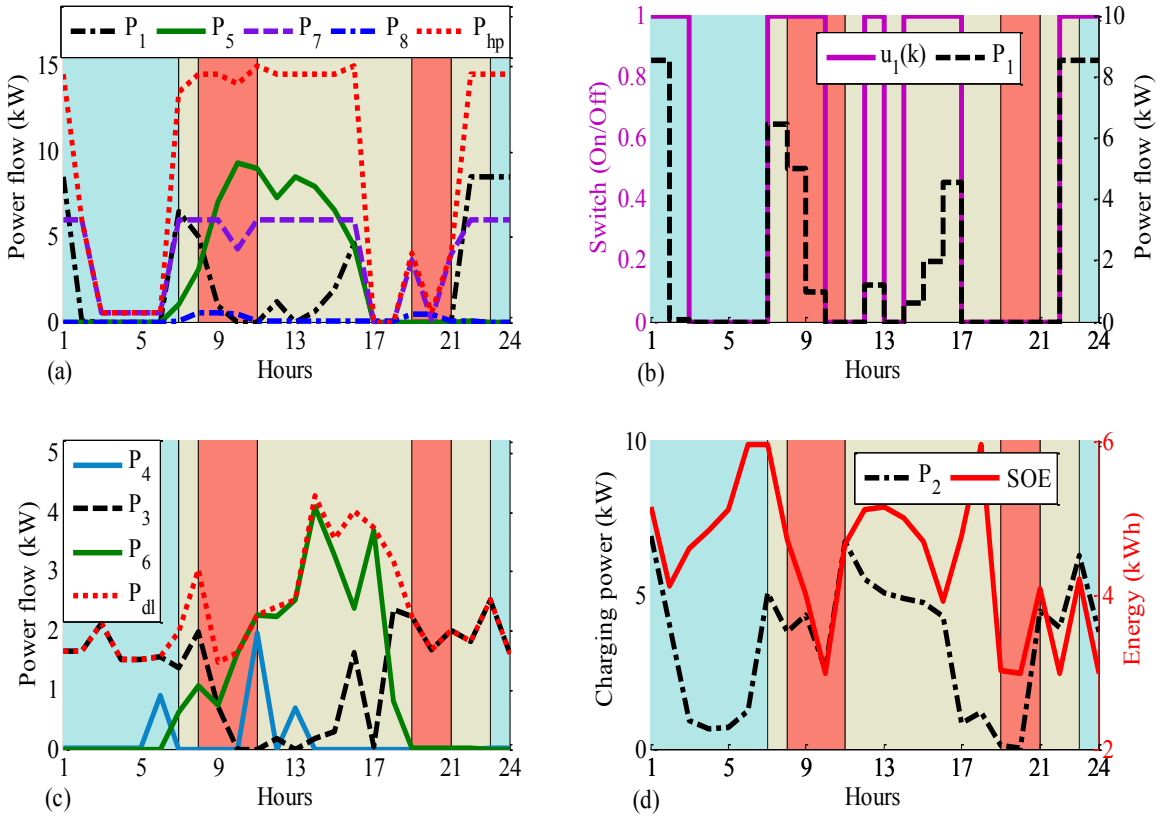

Figure 4.6. (a) OC of power to the HPWH; (b) OC switching to the HPWH; (c) Domestic load and solar sales ;(d) Battery SOE

the early morning, with minor grid P_1 support. The DG P_8 came in only at 07:00 concurrently with the solar PV P_5 when it began power generation, to complement the battery. The OC dropped P_1 at the approach of the standard TOU period to avoid using expensive energy. The switching frequency increased, as indicated in Figure 4.6(b), because of high load demand. The grid P_1 supplied part of the

standard periods. The scheduling, however, did not bring in the grid in the evening peak period because the battery had stored enough energy to meet the HPWH demand, supplemented by the DG.

The power scheduling in Figure 4.6(c) shows the domestic load supplies. The grid supply P_3 met the load demand from midnight till morning peak. However, the grid was dropped during the peak period and PV P_6 came in to sustain the load. There were relatively low solar energy sales P_4 in this month owing to higher load demand. The battery-charging activity is shown in Figure 4.6(d); the battery stored energy prior to the beginning of the morning standard period, as shown by the SOE upward trend. The sharp fall of SOE in the peak period is due to the switching off the direct grid supply to the HPWH. The strategy was similar in the evening peak period.

4.3.4 Optimal control strategy of the heat pump water heater and domestic load - August

The OC strategy illustrated in Figure 4.7(a) followed a similar pattern to the other months discussed above. The DG only supplied power during the morning peak period and the rest of the day it was off. The HPWH's operation was observed to oscillate; this was just the hotel's thermal usage on the selected day. The optimal schedule prioritised the battery's stored energy and the solar energy to supply the loads.

August had the highest solar irradiance in this case study, as shown in Figure 4.3 above. The solar energy sales were high at midday, though much of the PV-generated energy went to meet load demand.

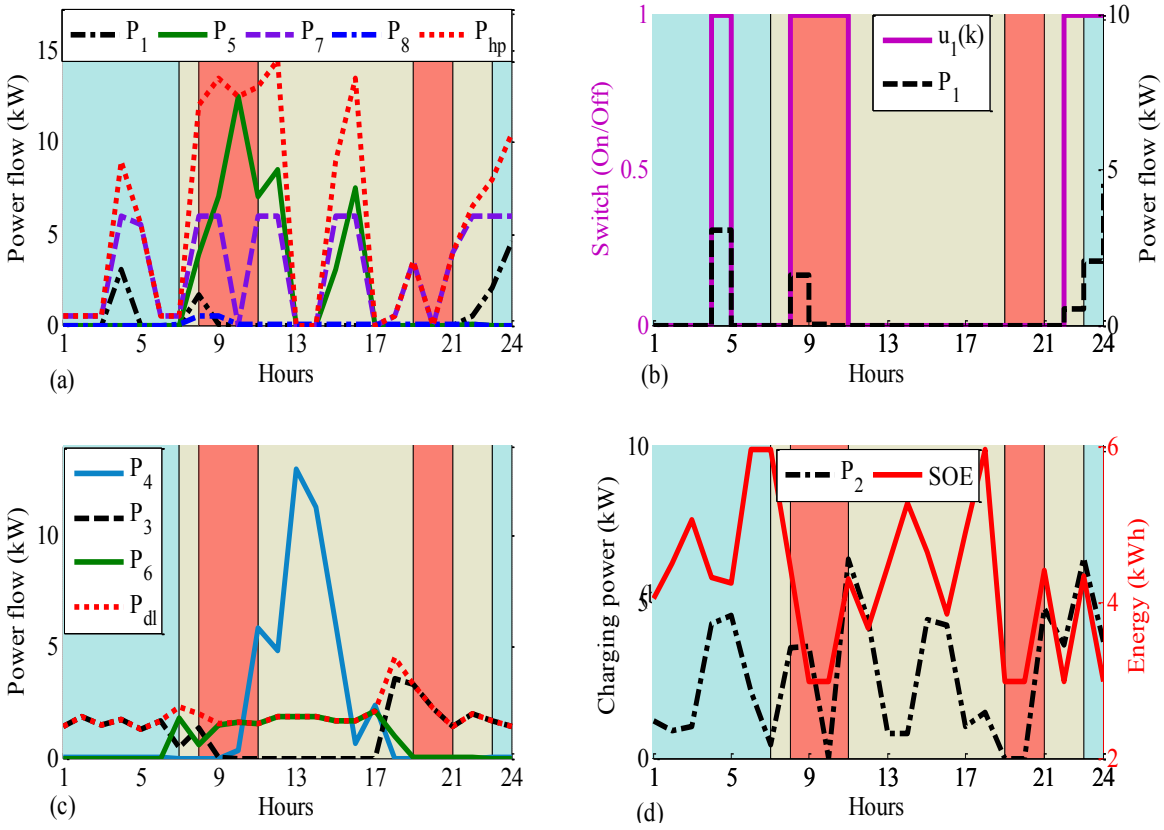

Figure 4.7. (a) OC of power to the HPWH; (b) OC switching to the HPWH; (c) Domestic load and solar sales ;(d) Battery SOE

4.3.5 Baseline and optimal energy costs

The daily energy and cost savings are presented in Table 4.2. Baseline cost is the bill which the hotel pays in the case study before the OC intervention while the optimal cost is the bill after OC intervention. This bill is for the grid energy consumed by the domestic load, HPWH and battery charging. The PV energy sales is the generated revenue from sales to the grid.

The energy saved, on the other hand, represents the grid power not delivered (energy not served) to the load, which would have been delivered without the OC intervention of this model. This energy is the difference between the baseline and the energy saved owing to the OC strategy. This energy not served directly translates into a relief on the utility company's primary input (e.g gas, coal, biomass, nuclear energy, water) in power generation. The reduction in primary energy input helps to mitigate climate change and greenhouse gases emission. However, these impacts are not considered in this

chapter. The results in Table 4.2 show the energy and cost savings per day on the selected dates in the case study.

Table 4.2. Daily optimal energy and cost savings

Month	Baseline cost (R/day)	Optimal cost (R/day)	Solar sales (R/day)	Baseline energy (kWh)	Energy saved (kWh)	Cost savings (%)
December	140.52	62.79	170.02	155.95	80.01	55.32
March	113.94	36.36	251.22	96.76	98.56	68.09
June	253.97	129.48	13.96	274.85	95.69	49.02
August	190.19	79.33	174.32	184.11	114.06	58.29

The maximum cost saving was in March, with 68.09%, and a corresponding energy saving of 114.06 kWh in August. The OC strategy is beneficial to the building owner; for example, in March, with baseline cost of $R113.94/day$ the bill after optimization reduced to $R36.36/day$, translating into a cost saving of 68.09%. The monthly energy cost can be found by multiplying the calender days of each month. The optimal schedule presented a huge benefit, especially with the proposed battery connection model that acted as storage for the off-peak energy. The OC strategy achieved both energy and cost savings. Strictly speaking this model is cost-positive on certain days of the month; the income from the solar energy sales can offset the energy bill (e.g. December)

Table 4.3 below shows the uncertainty error analysis of the model, when December was sampled. The percentage error is 5.7% when using the true values. From the results in Table 4.3 of the measured and true value, the conclusion is drawn that uncertainty analysis for the rest of the months in the case study are within the range of December's relative uncertainty.

Table 4.3. Uncertainty error of the performance index using measured true value

December:	Baseline cost (R/day)	Optimal cost (R/day)	Solar sales (R/day)	Baseline energy (kWh)	Energy saved (kWh)	Cost savings (%)
Experimental value	140.52	62.79	170.02	155.95	80.01	55.32
True value	140.52	58.08	188.17	155.95	79.92	58.67

The experimental measurements and true values used in this model are generally in agreement with each other. The performance index using true values is higher by 5.7%. The total cost saving is R 140.52 - R 62.79 = R77.73/day, therefore, the performance index is multiplied by the largest

relative uncertainty $(77.73)(0.02) = 1.555$. The final absolute uncertainty of the model on cost saving $= R(77.74 \pm 1.55)/day$.

4.4 SUMMARY

The OC strategy proposed in this chapter achieved huge savings both on energy and cost. The OC opted to use the stored off-peak energy in the battery and minimised the DG operation to the peak period only. The model has the potential to save up to 114.06 kWh of energy daily, with a maximum cost saving of 68.09%. The higher cost saving is owed to the battery connection model being used only as storage of cheaper-to-buy grid energy. The TOU electricity tariff played an important part in the further reduction of energy cost because the battery could be charged in off-peak TOU. This model enables building owners to trade off solar energy in return for incentives.

The payback period could be shorter owing to huge revenues from solar energy sales. In addition to the benefits mentioned above in this case study, Eskom gives a rebate upon replacement of resistive element heaters (geysers) with an HPWH, which is not considered in this chapter. In respect of the global call for climate change awareness most building owners are now looking for energy-efficient and sustainable technologies. It has proven to be cost-positive on certain days.

Further integration of other renewable energy resources such as wind and their operational modeling has been developed in the next chapter. All the previous chapters treated HPWH as input data only. The next chapter 5 looks at the actual HPWH control using the status of the hot water as the state variable.

CHAPTER 5 OPTIMAL CONTROL OF A WIND-PV-HYBRID POWERED HEAT PUMP WATER HEATER

5.1 INTRODUCTION

The previous chapters dealt mainly with the optimal scheduling strategies and integration of grid-tied renewable hybrid systems supplying HPWH and domestic loads. Chapters 3, 4 developed optimal integration models without necessarily controlling the HPWH, which is treated as input data. Here the HPWH is controlled by switching it into operation or off depending on the desired hot water temperature. Traditionally all HPWHs are fitted either with bang-bang controllers or digital thermostat controllers that do not operate in line with dynamic pricing or demand prediction. It will always heat the water till the temperature set point is reached regardless of whether there is a demand for hot water or not. This process is repeated; the actuator will keep turning on/off the geyser or HPWHs whenever the temperature drops, consuming a lot of energy.

The main problem with digital thermostat control systems used in HPWHs and some tank hot water heaters (geysers) on the market, is the dependency of their operation on temperature set-points only and not changing their assumed operating state between the intervals. Digital thermostat actuation occurs upon hitting the lower/upper set-point, which prolongs the operational time and consumes lots of energy. This control system is unable to control either demand prediction or load-shifting optimally to avoid operation during peak TOU electricity tariff periods, that could save energy and cost. Most geysers in South Africa are fitted with a thermostat control system actuating only every lapse of thermostat dead-band interval below the set-point, operating continuously even in periods

when there is no demand for hot water. Moreover, this hot water generating equipment, accounting for 23.60% energy consumption in the building, is rarely integrated into DREs.

Therefore, this chapter proposes a first attempt at an OC system application in HPWHs that is superior to digital thermostat control limitations. A further novelty is the successful optimal integration of the DREs, such as wind, into the supply of heat pumps, which has not yet been explored in literature. In comparison to the digital thermostat control system, this chapter's OC technology can effectively predict within the control horizon with known hot water demand, an optimal hot water temperature without necessarily reaching the set-points. This in turn minimizes the energy required to raise the water temperature to set-point.

The objective function is energy cost minimization, taking into account the TOU electricity tariff, which is an important control parameter. The control variables are the supply switch to the HPWH and the power from the grid, while the hot water temperature inside the tank is the state variable. The work in this chapter has been published in [13].

5.2 MODEL DEVELOPMENT

5.2.1 Schematic model layout

The optimal switching strategy schematic diagram of the heat pump shown in Figure 5.1 comprises the wind generator $P_w(t)$, PV modules $P_{pv}(t)$, grid $P_g(t)$ and an air-sourced heat pump with tank-wrapped condenser $P_{hp}(t)$. The switch $u(t)$ controls the power supply to the HPWH. The excess renewable power is fed into the grid. The grid power $P_g(t)$ accepts power from renewable power sources as well, as it supplements the heat pump whenever their combined output fails to meet the demand.

The TOU electricity tariff is one of the important control parameters in the optimal switching strategy of the HPWH, especially in the peak period. $T(t)$ is the state variable, viz the temperature of the water inside the storage tank. The hot water demand $W_D(t)$ is the flow rate in liters/hour taken from the case study. The desired hot water temperature is predetermined at between T_{low} and T_{up}, which are the lower and upper temperature set-points respectively. However, these limits may vary from one

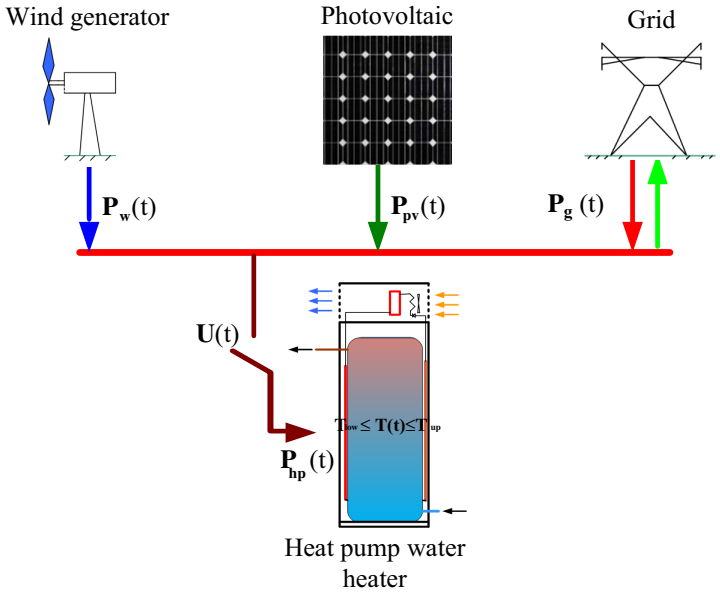

Figure 5.1. Schematic layout of the model.

individual to another. The control variables in this chapter are the grid power $P_g(t)$ and heat pump supply switch $u(t)$.

5.2.2 Sub-models

5.2.2.1 Heat pump water heater

The heat pump model is developed according to [102], with a fixed power demand P_{hp} rating, operating at full capacity. The temperature distribution of the hot water is assumed to be uniform in a constant water volume, neglecting stratification. For modeling simplicity, the energy losses in the evaporator, refrigerant and compressor are neglected; however, the efficiency of the electric motor driving the compressor is around 96%. The overall efficiency of other thermal components of the HPWH is accounted for by COP in the case study. In order to minimize the complexity of this modeling problem, a constant COP is assumed as well, though in practice it varies. Therefore, only energy losses due to hot water demand $Q_D(t)$ and convectional (standby) loss $Q_L(t)$ are modeled in this chapter.

The standby losses, $Q_L(t)$, are thermal losses dispatched through the tank's casing material. These losses can be minimised through increased thermal insulation and application of low thermal conductivity materials. The per second convention loss q_{loss} in W/m^2, according to [103], is given in equation (5.1),

$$q_{loss}(T(t), T_a) = \frac{T(t) - T_a}{\frac{\triangle x}{\kappa} + \frac{1}{h}}, \tag{5.1}$$

where $\triangle x$ and κ are the insulation thickness and thermal conductivity coefficients respectively, h is the surface heat transfer coefficient of the tank and $T(t)$, T_a are the hot water and ambient temperature respectively. Therefore, for a given tank surface area S_{area}, the total standby losses are:

$$Q_L(T(t), T_a) = q_{loss} S_{area}. \tag{5.2}$$

The other loss is associated with the hot water demand $Q_D(t)$, which triggers the inlet cold water into the tank to maintain a constant volume. Therefore, $T(t)$ drops during the period of hot water demand because of the inlet of cold water into the tank. Losses associated with the hot water demand are given as [104, 105] in equation (5.3):

$$Q_D(t) = cW_D(t)(T(t) - T_{in}), \tag{5.3}$$

where $c = 4180 J/kg/^{\circ}\mathrm{C}$ is the specific heat capacity of water. T_{in} is the municipal inlet water temperature whereas $W_D(t)$ is the hot water demand flow rate in liters/hour.

In order to satisfy the HPWH thermal output requirements, the corresponding electrical power input is [59, 104]:

$$P_{hp}(t) = \frac{Q_D(t) + Q_L(t)}{COP}. \tag{5.4}$$

The power balance is a dynamic equation. Let $Q_H(t)$ be the total HPWH heat output kilowatts and L the water mass (tank capacity) in kilograms. Therefore, the power balance becomes a first derivative differential function given in equation (5.5) [106].

$$cL\dot{T}(t) = Q_H(t) - Q_L(t) - Q_D(t), \tag{5.5}$$

$$Q_H(t) = P_{hp}COPu(t). \tag{5.6}$$

By substituting equation (5.1) to (5.4) into equation (5.5), one gets

$$\dot{T}(t) = \frac{P_{hp}COPu(t) - S_{area}\left(\frac{T(t)-T_a}{\frac{\triangle x}{\kappa}+\frac{1}{h}}\right) - cW_D(t)\left(T(t) - T_{in}(t)\right)}{cL}, \tag{5.7}$$

denoting:

$$\alpha(t) = \frac{S_{area}}{cL\left(\frac{\triangle x}{\kappa}+\frac{1}{h}\right)} + \frac{W_D(t)}{L}, \tag{5.8}$$

$$\beta = \frac{P_{hp}COP}{cL}, \tag{5.9}$$

$$\gamma(t) = \frac{S_{area}T_a}{cL\left(\frac{\triangle x}{\kappa}+\frac{1}{h}\right)} + \frac{W_D(t)T_{in}(t)}{L}, \tag{5.10}$$

then equation (5.7) becomes:

$$\dot{T}(t) = -\alpha(t)T(t) + \beta u(t) + \gamma(t). \tag{5.11}$$

5.2.2.2 Wind generator

In this study a simplified wind generator model is given in equation (5.12), according to [98]:

$$P_w(t) = \eta_t \eta_g 0.5 \rho_a C_p A_w V_r^3, \tag{5.12}$$

where η_t and η_g are the mechanical gearbox and generator efficiency respectively, ρ is the air density factor, C_p is the turbine power coefficient (Betz limit), A_w is the turbine rotor sweeping area and lastly, V_r is the wind speed. Though, rated wind speed is given by the manufacture, it is important for wind generator sizing purposes as given equation (5.13) [107].

$$V_N = \sqrt[3]{\frac{P_{wr}}{\eta_t \eta_g 0.5 \rho_a C_p A_w}}, \tag{5.13}$$

where V_N and P_{wr} are the rated wind speed and power respectively. Though this is a simplified model, a typical turbine power output characteristic is proportional to cubed wind speed between the cut-in wind speed V_i and rated wind speed V_N at the maximum aerodynamic efficiency. Above V_N, the pitched blades reduce the aerodynamic efficiency, hence keeping the power output constant. If the speed exceeds the pitch control limit, it reaches a cut-out wind speed V_c, cutting the power production. The hub height of the turbine with annual mean wind speeds [29] between $6-8$m/s at 10m height anemometer is calculated at approximately 1.2 times the rotor sweeping diameter [107]. The wind model parameters are from the case study given in Table 5.2. The excess wind power is fed into the grid using the established wind energy feed-in tariff.

5.2.2.3 Photovoltaic power

The PV power generation $P_{pv}(t)$ are input data in this model. A power source from zero to its maximum rated measured value is taken from the case study of our previous research [23, 32]. The PV power input data are given in Figure 5.5. The PV supplies $P_{pv}(t)$ to the HPWH and the excess is sold to the grid at the prevailing feed-in tariff. This model excludes the energy storage system in order to lower the initial investment cost, which hampers the implementation of these systems at household level. The grid acts as the DREs' energy storage system. The PV power generation is bounded by:

$$0 \leq P_{pv}(t) \leq P_{pv}^{max}. \tag{5.14}$$

5.2.2.4 Grid power

The grid is modeled as an infinite bar capable of simultaneously supplying and accepting power from the solar PV and wind generator. The TOU electricity tariff is one of the most important OC parameters. In South Africa, Eskom is the main power supply utility company and has both a flat and a dynamic TOU electricity tariff pricing $p(t)$ system. In this model the TOU electricity tariff is considered: off-peak (p_o), standard (p_s) and peak (p_p). The recent Eskom [1] megaflex active energy-TOU tariff is incorporated as a control parameter. The Eskom TOU electricity tariff is:

$$p(t) = \begin{cases} p_o = 0.3656\text{R/kWh} & \text{if } t \in [0,7] \cup [23,24], \\ p_s = 0.6733\text{R/kWh} & \text{if } t \in [7,8] \cup [11,19] \cup [21,23], \\ p_p = 2.2225\text{R/kWh} & \text{if } t \in [8,11] \cup [19,21], \end{cases} \tag{5.15}$$

where R is the South African rand and t is the time of day with $t = 0,\ldots,23$.

The grid can accept excess power from wind and PV and complement the renewable resources in meeting the heat pump load. However the feed-in and supply do not happen concurrently owing to the linear nature of the grid power constraint. The power balance is written as:

$$P_{hp}u(t) - P_g(t) = P_w(t) + P_{pv}(t). \tag{5.16}$$

The DREs' feed-in tariff is regulated by NERSA[2], a regulatory to establish the renewable energy feed-in tariff for South Africa. NERSA, through the renewable energy purchasing agency in South Africa, is the SBO of the national electricity utility, Eskom, under phase II (PV systems large ground or roof-mounted). These regulatory measures and SBO provide the necessary incentive to DRE developers and private investors. They guarantee the availability of a renewable energy market and provide venture capital at low financial risk. The prevailing PV feed-in tariff is $3.94R/kWh$, whereas for wind it is $1.25R/kWh$.

[1] http://www.eskom.co.za/
[2] http://www.nersa.org.za/

5.3 DISCRETE MODEL FORMULATION

5.3.1 Discretized hot water temperature

The water demand flow rate $W_D(t)$ and the inlet water, $T_{in}(t)$, are functions of time taken from the case study. The general discrete formulation of equation (5.11) in terms of the *k-th* hot water temperature is given in equation (5.17):

$$T_{k+1} = (1 - t_s\alpha_k)T_k + t_s\beta u_k + t_s\gamma_k. \tag{5.17}$$

Then, T_{k+1} at each interval can be derived as:

$$\begin{aligned}
T_1 =& (1 - t_s\alpha_0)T_o + t_s\beta u_0 + t_s\gamma_0,\\
T_2 =& [(1 - t_s\alpha_1)(1 - t_s\alpha_0)]T_o + t_s\beta\left[(1 - t_s\alpha_1)u_0 + u_1\right] + \left[(1 - t_s\alpha_1)t_s\gamma_0 + t_s\gamma_1\right],\\
T_3 =& [(1 - t_s\alpha_2)(1 - t_s\alpha_1)(1 - t_s\alpha_0)]T_o + t_s\beta\left[(1 - t_s\alpha_2)(1 - t_s\alpha_1)u_0 + (1 - t_s\alpha_2)u_1 + u_2\right]\\
&+ \left[(1 - t_s\alpha_2)(1 - t_s\alpha_1)t_s\gamma_0 + (1 - t_s\alpha_2)t_s\gamma_1 + t_s\gamma_2\right],\\
&\vdots\\
T_{k+1} =& T_o\prod_{j=0}^{k}(1 - t_s\alpha_j) + t_s\beta\sum_{j=0}^{k}u_j\prod_{i=j+1}^{k}(1 - t_s\alpha_i) + \sum_{j=0}^{k}t_s\gamma_j\prod_{i=j+1}^{k}(1 - t_s\alpha_i),
\end{aligned} \tag{5.18}$$

where; T_o and T_k are the initial and *k-th* water temperatures inside the tank respectively. t_s is the sampling time, whereas u_k is the *k-th* switch status, which is either 1 or 0. α_j and γ_j are functions of equation (5.8) and equation (5.10) respectively and β represents a constant given equation (5.9). The acceptable hot water temperature set points are given by inequality (5.19):

$$T_{low} \leq T_k \leq T_{up}, \tag{5.19}$$

where, T_{low} and T_{up} are the lower and upper desired temperatures respectively.

5.3.2 Objective function

The objective function is the grid energy cost J minimization under the TOU tariff p_k in discrete time; the control variable is the grid power, $P_{g,k}$. The control horizon is one day, with t_s being the sampling time, and the sampling interval is $(1 \leq k \leq N)$.

The objective function:

$$J = t_s \sum_{k=1}^{N} P_{g,k} p_k, \tag{5.20}$$

subject to the following constraints:

$$T_{low} \leq T_o \prod_{j=0}^{k} (1 - t_s \alpha_j) + t_s \beta \sum_{j=0}^{k} u_j \prod_{i=j+1}^{k} (1 - t_s \alpha_i) + \sum_{j=0}^{k} t_s \gamma_j \prod_{i=j+1}^{k} (1 - t_s \alpha_i) \leq T_{up}, \tag{5.21}$$

$$P_{hp} u_k - P_{g,k} = P_{w,k} + P_{pv,k}, \tag{5.22}$$

$$0 \leq P_{pv,k} \leq P_{pv}^{max}, \tag{5.23}$$

$$0 \leq P_{w,k} \leq P_{w}^{rated}, \tag{5.24}$$

$$u_k \in \{0, 1\}, \tag{5.25}$$

where p_k is the TOU electricity tariff (R/kWh) at the *k-th* sampling interval. Inequality (5.21) shows the state variable (hot water temperature) at every sampling time k and lies between the lower and upper acceptable hot temperature set point. Whereas equation (5.22) represents the power balance, the summation of DREs and grid power is equal to the HPWH demand. The production of DREs continues even when the heat pump switch u_k is *off*(0); the excess power is fed into the grid. Inequality (5.23) and (5.24) are the power bounds of the PV and wind generator respectively. Equation (5.25) is a binary switch control variable. At any given sampling interval its value is either 0 or 1, depicting the switch status of *off* or *on*.

5.3.3 Algorithm formulation

The proposed model has a binary variable and real number control variables, solved using the *OPTI toolbox* SCIP algorithm in MATLAB.

5.3.3.1 The objective function

The objective function is the total daily electrical energy cost under the TOU tariff given by,

$$f^T\mathbf{X} = \begin{bmatrix} 0 & \dots & 0_N, & p_1 & \dots & p_N \end{bmatrix} \begin{bmatrix} u_0 \\ \vdots \\ u_{N-1} \\ P_{g,0} \\ \vdots \\ P_{g,N-1} \end{bmatrix}_{2N\times 1} . \tag{5.26}$$

subject to

$$\begin{aligned} \mathbf{AX} &\leq \mathbf{b} \ \text{(linear inequality constraint)}, \\ \mathbf{A_{eq}X} &= \mathbf{b_{eq}} \ \text{(linear equality constraint)}. \end{aligned} \tag{5.27}$$

The detailed optimization problem and constraints formulation are attached in A. The limits of the control variables are restricted between the lower and upper bounds, given in equation (5.28) and equation (5.29).

lower bounds

$$lb^T = \begin{bmatrix} 0 & \dots & 0_N, & -\infty_1 & \dots & -\infty_N \end{bmatrix}, \tag{5.28}$$

upper bounds

$$ub^T = \begin{bmatrix} 1 & \dots & 1_N, & \infty_1 & \dots & \infty_N \end{bmatrix}. \tag{5.29}$$

5.3.4 Case study

The case study is based on a farmhouse situated in the coastal town of Port Elizabeth in South Africa. The main intervention of this model proposes an OC and renewable power integration solution to the HPWH installed at this farmhouse. The current (baseline) situation is that the HPWH installed at the farmhouse is controlled by the digital thermostat and supplied by the grid alone. Despite this being the normal mode of control/operation, it is far from optimal from a daily operational point of view.

Because of the operation constraints of the HPWH, the sampling time t_s is taken to be 30 minutes, giving the total sampling interval $N = 48$ per 24-h horizon. The 24-h daily simulation has been

mentioned earlier in section 5.1, because of several other factors such as lack of annual consolidated water demand and DREs output data in South Africa [108]. It is expected that the results of a day's performance may vary if modeled on an annual basis, because of variations in input data such wind power, PV power, and inlet water temperature over seasons. In this chapter, a typical winter day is assumed because of its relatively higher hot water and energy demand, to simulate the worst case scenario. There are errors an a 24-h model's performance resulting from a variation of DREs and other input data over the season. However, these can be minimized by application of MPC in future research, as recommended in section 5.5. Since cost minimization is the objective, for precise economic and payback (break-even) period estimation, simulations are done on each selected day in all seasons: summer, autumn, winter and spring in the case study. This increases the confidence level of the results with changing seasonal hot water demand, PV power generation, wind power generation and inlet cold water temperature variation that directly affect the annualised energy and cost savings calculated in subsection 5.4.4.

The average inlet cold water temperature[3], T_{in}, in Port Elizabeth in early winter is shown in Figure 5.2. The TOU electricity tariff color bar legend, off-peak (p_o), standard (p_s) and peak (p_p), in Figure 5.2 applies to all associated figures in this chapter.

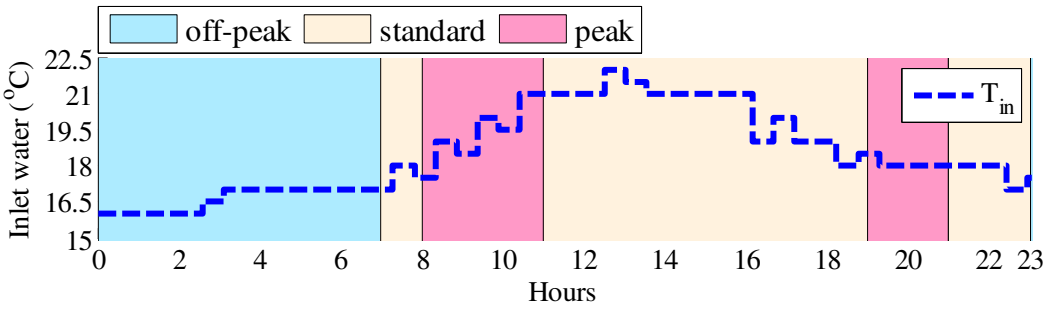

Figure 5.2. Hourly inlet cold water temperature

The hot water demand flow rate $W_D(k)$ is shown in Figure 5.3. According to the Department of Water Affairs and Forestry in South Africa, there is no consolidated database of information on household water consumption from water utilities [108]. It is only estimated to be around 50% of the total water demand used in homes. Because of lack of accurate hot water demand data in the case study and at national level for this specific location, the average hot water demand survey conducted by Meyer [109, 110] in selected cities of South Africa is adopted to validate this model's results.

[3] http://www.wunderground.com/weather-forecast/ZA/Port_Elizabeth.html?MR=1

The end-user at this farmhouse rarely uses hot water in the early and late hours of the day. June 3 is the sampled winter day in the case study; however, on this day there is no hot water usage between 00:00-05:00 and 22:00-00:00 mainly because the occupants are asleep during these periods. The preferred hot water temperature is set to $55\,^{\circ}\text{C} \leq T_k \leq 65\,^{\circ}\text{C}$; the average country ambient temperature of $T_a = 25\,^{\circ}\text{C}$ is used. The initial water temperature is set to $T_o = 60\,^{\circ}\text{C}$. However, the above desirable temperature varies from one individual to another.

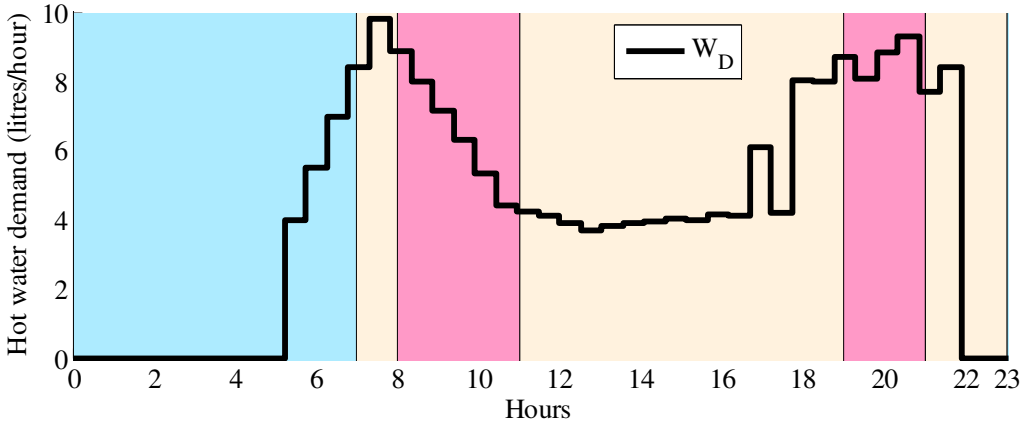

Figure 5.3. Flow rate of hot water in winter

5.3.4.1 Heat pump water heater parameters

The HPWH type is an air source tank-wrapped condenser coil, with the following parameters shown in Table 5.1.

Table 5.1. Heat pump parameters

Power input (kW)	COP	Storage capacity (l)	Compressor (cc)	Tank (h/ø) (m)	$\triangle x\,(m)$	$\kappa\,(W/m.K)$	$h\,(W/m^2K)$
6	3.8	270	39.0	1.41×0.66	0.035	0.055	6.3

5.3.4.2 Wind generator parameters

The wind generator in the case study is a Ruam Energy[4] turbine with technical specifications given in Table 5.2. In this chapter, η_t is the mechanical gearbox efficiency only. However, the overall wind-to-turbine power convention coefficient or the Betz limit C_p is factored in as well. The wind turbine

[4] www.raumenergy.com

Table 5.2. Wind generator parameters

P_{wr}(kW)	η_t (%)	η_g (%)	ρ_a (kg/m^3)	C_p	A_w (m^2)	V_i (m/s)	V_N (m/s)	V_c (m/s)
3.5	0.9	0.8	1.22	0.48	11.3	3.2	11	50

rated revolution per minute (RPM) is 280 *RPM* and a tower height to nacelle is approximately 16.6 m. The hourly wind speed at Port Elizabeth[5] and the consequent wind power generation, according to equation (5.12), are presented in Figure 5.4.

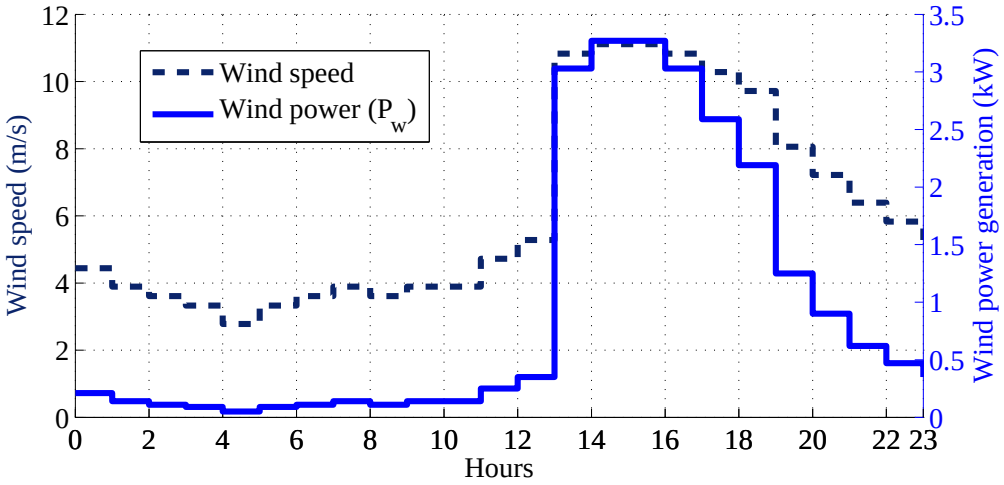

Figure 5.4. Wind power output and speed for Port Elizabeth

5.3.4.3 Photovoltaic power generation

The PV power is input data in this model taken from our previous research [23, 32].

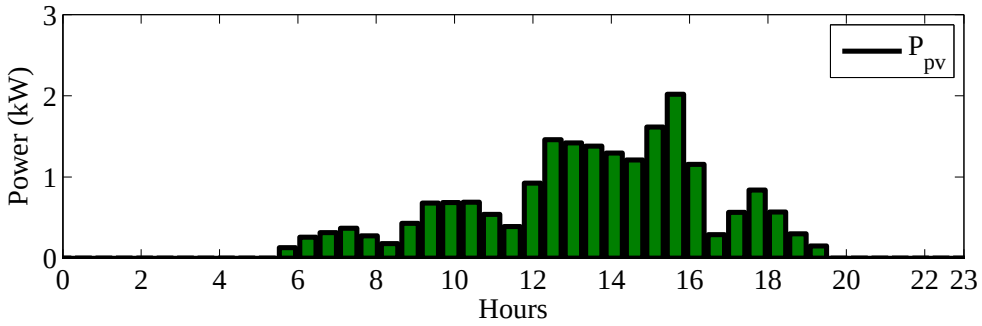

Figure 5.5. Photovoltaic power output

[5]http://www.timeanddate.com/weather/south-africa/port-elizabeth/hourly

In this model neither the PV nor the wind power generation is a control variable. Depending on the status of the HPWH, all DRE's power produced is fed into the grid during non-operational periods.

5.4 SIMULATION RESULTS AND DISCUSSION

5.4.1 Optimal heat pump switching control strategy in winter

In Figure 5.6 OC turns *on* the HPWH supply switch from 00:00 to 01:00 in the morning; thereafter, it keeps it turned *off* between 01:00 and 04:00. Thereafter, in order to avoid operating in peak TOU, the OC turns *on* after 04:00 to heat the water in advance to meet the anticipated hot water demand, which starts at 05:30, using the cheaper off-peak energy. It turns it *off* again towards 07:00, to avoid the standard TOU tariff so as to save energy cost. The HPWH is kept *off* till 16:00, when it turns *on* again to preheat the water before the evening peak period, as a load-shifting strategy. Subsequently, after the evening peak it only comes *on* once again for 30 minutes to preheat the water. The OC finally turns *off* at 21:30 because at that time the hot water demand W_d declines to zero and the temperature is still above T_{low}, shown in Figure 5.8.

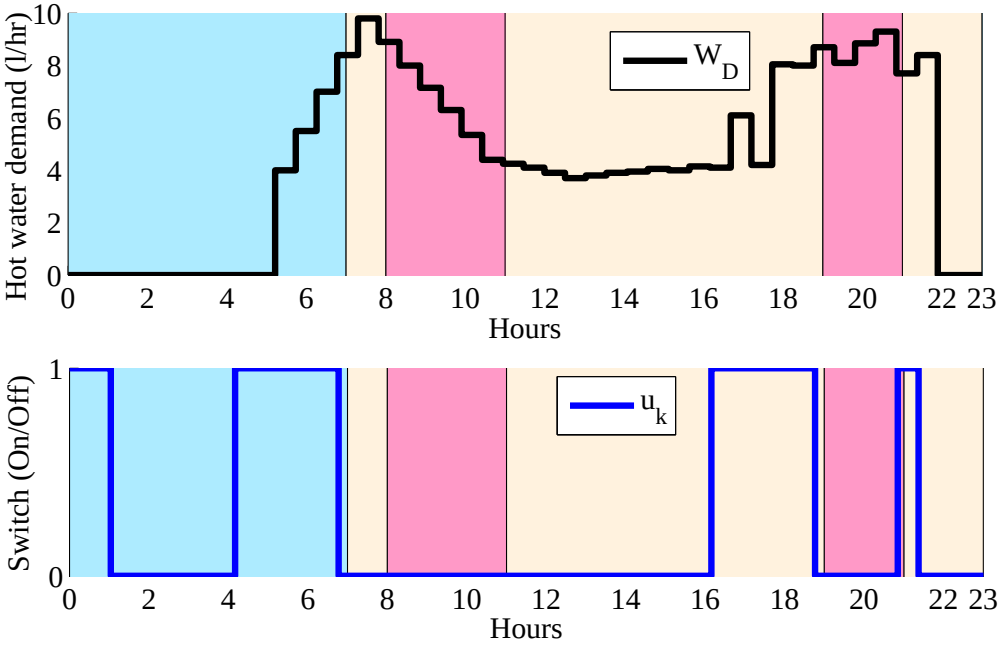

Figure 5.6. Optimal heat pump power supply switching

The OC shows the ability to predict the demand and TOU accurately in order to save energy cost through load shifting, overcoming the limitation of a digital thermostat control strategy used in most HPWHs, as discussed in subsection 5.4.3.

5.4.2 Optimal grid and feed-in power supply strategy in winter

The results of the OC power scheduling are presented in Figure 5.7, showing wind power P_w, PV power P_{pv}, grid power P_g and HPWH P_{hp} demand. The grid power assumes negative values during feed-in and positive ones when supplying the HPWH load. In Figure 5.7, P_g supplies the HPWH from midnight to 01:00, with very little supplement from wind power P_w. The slight deviation between HPWH demand P_{hp} and P_g is due to the low amount of power supplied by the wind generator. The grid stops supplying power between 01:00 and 04:00 because the HPWH is turned *off*, shown in Figure 5.6, and begins accepting the little available wind power. At 04:00 the OC resumes grid supply till about 06:30 when the demand declines. PV power generation P_{pv} begins around the same time and the OC instantly resumes excess power feed-in into the grid.

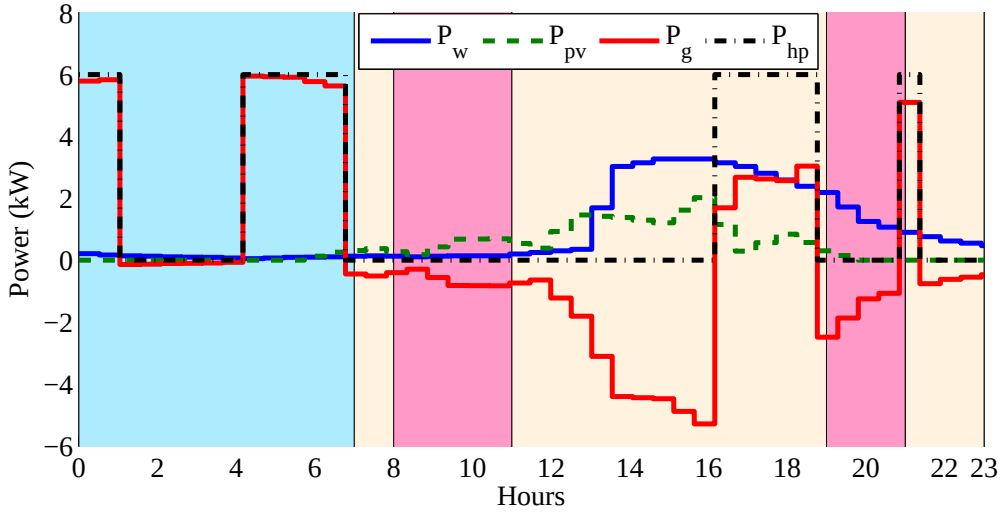

Figure 5.7. Optimal grid and renewable power scheduling strategy

From 07:00 the OC continues power feed-in to the grid till 16:00. At 16:00, the OC stops feed-in; all the DREs' power is now used to meet the whole HPWH load turned *on*, though their combined power is unable to satisfy demand, prompting OC to bring in the grid P_g to supplement the deficit. OC is shown opting for cheaper renewable power whenever available to supply the HPWH as a mean

of reducing energy cost. It manages to schedule load-shifting and avoid using peak TOU expensive energy, giving a cost benefit to the end-user.

5.4.3 Comparison between optimal and digital thermostat control strategies

Figure 5.8 shows the hot water demand flow rate, a comparison of optimal and digital thermostat switching and finally the hot water temperature T_k. The OC switches *on* the HPWH from 00:00 to 01:00; the hot water temperature rises gradually from the initial $T_o = 60\,^{\circ}\text{C}$ to $61.5\,^{\circ}\text{C}$. Then temperature is observed to stay almost constant between 01:00 and 04:30, with a marginal decrease caused by convectional losses. Though the temperature in the above interval appears constant, it is merely because of the axis scaling; the half-hour temperature between 01:00 and 04:30 shows a minimal temperature fall of 0.0008% due to the marginal standby losses. The limited hot water temperature drop in the absence of flow rate is owed to the good insulation of the HPWH tank in the case study.

Thereafter, the HPWH turns *on* again at 04:00, causing the water temperature to rise further. The non-linearity rise of T_k rise is due to the inlet of cold water into the tank as a result of hot water demand resumption. The temperature decrease after 07:00 is steady mainly because of the hot water consumption pattern. Since no water heating takes place from 07:00 to 16:00, the only major factors causing the decrease of T_k are inlet of cold water and steady hot water demand usage. OC turns *on* the HPWH at 16:00 to preheat the water before evening peak TOU, effectively shifting the load. OC can predict the right time to turn *on* the HPWH so that the end-user is not inconvenienced and has hot water available at the right temperature.

The baseline situation is simulated as well to compare the benefits of OC over a digital thermostat control strategy, which is used in most HPWHs on the market. The results of the comparison are also shown in Figure 5.8. The digital thermostat (u_k – digital thermostat) turns *on* the HPWH from midnight till 03:30 and continues heating the water until T_k has reached the upper set point. It keeps it in operation regardless of whether there is hot water demand or not, using more energy. The hot water demand keeps decreasing T_k. By 18:00 it reaches the lower set point, hence the thermostat turns *on* again. Since it has no capability of load shifting, it runs throughout the peak period, incurring huge energy cost. In this study the switching *on* frequencies in the 24-h horizon are 13 and 20 times for the

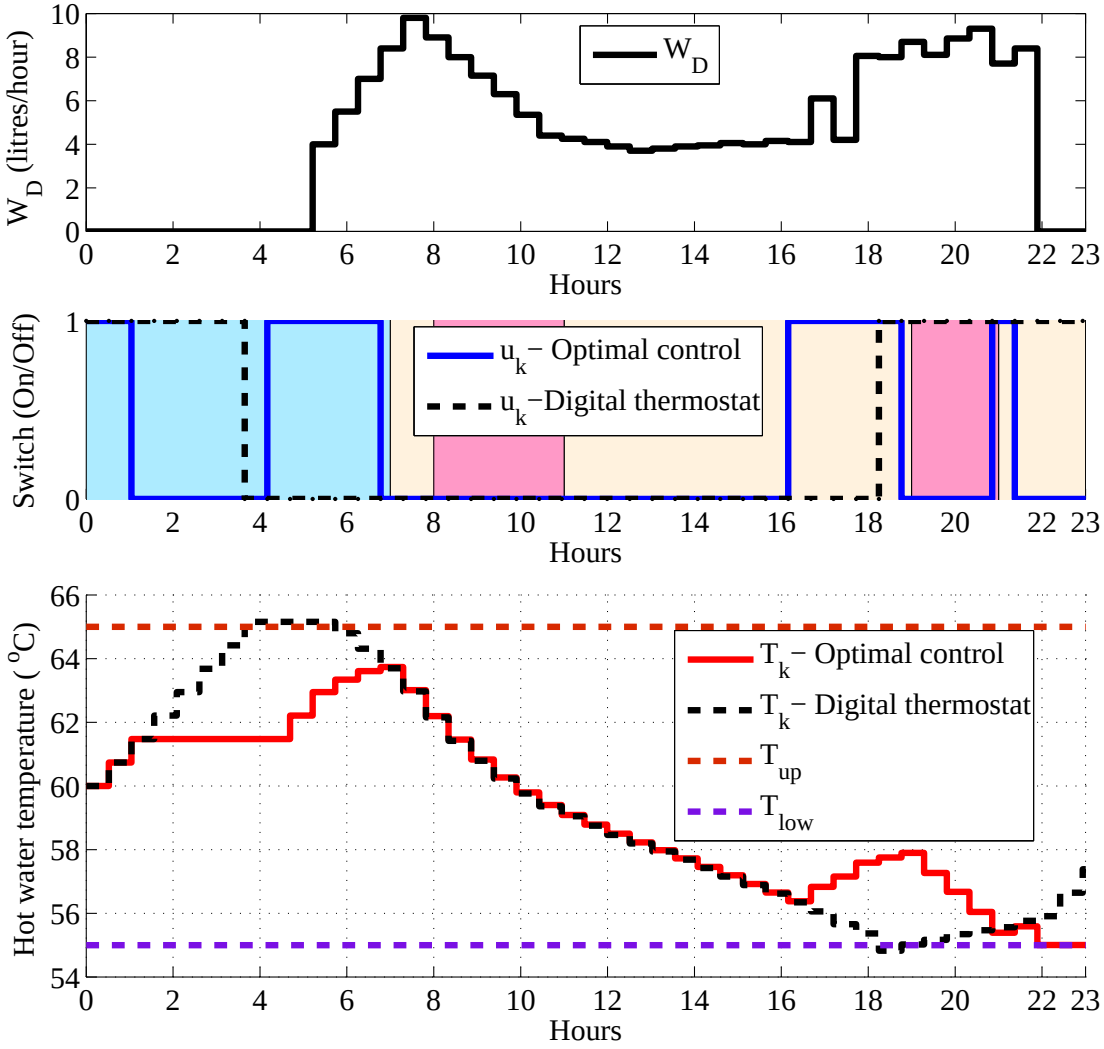

Figure 5.8. Hot water temperature's dependency on switching and water usage

optimal and digital thermostat control strategy respectively. The OC has a lower switching frequency, which saves on energy and prolongs the compressor's life cycle.

However, it is worth pointing out that the desired temperature should not be set too high, beyond the rated capacity of the HPWH, as it will never reach that required temperature when demand for hot water occurs. A realistic temperature should be set within the range of the HPWH power rating, otherwise the end-user has to raise the water temperature inside the tank beforehand by some other means (e.g. by using an in-line resistive element heater).

5.4.4 Baseline and optimal energy savings in winter

Table 5.3 shows the daily energy and cost saving: baseline (digital thermostat control strategy) and OC strategy. The baseline energy is the current situation in the case study, where the 6 kW HPWH operates on the digital thermostat control strategy and is supplied by the grid alone, analogous. The baseline cost is the money paid for grid energy under the TOU electricity tariff prior to this proposed intervention. The optimal energy is the grid energy consumption after the implementation of this OC model integrated with DREs. The difference between the baseline energy and the optimal energy is what is referred to as the saved energy on the grid side, whereas, the optimal cost is the grid energy cost after intervention. In this model, the DREs' power consumed by the HPWH is assumed to be free energy, since after the initial investment cost the end-user uses this energy without paying for it. However, this energy is not necessarily free because of the invested resources. This is reflected in increased time to reach the break-even point in subsection 5.4.7. The total feed-in energy, on the other hand, is the excess PV and wind energy fed into the utility grid when the HPWH is turned *off*.

Table 5.3. Daily optimal energy savings

Baseline (kWh/day)	Optimal (kWh/day)	Total feed-in (kWh/day)	Baseline cost (R/day)	Optimal cost (R/day)	Energy saving (%)	Cost saving (%)
60.00	29.26	23.24	48.83	14.29	51.23	70.74

The OC strategy yields 51.23% less energy consumption from the grid owing to a substantial supplement from wind and PV energy, which meets the HPWH load whenever available. The reduction of energy consumption from the grid consequently offers the power utility company positive climate mitigation and primary energy input relief that are not quantified in this chapter. Hence, the proposed model is a near NZEB. A cost saving of 70.74% is realised, implying that this model has the potential to be cost-effective with the revenue from DREs sales.

The combined power output of DREs and the grid is shown in Figure 5.9. The power flow of P_w and P_{pv} has been discussed earlier in subsection 5.4.2. The baseline power $P_{g,baseline}$ supplies the HPWH from midnight till 04:00, meeting all the HPWH demand, since the grid is the only source of power. It is observed in the baseline scenario in Figure 5.8 that the digital controller turns *on* the HPWH in the evening at 18:00 when the hot water temperature reaches the lower set point. The grid powers the HPWH throughout till 23:00 without consideration of the peak TOU, which is the major setback of

this digital controller that reacts only to the state variable set point. On the contrary, the OC strategy is seen to schedule the grid power $P_{g,optimal}$ effectively to supplement DREs and avoids the peak periods. The load shifting strategy is to avoid expensive peak TOU electricity tariff. This effects a huge saving on energy cost. Here the OC shows the capability of load shifting, predicting and optimally keeping the hot water temperature within the desired set point using less energy to heat it to set points, while the digital thermostat controller clearly shows its limitation on T_k and load shifting.

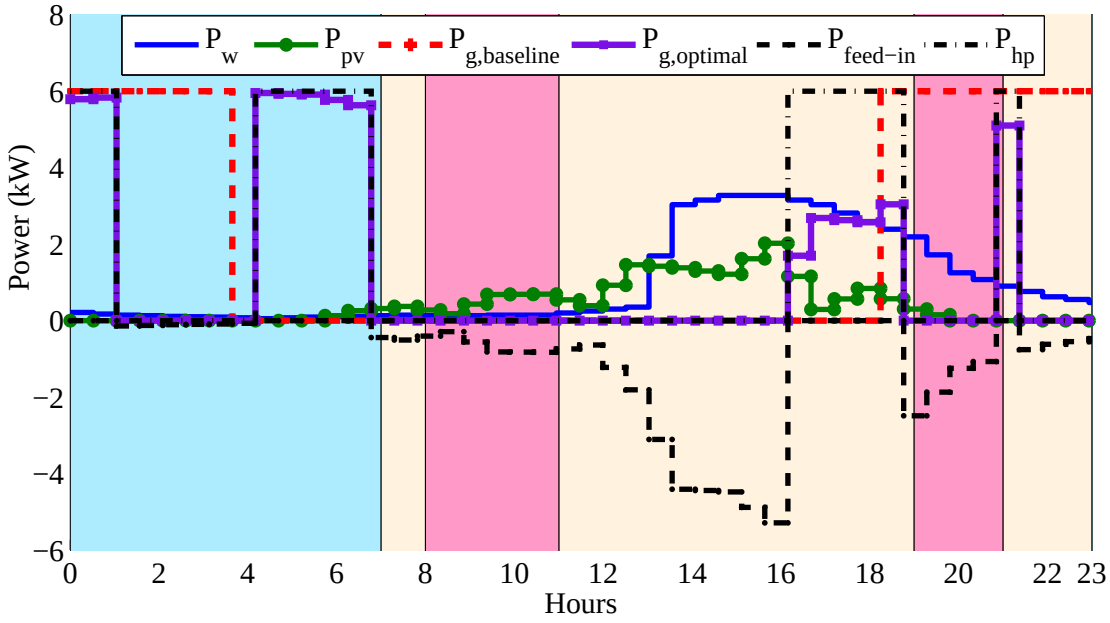

Figure 5.9. Baseline and optimal power output

Lastly, the feeding in of DREs' power occurs only when the HPWH turns *off*. The OC prioritizes the renewable power to supply the HPWH, only in cases where their combined power output is less than the demand. A marginal feed-in $P_{feed-in}$ of the available P_w power takes place from 01:30 to 04:00 owing to the absence of HPWH P_{hp} load. In the early morning at 06:30, the OC resumes the solar PV P_{pv} and wind P_w power feed-in into the main grid till 16:00. The OC stops the feed-in of power to the grid between 16:00 and 18:30 when the HPWH switches *on*; instead the grid $P_{g,optimal}$ is used to supplement the HPWH load deficit. Thereafter, the feed-in resumes till around 21:00 when it stops for a moment to aid the DRE. P_{pv} production ceases in these late hours of the day, so only wind energy is fed to the grid.

5.4.5 Effects of seasonal hot water demand variation on optimal temperature

The model is further simulated on a selected day in each of the four seasons to account for the varying hot water demand given in the case study, as shown in Figure 5.10. The changing hot water demand shows an effect on the optimal energy and cost saving, because of the different scheduling strategy. Many factors affect the consumption of hot water, such as behavioral, and social ones, as well as ambient and inlet water temperatures. The simulation is run in each season to account for the consumption factor in order to determine the optimal cost and energy savings accurately. The savings, optimal benefit and sales of DREs sales are further averaged over the season and annualized for the calculation of the break-even period in subsection 5.4.7

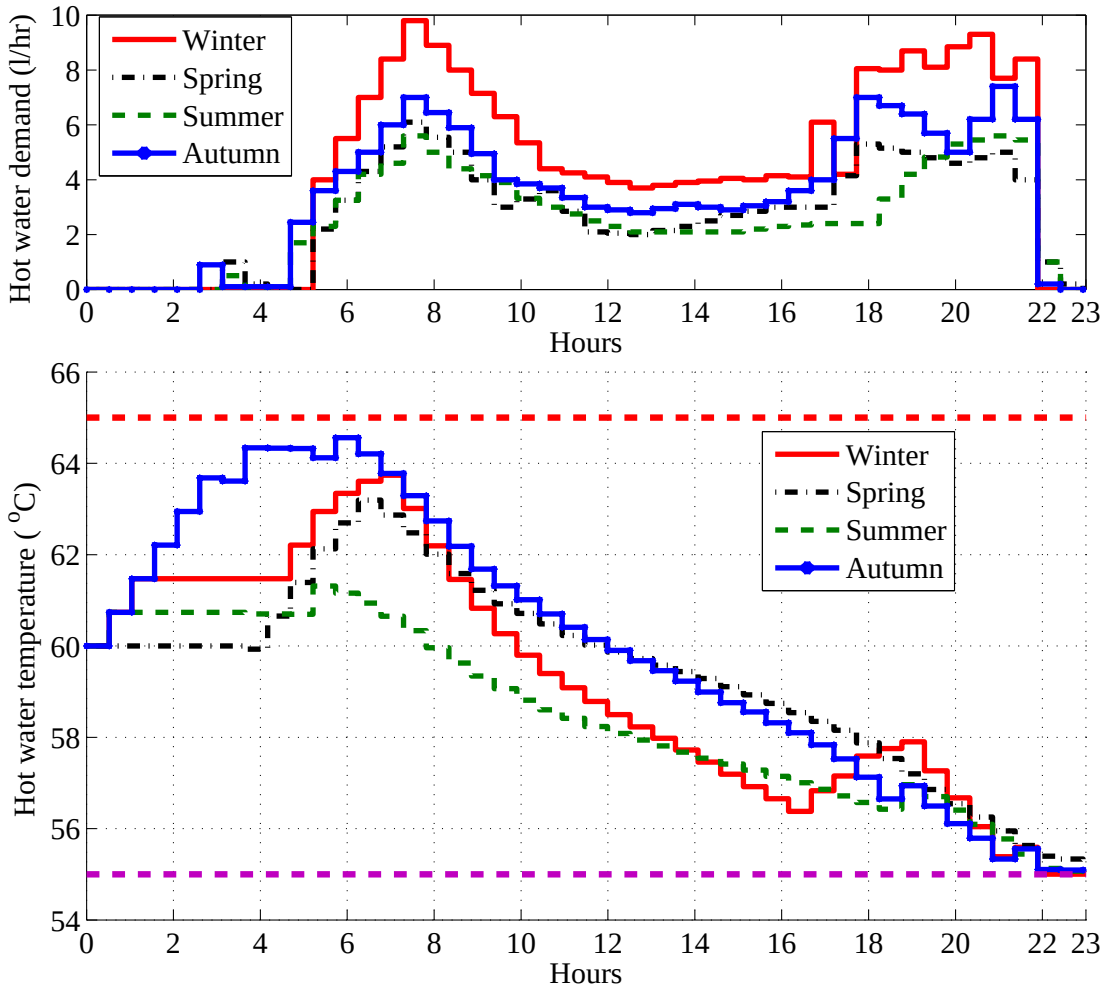

Figure 5.10. Effects of seasonal hot water demand on optimal water temperature

The optimal hot water temperature is relatively similar in each season because of the similarity in the hot water usage in the house. In Figure 5.10, autumn T_k steadily rises above other seasons because

of the hot water consumption that starts earlier, around 02:30, making the OC turn *on* the HPWH before the demand for hot water starts. There is a reduction in the switching *on* frequency in the afternoons in most seasons owing to the improved inlet water temperature. However, in a typical situation, people still bath the same number of times regardless of the season, but; what reduces is the hot water requirement for mixing during a bath owing to the improved ambient temperatures.

5.4.6 Annualized feed-in energy and revenue

In order to estimate the reflective energy and revenue over a period of the year accurately, the simulation is run in each season on a selected day to account for demand variation and seasonal changes of wind and solar production, as well as inlet water temperature. The feed-in energy and revenue of each season are then averaged to reflect the day's value. The average value is annualized to reflect an average amount per annum. The energy cost saved after intervention is translated as a benefit cost or rather the amount the end-user would have spent had it not been for this intervention. The optimal benefit is the difference between baseline and optimal cost of a winter day, both in this simulation and in an annualized calculation. The HPWH operated for a total of 6.5 hours in the case study. The switching *on/off* was dependent on the state variable, therefore the operation time varied on each day.

Table 5.4. Seasonal solar PV and wind generator feed-in

Seasons :	Winter	Spring	Summer	Autumn
Feed-in energy (kWh)				
Wind feed-in	15.08	22.72	21.58	20.80
Solar feed-in	8.17	10.01	9.79	9.79
Optimal grid energy	29.26	14.75	7.38	24.60
Revenue(R)				
Wind feed-in sales	18.84	28.40	26.97	25.99
Solar feed-in sales	32.17	39.42	38.55	38.55

Table 5.4 shows the calculated seasonal energy and revenue. In order to calculate for example wind energy sales, a seasonal day's revenue is added $(R18.84 + R28.40 + R26.97 + R25.99)/4 = R25.05$ and averaged to determine a day's value over the year. Then this day value is multiplied by the number of days in a year $R25.05 \times 365 = R6638.66/\text{annum}$. This annualized revenue is then used to calculate the the economic analysis of this proposed model. The averaging and simulation of a day

in each season, increases the reliability of the proposed model and its financial feasibility, while at the same time meeting the technological and operational constraints of HPWH in the 24-h control horizon.

5.4.7 Economic analysis and payback period

In order to ascertain the economic viability of any project, investors and decision makers use the discounted payback period [111]. This approach firstly discounts the cash flows to determine a present value (PV_E) of money in the future. Then it establishes the period when the net present value (NPV) equals the total capital cost (CC) or the invested money, which is when break-even point (payback period) occurs. This is when the investor has recovered all his invested money. The initial capital investment in Table 5.4 is a negative cash flow in the financial statement (e.g., solar PV cost = -*R*27 500.00) represented in brackets as $(27\ 500.00)$. The negative cash flows are the initial capital investment and all running cost of the project. Several assumptions are made when calculating the present value and payback period, the variation of inflation rate, depreciation, running and maintenance cost over time. However, for the purpose of present value and payback period calculation, the inflation rate, revenue and operational costs are assumed to be constant. Although it is expected that there would be an increase in all these factors, it cannot be reliably estimated at this time.

The payback period in this chapter is obtained from the NPV of the present value PV_E. The present value of the cash flow during the n-th year, $PV_E(n)$, formulated as [112]:

$$PV_E(n) = \frac{\text{Cash flow}(n)}{(1+r)^n}, \tag{5.30}$$

where cash flow(n) denotes the cash flow of the n-th year and r denotes the discount rate. The formula of the cash flow is project-specific and the tabulation of the results are shown in Table 5.4.

Table 5.5 shows the revenue from solar energy sales, wind energy sales and OC benefit. The cash flows and pay-back period is calculated making the assumption that the solar sales, wind sales, cost saving, operational and maintenance costs will remain constant throughout the period. A discount factor or interest rate of 4.4% for February 2015 in the case study is used to reflect the time value of money.

The 4.4% is indicative of the inflation rate in South Africa. The prices[6] of most components are based on the local product supplier and all amounts are in South African rand, while the wind generator and PV_E size are shown in Table 5.2 and subsection 5.3.4.3 respectively.

Table 5.5. Present value discounting

Years :	0	1	2	3	4	5
Initial capital investment						
Solar PV cost (R)	(27 500.00)					
Wind generator cost (R)	(23 500.00)					
Controllers cost (R)	(22 900.00)					
Inverters and accessories cost (R)	(15 000.00)					
Installation cost (R)	(14 000.00)					
Total investment cost (R)	(102 900.00)					
Maintenance and operation cost (R)		(2 500.00)	(2 500.00)	(2 500.00)	(2 500.00)	(2 500.00)
Expected annualised revenue						
Wind energy sales (R)		6 638.66	6 638.66	6 638.66	6 638.66	6 638.66
Solar energy sales (R)		13 568.47	13 568.47	13 568.47	13 568.47	13 568.47
Optimal benefit cost (R)		12607.10	12607.10	12607.10	12607.10	12607.10
Cash flows		30 314.24	30 314.24	30 314.24	30 314.24	30 314.24
Discount factor $(1+r)^{-n}$	1.00	0.96	0.92	0.88	0.84	0.81
Present value	(102 900.00)	29 036.63	27 812.86	26 640.67	25 517.88	24 442.42

Usually, for most energy-efficiency project economic analysis, the operating cost, maintenance cost and cost savings are taken into account. Having obtained $PV_E(n)$, the net present value is:

$$\mathrm{NPV}_{n=1}^{m} = \sum_{n=1}^{m} \mathrm{PV}_E(n) - \mathrm{CC}, \tag{5.31}$$

where CC is the initial capital cost of the project. Thereafter, the discounted payback period is obtained as

$$\text{Payback period} = m_y + \frac{-NPV_{n=1}^{m}}{\mathrm{PV}_E(m_y+1)}, \tag{5.32}$$

where m_y denotes the last year with a negative NPV and the results are presented in Table 5.6.

The NPV continues to decrease in negative cash flow till a point when it crosses to positive cash flows. The payback/break-even stage occurs at the point when the cumulative cash flow equals zero. This

[6] www.dako.co.za

is the point at which all the invested capital is recovered. Thereafter, NPV goes into positive values, meaning the whole capital cost has been fully recovered, all the revenue in subsequent years to follow is pure profit; though maintenance cost is expected to be high owing to ageing equipment, it is not considered in this chapter.

Table 5.6. Discounted payback period

Years	Present value	Net present value
0	(102 900.00)	(102 900.00)
1	29 036.63	(73 863.37)
2	27 812.86	(46 050.51)
3	**26 640.67**	**(19 409.84)**
4	25 517.88	6 108.04
5	24 442.42	30 550.46

According to Table 5.6, the pay-back period is three years and nine months. The break-even period is shorter owing to the optimal benefits. The money generated from the feed-in sales can still assist to offset the power utility bills. Therefore, this optimal switching control is beneficial for those intending to transform their homes into cost-effective and net-zero energy buildings in countries with an attractive feed-in tariff.

5.5 SUMMARY

The TOU based optimal switching control shows the potential to save energy cost, as well as energy not delivered on the utility side, thus a reduction on primary inputs and greenhouse gases. This model yields a maximum energy saving of 51.23% and has the potential to be cost-effective on energy bills. This intervention provides a practical optimal integration of wind and other DREs into homes, with the benefit of energy trade-off and the possibility of achieving a NZEB.

The economic analysis shows a payback period of three years and nine months. There are other incentives pertaining to rebates on HPWH, wind power and solar PV application that are not considered in this chapter, which are evident in the case study and could further reduce the payback period.

This model is suitable for application in both peri-urban and rural areas, in the generation of hot water, space heating and renewable energy integration. It can be adopted by home-owners who want to integrate renewable energy sources using energy-efficient equipment such as HPWH to save energy with the minimum environmental impact. The OC strategy offers the potential to be cost-effective and to overcome the limitations of digital thermostat control used in most heat pumps on the market.

The following chapter looks at the integration of the FC into energy-efficient devices.

CHAPTER 6 OPTIMAL CONTROL OF A FUEL CELL/WIND/PV/GRID HYBRID SYSTEM WITH THERMAL HEAT PUMP LOAD

6.1 INTRODUCTION

In most of the work done in the previous chapters, diesel generator and battery storage are the common power back-up in RE hybrid systems, instead of the greener hydrogen FC. This promising next generation hydrogen economy and the optimal FC sizing and life cycle cost have been evaluated in [113], [114]. However, little has been done on FCs' OC and integration on the demand side. While most of these back-up systems. For example, DGs have expensive running costs and negative environmental effects, FC technology is green energy, has multiple environmental benefits and can be used in the transportation sector. In this case we have looked at the application of FCs at domestic level in supplying energy-efficient devices, its electrolyzer powered by renewable energy.

This chapter presents a first-ever OC strategy model on an integrated RE-FC-grid system with an energy-efficient thermal load under a TOU tariff. The work in this chapter has been published in [115].

6.2 MATHEMATICAL MODEL FORMULATION

6.2.1 Schematic model layout

The schematic layout is shown in Figure 6.1. The PV modules $P_{pv,t}$ and wind generator $P_{w,t}$ feed through their respective inverters into the DC bus. The DC bus then supplies through $P_{RE-IN,t}$ to the loads and the other $P_{el,t}$ to the FCs electrolyzer for the generation of hydrogen. The generated hydrogen, $P_{H2,t}$, is stored in the hydrogen storage tank, H_2, which later supplies hydrogen, $P_{FC,t}$, to the FC. The FC output is rectified and feeds into the grid AC bus through $P_{FC-IN,t}$ where the loads are connected.

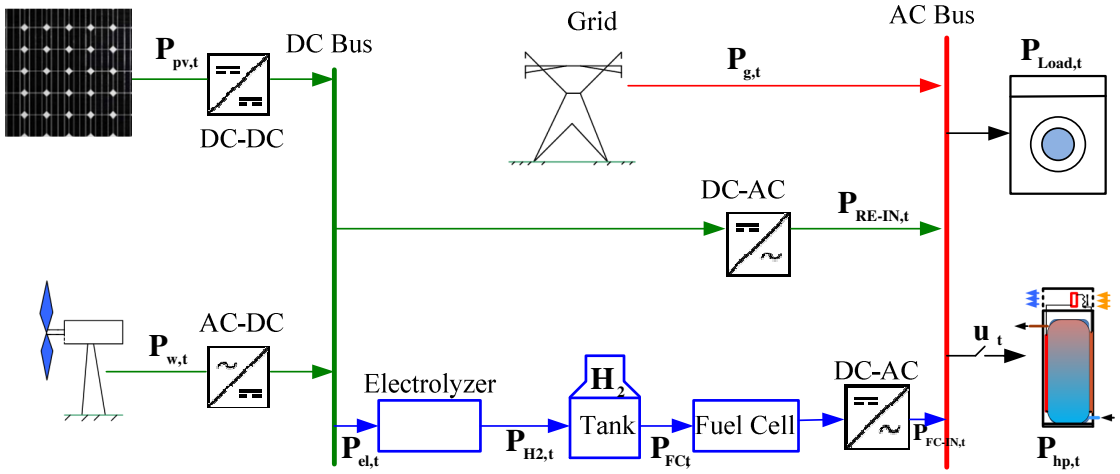

Figure 6.1. Schematic layout of a renewable energy-grid integrated model

The grid power, $P_{g,t}$, supplies the load via the AC bus directly with a possibility of REs feed-in. The domestic load $P_{\text{Load,t}}$ represents all other loads in the building apart from the thermal loads. The thermal load considered in this model is the heat pump water heater because of its high energy efficiency. The heat pump, $P_{hp,t}$, works at full load at its rated power whenever it is in operation, and is controlled by switch u_t. The control variables are $P_{RE-IN,t}$, $P_{el,t}$, $P_{H2,t}$, $P_{FC,t}$, $P_{FC-IN,t}$, $P_{g,t}$ and switch u_t. The state of hydrogen energy in the tank $H_{2,t}$ and the heat pump's hot water temperature T_t are the two state variables.

6.2.2 Sub-models

6.2.2.1 Heat pump water heater

The heat pump model is developed according to [13, 102], with a fixed power demand P_{hp} rating, operating at full capacity. The HPWH model used in this chapter was developed in the previous chapter 5 subsubsection 5.2.2.1.

6.2.2.2 Wind generator

The wind turbine power output is dependent on the wind velocity at hub height and turbine specifications. The standard height or reference for wind speed measurements for wind resource assessment is usually 10 m above the effective ground level, these measurements are extrapolated to the wind speed at hub height. This is important because it is the wind speed experienced by the rotor of the wind turbine (hub height wind speed) that determines the actual power radiated by a particular turbine. The most common expression used for this purpose is the power-law equation, expressed as [116, 117, 75, 107]:

$$v_{hub} = v_{ref} . \left(\frac{h_{hub}}{h_{ref}} \right)^{\varphi}, \tag{6.1}$$

where v_{hub} is the wind speed at the desired height h_{hub}, v_{ref} is the wind speed at the reference height h_{ref} and φ is the power law exponent, which represents the ground surface friction coefficient. The exponent is a function of height, season, nature of the terrain and time of day as well as the temperature and wind velocity. It is low for smooth terrains, high for rough terrains and the values for typical classes are given in [117]. The coefficient ranges from $\frac{1}{7}$ to $\frac{1}{4}$. In this chapter $\frac{1}{7}$ is used, typical of the case study which is an open land. The v_{hub} obtained is then used in the wind power equation. The power output of a wind turbine thus depends on many factors; the air density, rotor sweeping area, wind speed and the overall Betz limit.

The hub height velocity is used in the output power model to calculate the power generated by the wind turbine generator. The models used to describe the performance of wind generator (WG) are different since different WGs have different power output performance curves. Different wind turbine models and their power output characteristics are presented in [98, 117]. Various authors have developed different models for calculating the power output by making various assumptions and assuming that

the turbine power curve has a linear, quadratic or cubic form [118, 119]. The general expression used is as follows:

$$P_w = \begin{cases} P_r \frac{V^\chi - V_{in}^\chi}{V_r^\chi - V_{in}^\chi}, & (V_{in} \leq V \leq V_r) \\ P_r, & (V_r \leq V \leq V_{out}) \\ 0, & (0 \leq V_{in} \text{ and } V \leq V_{out}) \end{cases} \tag{6.2}$$

where V is the wind speed at the hub height, χ is the Weibull shape parameter taken as 2 in this chapter, P_r is the rated electrical power; V_{in} is the cut-in wind speed; V_r is the rated wind speed and V_{out} is the cut-off wind speed. The wind model parameters are presented in the case study as given in Table 6.2.

6.2.2.3 Hydrogen Fuel Cell

The FC hydrogen storage system comprises the electrolyzer and a tank. The input energy for the electrolyzer is supplied by the RE sources. The hydrogen is produced by electrolysis of water and is stored in the tank. The FC complements the grid during periods of peak TOU tariff or the RE is insufficient to meet the load. The storage tank is operated within the maximum and minimum levels of hydrogen storage and a minimum amount of hydrogen should remain in the tank to maintain a security limit. The electrolyzer is connected directly to the hydrogen tank and power from the electrolyzer to the tank, $P_{el,t}$, is given by:

$$P_{el,t} = \frac{P_{H2,t}}{\eta_{el}}, \tag{6.3}$$

where $P_{el,t}$ is the renewable power input to the electrolyzer, $P_{H2,t}$ is the hydrogen power output and η_{el} is the efficiency of the electrolyzer and is assumed to be constant. The energy in the hydrogen storage tank at any given time is expressed as:

$$\dot{E}_{s,t} = P_{el,t} - \frac{1}{\eta_s} P_{FC,t} \tag{6.4}$$

in which, η_s is the storage discharging efficiency taken as 95% owing to leakages and pumping [120]. The following general expression thus applies to the storage dynamics in descrete time with a sampling time, t_s:

$$E_{s,t} = E_s(0) + \sum_{\tau=1}^{t} P_{el,\tau} t_s - \frac{1}{\eta_s} \sum_{\tau=1}^{t} P_{FC,\tau} t_s, \tag{6.5}$$

where $E_s(0)$ is regarded as the initial SOC of the storage tank.

$P_{H2,\tau}$ is the power accepted by the storage at time t, and $\frac{1}{\eta_s} \sum_{\tau=1}^{t} P_{FC,\tau}$ is the power drawn from the storage at time t. The mass of hydrogen stored in the tank at any given time t is given by:

$$Mass_{h,t} = \frac{E_{s,t}}{HHV_h}, \tag{6.6}$$

where $HHV_h = 39.7\ kWh/kg$ is the hydrogen heating value [74, 121]. The storage operates within maximum and minimum limits.

FC stacks produce direct current at a voltage that varies with the load. A switching power converter is used to match the voltage produced by the FC to the needs of the application and to protect the FC from over-current or under-voltage conditions. In this work the application requires AC, so the electricity is then processed through a DC/AC inverter. FCs also produce thermal energy but this is not considered in this work. There are various types of FCs and in this work the proton exchange membrane FC is considered owing to its reliable performance under variable supply and its availability in a wide range of capacities. The output power, $P_{FC-IN,t}$ is a function of the input power, $P_{FC,t}$, and efficiency η_{FC} (assumed constant) of the FC given by:

$$P_{FC-IN,t} = \eta_{FC} P_{FC,t}. \tag{6.7}$$

The FC output is restricted within:

$$E^{min} \leq E_{s,t} \leq E^{max}. \tag{6.8}$$

6.2.2.4 Photovoltaic power

The PV power output profile $P_{pv}(t)$ is input data, taken from the case study in our previous research [23, 32]. The PV power input data are given in Figure 6.4. The PV power generation is bounded by:

$$0 \leq P_{pv,t} \leq P_{pv}^{max}. \tag{6.9}$$

6.2.2.5 Grid power

The grid is capable of accepting and supplying power to the AC bus where the load is connected. The formulation of TOU electricity tariff is same as in the previous chapters.

6.2.2.6 DC and AC bus power balance

The power balance at the DC bus is given as:

$$P_{el,t} + P_{RE-IN,t}/\eta_{in} = P_{w,t}\eta_w + P_{pv,t}\eta_{pv}, \tag{6.10}$$

where $P_{el,t}$ is the renewable power input to the electrolyzer and $P_{RE-IN,t}$ is the direct renewable energy power supply to the loads. η_{in},η_w and η_{pv} are the efficiency of the DC/AC, wind generator and PV inverters respectively.

The power balance at the AC load bus is given as:

$$P_{g,t} + P_{RE-IN,t} + P_{FC-IN,t} = P_{\text{Load},t} + P_{hp,t}u_t, \tag{6.11}$$

where $P_{g,t}$ is the grid power ,and $P_{FC-IN,t}$ is the FC power output. $P_{\text{Load},t}$ and $P_{hp,t}u_t$ are the domestic load and heat pump demand respectively, whereas u_t is the heat pump's power supply switch.

6.3 DISCRETE FORMULATION OF THE MODEL

6.3.1 Hot water temperature model

The water demand flow rate $W_{D,t}$ and the inlet water, $T_{in,t}$, are functions of time as developed in the previous chapter 5 subsection 5.3.1

6.3.2 Objective function

The multi-objective function consists of energy cost, $w_1 t_s \sum_{k=1}^{N} P_{g,k} p_k$, minimization and maximization of FC usage, $w_2 t_s \sum_{k=1}^{N} P_{FC-IN,k}$, in discrete time with weighting factors, w_1 and w_2. The objective function is normalized to level the sensitivity of the weighting factor by dividing the grid power variable by 1000 units. The control horizon is 24 h, with t_s being the sampling time, and the sampling interval is $(1 \leq k \leq N)$ whereas p_k is the TOU tariff. N is the final sampling point.

The objective function is expressed as follows:

$$J = \frac{1}{1000} w_1 t_s \sum_{k=1}^{N} P_{g,k} p_k - w_2 t_s \sum_{k=1}^{N} P_{FC-IN,k}, \tag{6.12}$$

subject to:

$$P_{el,k} + P_{RE-IN,k}/\eta_{in} = P_{w,k}\eta_w + P_{pv,k}\eta_{pv}, \tag{6.13}$$

$$P_{g,k} + P_{RE-IN,k} + P_{FC-IN,k} = P_{\text{Load},k} + P_{hp,k} u_k, \tag{6.14}$$

$$0 \leq P_{pv,k} \leq P_{pv}^{max}, \tag{6.15}$$

$$P_{el,k} = \frac{P_{H2,k}}{\eta_{el}}, \tag{6.16}$$

$$P_{FC-IN,k} = \eta_{FC} P_{FC,k}, \tag{6.17}$$

$$T_{low} \leq T_o \prod_{j=0}^{k} (1 - t_s \alpha_j) + t_s \beta \sum_{j=0}^{k} u_j \prod_{i=j+1}^{k} (1 - t_s \alpha_i) + \sum_{j=0}^{k} t_s \gamma_j \prod_{i=j+1}^{k} (1 - t_s \alpha_i) \leq T_{up}, \tag{6.18}$$

$$E^{min} \leq E_s(0) + \sum_{\tau=1}^{k} P_{H2,\tau} t_s - \frac{1}{\eta_s} \sum_{\tau=1}^{k} P_{FC,\tau} t_s \leq E^{max}, \tag{6.19}$$

$$P_w = \begin{cases} P_r \frac{V^{\chi} - V_{in}^{\chi}}{V_r^{\chi} - V_{in}^{\chi}}, & (V_{in} \leq V \leq V_r) \\ P_r, & (V_r \leq V \leq V_{out}) \\ 0, & (0 \leq V_{in} \text{ and } V \leq V_{out}) \end{cases} \tag{6.20}$$

$$u_k \in \{0, 1\}. \tag{6.21}$$

6.3.3 Algorithm formulation

The OC problem is solved using SCIP algorithm in *OPTI toolbox* in MATLAB.

6.3.3.1 The objective function

The objective function minimizes the grid energy cost under the TOU tariff while maximizing FC power output.

For grid energy cost minimization J_e:

$$J_e = f^T\mathbf{X} = \left[0\dots0_N, p_1\dots p_N, 0\dots0_N, 0\dots0_N, 0\dots0_N, 0\dots0_N\right]_{1\times6N} \times \\ \times \left[u_1\dots u_N, P_{g,1}\dots P_{g,N}, P_{RE-IN,1}\dots P_{RE-IN,N}, P_{H2,1}\dots P_{H2,N}, \right. \\ \left. P_{FC-IN,1}\dots P_{FC-IN,N}, P_{FC,1}\dots P_{FC,N}\right]'_{6N\times1}, \quad (6.22)$$

for FC power output maximization J_{FC}:

$$J_{FC} = f^T\mathbf{X} = \left[0\dots0_N, 0\dots0_N, 0\dots0_N, 0\dots0_N, 1\dots1_N, 0\dots0_N\right]_{1\times6N} \times \\ \times \left[u_1\dots u_N, P_{g,1}\dots P_{g,N}, P_{RE-IN,1}\dots P_{RE-IN,N}, P_{H2,1}\dots P_{H2,N}, \right. \\ \left. P_{FC-IN,1}\dots P_{FC-IN,N}, P_{FC,1}\dots P_{FC,N}\right]'_{6N\times1}. \quad (6.23)$$

Finally the multi-objective function is:

$$minJ = t_s w_1 \sum_{k=1}^{N} J_e - t_s w_2 \sum_{k=1}^{N} J_{FC}, \quad (6.24)$$

subject to

$$\mathbf{AX} \leq \mathbf{b} \text{ (linear inequality constraint)}, \\ \mathbf{A_{eq}X} = \mathbf{b_{eq}} \text{ (linear equality constraint)}. \quad (6.25)$$

6.3.3.2 Inequality matrices

The general formulation of the inequality constraint is shown in equation (6.26):

$$\mathbf{AX} \leq \mathbf{b}. \tag{6.26}$$

Vector $\mathbf{X}$ comprises all the control variables and they are given in matrix 6.27:

$$\mathbf{X} = \Big[u_1 \dots u_N, P_{g,1} \dots P_{g,N}, P_{RE-IN,1} \dots P_{RE-IN,N}, P_{H2,1} \dots P_{H2,N}, P_{FC-IN,1} \dots P_{FC-IN,N}, P_{FC,1} \dots P_{FC,N}\Big]'_{6N\times 1}. \tag{6.27}$$

The spacial matrix $\mathbf{A}$ and vector $\mathbf{b}$ are formulated as follows:

Let $\mathbf{A_1}$, an $N \times N$ matrix, represent the state variable of the thermal load, shown in equation (6.28):

$$\mathbf{A_1} = t_s\beta \times \begin{bmatrix} 1 & 0 & 0 & 0 & \dots & 0 \\ (1-t_s\alpha_1) & 1 & 0 & 0 & \dots & 0 \\ (1-t_s\alpha_2)(1-t_s\alpha_1) & (1-t_s\alpha_2) & 1 & 0 & \dots & 0 \\ \vdots & \vdots & \vdots & \ddots & \vdots & \\ (1-t_s\alpha_{N-2})\times\dots\times(1-t_s\alpha_1) & (1-t_s\alpha_{N-2})\times\dots\times(1-t_s\alpha_2) & \dots & \dots & 1 & 0 \\ (1-t_s\alpha_{N-1})(1-t_s\alpha_{N-2})\times\dots\times(1-t_s\alpha_1) & (1-t_s\alpha_{N-1})\times\dots\times(1-t_s\alpha_2) & \dots & \dots & (1-t_s\alpha_{N-1}) & 1 \end{bmatrix}, \tag{6.28}$$

The $2N \times 6N$ matrix below represents a combined inequality (6.28) and the FC status of energy inequality (6.19), in this appendix each sub-matrix inside the bigger matrix is an $N \times N$ dimension:

$$\mathbf{A_2} = \left[\begin{array}{c|c|c|c|c|c} \mathbf{A_1} & 0\ldots0 & 0\ldots0 & 0\ldots0 & 0\ldots0 & 0\ldots0 \\ & \vdots & \vdots & \vdots & \vdots & \vdots \\ & 0\ldots0 & 0\ldots0 & 0\ldots0 & 0\ldots0 & 0\ldots0 \\ \hline 0\ldots0 & 0\ldots0 & 0\ldots0 & t_s\ldots0 & 0\ldots0 & -\frac{t_s}{\eta_s}\ldots0 \\ \vdots & \vdots & \vdots & \ddots & \vdots & \ddots \\ 0\ldots0 & 0\ldots0 & 0\ldots0 & 0\ldots t_s & 0\ldots0 & -\frac{t_s}{\eta_s}\ldots-\frac{t_s}{\eta_s} \end{array}\right]_{2N\times 6N}, \tag{6.29}$$

inequality (6.18) is reformulated into inequality (6.30) and inequality (6.31):

$$t_s\beta\sum_{j=0}^{k}u_j\prod_{i=j+1}^{k}(1-t_s\alpha_i)\leq T_{up}-T_o\prod_{j=0}^{k}(1-t_s\alpha_j)-\sum_{j=0}^{k}t_s\gamma_j\prod_{i=j+1}^{k}(1-t_s\alpha_i), \tag{6.30}$$

$$-t_s\beta\sum_{j=0}^{k}u_j\prod_{i=j+1}^{k}(1-t_s\alpha_i)\leq -T_{low}+T_o\prod_{j=0}^{k}(1-t_s\alpha_j)+\sum_{j=0}^{k}t_s\gamma_j\prod_{i=j+1}^{k}(1-t_s\alpha_i). \tag{6.31}$$

According to inequality (6.30) and inequality (6.31), the element of vectors $\mathbf{b_1}$ and $\mathbf{b_2}$ is:

$$b_{1,k}=T_{up}-T_o\prod_{j=0}^{k}(1-t_s\alpha_j)-\sum_{j=0}^{k}t_s\gamma_j\prod_{i=j+1}^{k}(1-t_s\alpha_i), \tag{6.32}$$

$$b_{2,k}=-T_{low}+T_o\prod_{j=0}^{k}(1-t_s\alpha_j)+\sum_{j=0}^{k}t_s\gamma_j\prod_{i=j+1}^{k}(1-t_s\alpha_i). \tag{6.33}$$

Vector $\mathbf{b_1}$ in equation (6.32) is the difference of the three vectors $\mathbf{b_3}$, $\mathbf{b_4}$ and $\mathbf{b_5}$, as shown in equation (6.34).

$$\mathbf{b_1}=\mathbf{b_3}-\mathbf{b_4}-\mathbf{b_5}, \tag{6.34}$$

where,

$$\mathbf{b_3}=\begin{bmatrix}T_{up}\\ \vdots \\ T_{up}\end{bmatrix}_{N\times 1}, \tag{6.35}$$

then vector $\mathbf{b_4}$ is given in equation (6.36),

$$\mathbf{b_4} = T_o \begin{bmatrix} (1-t_s\alpha_0) \\ (1-t_s\alpha_1)(1-t_s\alpha_0) \\ (1-t_s\alpha_2)(1-t_s\alpha_1)(1-t_s\alpha_0) \\ \vdots \\ (1-t_s\alpha_{N-2})(1-t_s\alpha_{N-3})\times\ldots\times(1-t_s\alpha_0) \\ (1-t_s\alpha_{N-1})(1-t_s\alpha_{N-2})(1-t_s\alpha_{N-3})\times\ldots\times(1-t_s\alpha_0) \end{bmatrix}_{N\times 1}, \tag{6.36}$$

and finally, $\mathbf{b_5}$ is given in equation (6.37) below,

$$\mathbf{b_5} = \begin{bmatrix} t_s\gamma_o \\ (1-t_s\alpha_1)t_s\gamma_o + t_s\gamma_1 \\ (1-t_s\alpha_2)(1-t_s\alpha_1)t_s\gamma_o + (1-t_s\alpha_2)t_s\gamma_1 + t_s\gamma_2 \\ \vdots \\ (1-t_s\alpha_{N-2})\times\ldots\times(1-t_s\alpha_1)t_s\gamma_o + (1-t_s\alpha_{N-2})\times\ldots\times(1-t_s\alpha_2)t_s\gamma_1 + \ldots + t_s\gamma_{N-2} \\ (1-t_s\alpha_{N-1})(1-t_s\alpha_{N-2})\times\ldots\times(1-t_s\alpha_1)t_s\gamma_o + (1-t_s\alpha_{N-1})\times\ldots\times(1-t_s\alpha_2)t_s\gamma_1 + \ldots(1-t_s\alpha_{N-1})t_s\gamma_{N-2} + t_s\gamma_{N-1} \end{bmatrix}. \tag{6.37}$$

The T_{low} vector is given in equation (6.38), the formulation of the $\mathbf{b_2}$ vector is analogous to $\mathbf{b_1}$ given in equation (6.39),

$$\mathbf{b_6} = \begin{bmatrix} T_{low} \\ \vdots \\ T_{low} \end{bmatrix}_{N\times 1}, \tag{6.38}$$

$$\mathbf{b_2} = -\mathbf{b_6} + \mathbf{b_4} + \mathbf{b_5}. \tag{6.39}$$

Finally, the FC vectors are given in matrix 6.40 and 6.41 for the maximum and minimum hydrogen storage capacity respectively:

$$\mathbf{b_7} = \begin{bmatrix} E^{max} - E(0) \\ \vdots \\ E^{max} - E(0) \end{bmatrix}_{N\times 1}, \tag{6.40}$$

$$\mathbf{b_8} = \begin{bmatrix} -E^{min} + E(0) \\ \vdots \\ -E^{min} + E(0) \end{bmatrix}_{N\times 1}. \tag{6.41}$$

The final inequality **A** matrices and vector **b** are given in 6.42 and 6.43 respectively.

$$\mathbf{A} = \begin{bmatrix} \mathbf{A_2} \\ -\mathbf{A_2} \end{bmatrix}_{4N\times 6N}, \tag{6.42}$$

$$\mathbf{B} = \begin{bmatrix} \mathbf{b_1} \\ \mathbf{b_7} \\ \mathbf{b_2} \\ \mathbf{b_8} \end{bmatrix}_{4N\times 1}, \tag{6.43}$$

6.3.3.3 Equality matrices

The power balance equality constraint in equation (6.13), equation (6.14) and equation (6.17), are sparse matrix $\mathbf{A_{eq}}$, given in equation (6.44):

$$\mathbf{A_{eq}} = \left[\begin{array}{c|c|c|c|c|c} 0\ldots0 & 0\ldots0 & \eta_{in}\ldots0 & \eta_{el}\ldots0 & 0\ldots0 & 0\ldots0 \\ \vdots & \vdots & \ddots & \ddots & \vdots & \vdots \\ 0\ldots0 & 0\ldots0 & 0\ldots\eta_{in} & 0\ldots\eta_{el} & 0\ldots0 & 0\ldots0 \\ \hline -P_{hp}\ldots0 & 1\ldots0 & 1\ldots0 & 0\ldots0 & 1\ldots0 & 0\ldots0 \\ \ddots & \ddots & \ddots & \vdots & \ddots & \vdots \\ 0\ldots-P_{hp} & 0\ldots1 & 0\ldots1 & 0\ldots0 & 0\ldots1 & 0\ldots0 \\ \hline 0\ldots0 & 0\ldots0 & 0\ldots0 & 0\ldots0 & -1\ldots0 & \eta_{FC}\eta_{in}\ldots0 \\ \vdots & \vdots & \vdots & \vdots & \ddots & \ddots \\ 0\ldots0 & 0\ldots0 & 0\ldots0 & 0\ldots0 & 0\ldots-1 & 0\ldots\eta_{FC}\eta_{in} \end{array}\right]_{3N\times 6N}, \tag{6.44}$$

The *k-th* total PV power, wind power and the demand constitute the elements of vector $\mathbf{b_{eq}}$ is shown in equation (6.45):

$$\mathbf{b_{eq}} = \begin{bmatrix} \eta_w P_{w,1} + \eta_{pv} P_{pv,1} \\ \vdots \\ \eta_w P_{w,N} + \eta_{pv} P_{pv,N} \\ \hline P_{load,1} \\ \vdots \\ P_{load,N} \\ \hline 0 \\ \vdots \\ 0 \end{bmatrix}_{3N\times 1} . \tag{6.45}$$

The canonical form is $\mathbf{A_{eq}X} = \mathbf{b_{eq}}$ where $\mathbf{A_{eq}}$ is given in equation (6.44) and $\mathbf{b_{eq}}$ in equation (6.45).

The limits of the control variables are restricted between the lower and upper bounds, given in equation (6.46) and equation (6.47):

lower bounds

$$lb^T = \left[0_1 \dots 0_N, -\infty_1 \dots -\infty_N, 0_1 \dots 0_N, E^{min} \dots E^{min}, 0_1 \dots 0_N, 0_1 \dots 0_N\right]_{6N\times 1}, \tag{6.46}$$

$$ub^T = \Big[1_1 \dots 1_N, \infty_1 \dots \infty_N, P^{rated}_{RE-IN,1} \dots P^{rated}_{RE-IN,N}, E^{max} \dots E^{max}, P^{rated}_{FC-IN,1} \dots P^{rated}_{FC-IN,N}, P^{rated}_{FC,1} \dots P^{rated}_{FC,N}\Big]'_{6N\times 1}. \tag{6.47}$$

6.3.4 Case study

The case study is done on a facility in Pretoria, South Africa. This facility intends to be a positive-energy building; the installation of wind, PV and FC generators is under way. The current control strategy on this equipment is a PID controller incapable of handling hard constraints and on-line

optimization. The baseline situation at the facility is that grid power supplies all the loads. Therefore, this chapter proposes an OC strategy incorporating RE sources and FCs at this facility. The sampling time $t_s = 30$ min, while $N = 48$ and the control horizon is 24 h.

Because of the difficulties of consolidated input data of this facility, relatively similar data are adopted from [13]. The inlet cold water temperature and hot water demand are shown in Figure 6.2:

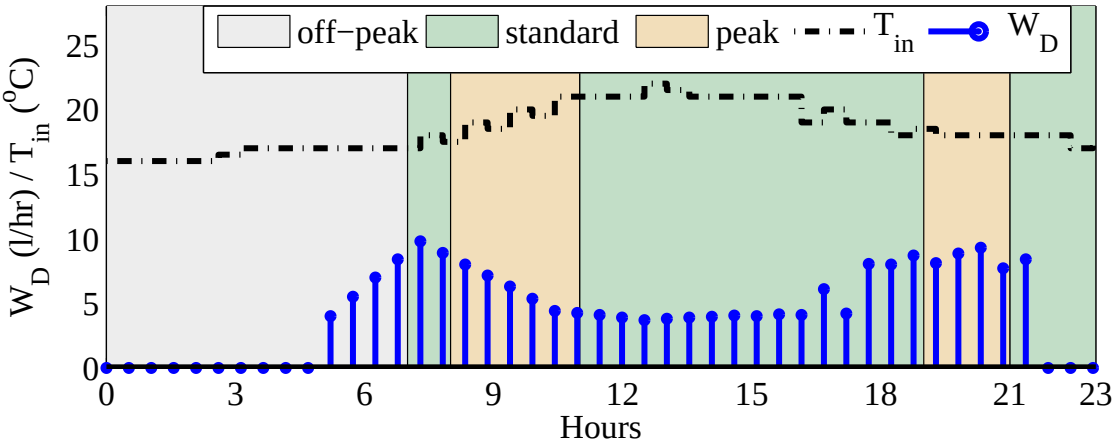

Figure 6.2. Flow rate

6.3.4.1 Heat pump water heater parameters

The HPWH considered in this chapter is a Quantum solar heat pump[1] air source tank-wrapped heat exchanger (condenser) and its parameters are shown in Table 6.1. The preferred hot water temperature

Table 6.1. Heat pump parameters

Power input (kW)	COP	Storage capacity (l)	Compressor (cc)	Tank (h/ø) (m)	$\triangle x\,(m)$	$\kappa\,(W/m.K)$	$h\,(W/m^2K)$
7	3.8	270	39.0	1.41×0.66	0.035	0.055	6.3

is set to $55\,^{\circ}\text{C} \leq T_k \leq 60\,^{\circ}\text{C}$; the average country ambient temperature of $T_a = 25\,^{\circ}\text{C}$ is used. The initial water temperature in the tank is set to $T_o = 57\,^{\circ}\text{C}$. However, the above desirable temperature varies from one individual to another.

[1] www.quantumecohotwater.com.au

6.3.4.2 Wind generator parameters

The wind generator in the case study is a Ruam Energy[2] turbine with technical specifications given in Table 6.2. The parameters are:

Table 6.2. Wind generator parameters

$P_r(kW)$	φ	$h_{ref}\ (m)$	$h_{hub}\ (m)$	χ	$V_{in}\ (m/s)$	$V_r\ (m/s)$	$V_{out}\ (m/s)$
7	1/7	10	30	2	2.0	11	50

The wind turbine revolution per minute is 280 RPM. The hourly measured wind and hub height speeds are shown in Figure 6.3:

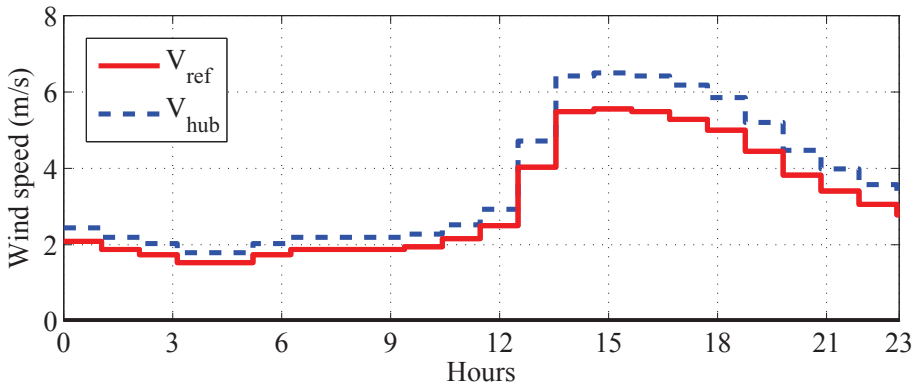

Figure 6.3. Hub height wind speed

6.3.4.3 Photovoltaic power generation

The PV power is input data in this model, taken from our previous research [23, 32] on the data measured on an installed facility in South Africa. The power output P_{pv} profile is given in Figure 6.4 on the far right.

6.3.4.4 Inverter and fuel cell parameters

The FC under consideration is a stationary type with a wider application in commercial, industrial, and residential use, which can supplement the grid power supply. The electrolyzer efficiency is taken to be

[2] www.raumenergy.com

$\eta_{el} = 0.65$, hydrogen storage tank $\eta_s = 0.95$ and overall FC efficiency $\eta_{FC} = 0.5$. The hydrogen tank energy storage capacity has a minimum $E^{min} = 0$ kWh and maximum $E^{max} = 25$ kWh, the initial status of hydrogen energy is taken to be $E_s(0) = 3$ kWh, while all the inverters' efficiency, both DC/DC and AC/DC or vice versa, is taken to be $\eta_{in} = 0.98$.

6.4 SIMULATION RESULTS AND DISCUSSION

The simulations are carried out to assess the feasibility and viability of implementing the proposed integrated FC hybrid system. Two simulation scenarios are analyzed: Case I without RE feed-in and Case II, having RE energy feed-in to account for all the possible applications of the proposed model.

CASE I

6.4.1 Optimal power control strategy of a fuel cell hybrid system

The optimal power scheduling strategy of the FC-grid-RE integrated system is shown in Figure 6.4. The weighting factors are set to $w_1 = 0.7$ and $w_2 = 0.3$, giving more weight on the minimization of grid energy. In Figure 6.4, the grid P_g meets all domestic load P_{load} and heat pump P_{hp} from 00:00 till 07:00 at the end of the morning off-peak TOU period, since wind energy P_w and PV P_{pv} are unavailable. There is no P_w generation in this period because the wind velocities are below cut-in speed on this simulated day. Though the FC has an initial status of energy $E_s(0) = 3$ kWh (Figure 6.5), the OC opts to avoid its usage because of poor energy conversion efficiency. The OC instead uses the off-peak TOU grid energy. The OC strategy changes as the TOU enters the standard period at 07:00; the energy becomes slightly more expensive, the OC cuts off the grid supply and brings in the RE power, P_{RE-IN}, to sustain the domestic load which is supplemented by the FC. Unfortunately the heat pump switches *on* (in Figure 6.6) at 8:00 in the peak period. The available FC and RE power cannot meet the demand and the grid comes in to supply power for an hour. During the afternoon standard TOU the FC is not used to supply power; the wind, PV and grid meet the load. The cutting off of supply from the FC can only be attributed to its huge power losses in terms of efficiency whenever it operates.

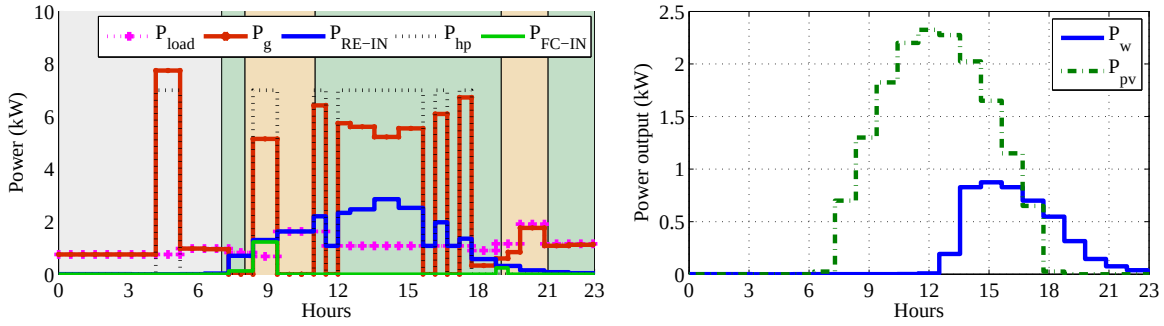

Figure 6.4. Optimal scheduling strategy and wind output

The optimal strategy in Figure 6.4, avoids using peak TOU energy as much as possible to save energy cost. The evening peak is mainly powered by the grid, FC and wind, since PV power is not available at night. The hot water temperature set point bounds reflected in Figure 6.6 are slightly stringent, prompting the OC to increase the heat pump's switching u_k frequency.

6.4.2 Fuel cell scheduling strategy and hydrogen storage dynamics

In Figure 6.5 optimal FC power dispatch is shown. The power source of the electrolyzer is the RE supply to generate hydrogen. The FC power P_{PF-IN} supply is *off* from 00:00 to 07:30, the loads are supplied by the grid during the off-peak period. The stored hydrogen energy H_2 drops at 07:30 owing to the resumption of the FC operation. P_{FC-IN} supplies the load from 07:30 to 9:30 in the morning peak period. The stored hydrogen H_2, sharply declines to minimum during this interval because the OC keeps the electrolyzer switched *off*. There is no hydrogen generation till 10:00 when the heat pump demand is reduced, and the excess RE is then used for hydrogen generation, P_{H2}, and the hydrogen mass builds in the tank. A steady increase in hydrogen storage is observed between 10:00 and 12:00. This is attributed to the low load demand. The OC again actuates the electrolyzer at 16:00 and hydrogen power P_{H2} production begins, further increasing the stored hydrogen. During the evening peak, the FC operates once again, as at this time only the FC has enough power reserve, since RE production has dwindled.

The OC avoids operating the FC at all times, the RE meanwhile can directly supply the loads, treating the FC as storage system. The OC just operates it in peak period or when the RE is completely unavailable. However, depending on the desired effect, the weighting factor can be adjusted to make

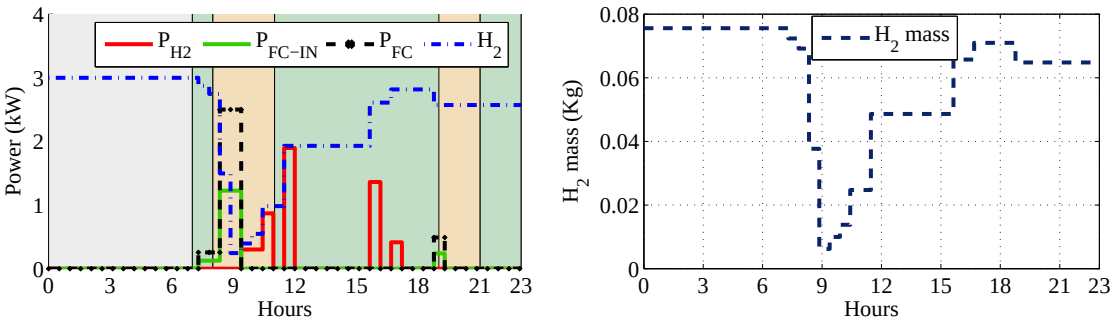

Figure 6.5. Fuel cell optimal control and hydrogen mass

sure the fuel, once in operation replenishes all the stored hydrogen. Because of a direct RE P_{RE-IN} supply circuit to the loads that causes minimal power loss on the inverter only, the OC gives higher priority to this circuit than the FC circuit that has output efficiency of $\eta_{FC} = 0.5$. Therefore, the OC opts to keep its usage to the bare minimum. In Figure 6.5, on the far right, the cumulative hydrogen mass plotted according to equation (6.6) is shown. The pressure drop inside the tank limits the complete utilization of hydrogen; because of this, a lower and upper limit are given for each specified storage tank.

6.4.3 Thermal load switching control

In this model, the domestic load is deterministic at each sampling interval. Only the thermal load is controllable; that is, the switching status of the heat pump in this case. Switch u_k is a variable dependent on the state of the hot water T_k in the tank. It is assumed that at any sampling time the heat pump operates at its full rated power demand of 7 kW. The lower and upper limits are set according to each individual's desired temperature range given in section 6.3.4. Figure 6.6 shows the optimal switching u_k and the hot water state variable T_k of the heat pump. The heat pump switch u_k turns *on* around 04:00 for an hour and a corresponding rise in hot water temperature T_k is observed. The water is preheated prior to the resumption of morning water demand (shown in Figure 6.2). From midnight to 04:30 when there is no hot water demand, a negligible drop in T_k is seen owing to the best heat pump insulation level. However, the preheated water temperature falls sharply at the beginning of demand between 05:00 and 09:00. The OC switches *on* the heat pump again at 08:30 to heat the water that is almost hitting the lower set-point. The inlet cold water is the major cause of the temperature drop inside the tank, in addition to hot water demand. The OC operates the heat pump from 12:00

to 15:30 in readiness for the evening peak demand, thereby avoiding operating it in the evening peak period and thus making use of standard TOU that is relatively cheaper.

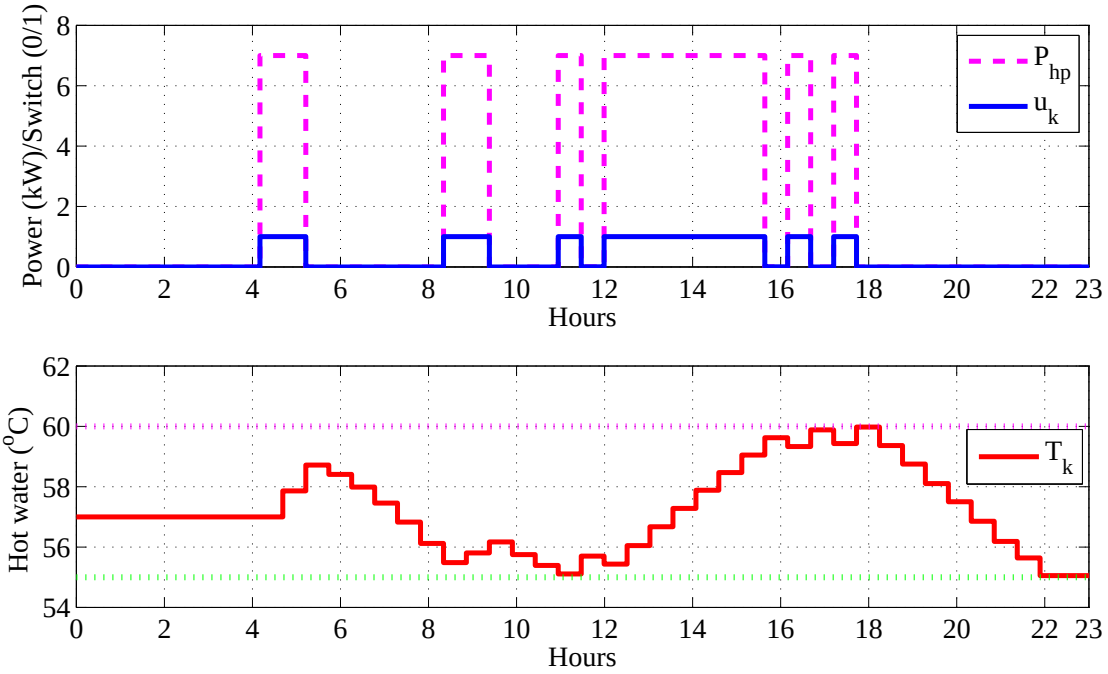

Figure 6.6. Optimal heat pump scheduling and hot water temperature

The heat pump water's temperature is highest between 17:00 and 18:30, enough to meet the evening demand and that of the rest of the night. The proposed models show the capacity to predict, control and meet the state variable water constraint.

CASE II

6.4.4 Optimal feed-in power control strategy

The notable major difference between the two operational scenarios in Figure 6.4 and Figure 6.7 is that the OC does not use the electrolyzer at all in case II. In Figure 6.7 the heat pump load scheduling strategy is rather spread throughout the whole control horizon. The RE feed-in takes place between 08:30 and 10:30 and later on between 11:30 and 14:00 only during the periods when the heat pump is not operational. The OC stops the feed-in during peak load, because all the generated RE is used to supplement the grid power, which is expensive to purchase.

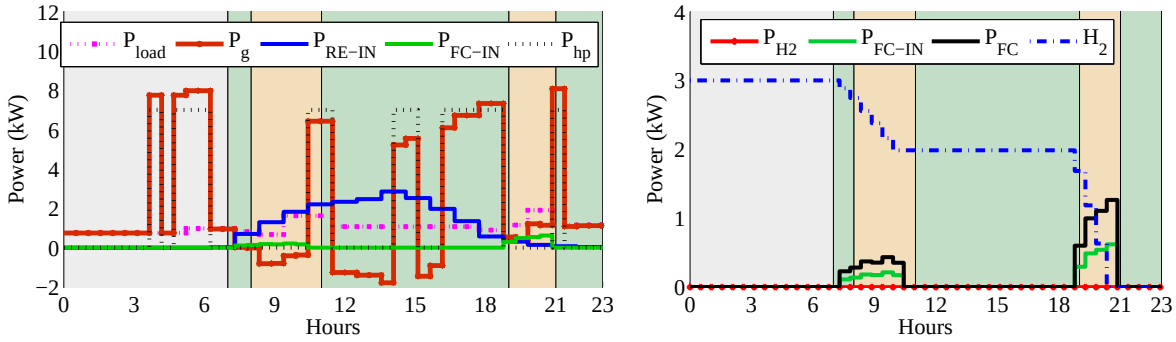

Figure 6.7. Optimal feed-in strategy

The FC P_{FC-IN} is used twice during the peak period. This can be attributed to higher FC system energy loss; the OC therefore, rather opts to sell to the grid. The proposed model has shown greater capability of power control and can effectively improve the scheduling strategy of these systems, mostly on programmable logic controllers. The OC technique maximizes operational efficiency.

6.4.5 Baseline and optimal control savings

The facility in the case study currently uses only the grid to sustain all the loads, here referred to as the baseline. The proposed intervention is the addition of wind, PV, FC and OC, referred to as the optimal situation. Table 6.3 shows the baseline/current and after implementation of the model, tabulating the predicted savings on a 24-h basis.

Table 6.3. Baseline and optimal energy/cost savings

Baseline (kWh)	Baseline cost (R/day)	Optimal (kWh)	Optimal cost (R/day)	Energy saving (%)	Cost saving (%)
74.00	66.08	53.52	43.69	27.68	33.8

The energy saving is about 27.68% owing to the addition of the RE sources coupled with an optimal load-shifting strategy. This translates into reduced grid energy cost of 33.8%. The proposed model has the potential of effecting savings for this facility in the case study, provided the REs rides on OC strategy instead of the traditional logical controllers. Though this chapter does not look into economic analysis and the payback period, it could be interesting in future research to quantify these estimates. The proposed model opens the door for integration and OC of FCs with other distributed

RE sources, especially in developing countries experiencing a power deficit (e.g. Zambia, Zimbabwe, South Africa).

6.5 SUMMARY

An OC model of an integrated FC-RE-grid hybrid energy system with a thermal load meeting all the operational constraints has been presented. The OC provides the required hot water demand and optimally schedules the RE system with FC mainly used as back-up/storage energy sources. The model can be used for feed-in and load shifting in order to minimize grid energy cost; it avoids operating the thermal load in the peak TOU period. The proposed model can effectively improve the operational and system efficiency, which results in minimization of energy losses. The engineering challenge facing RE and energy-efficient equipment integration has been solved in this chapter, especially on DSM. The traditional control methods, e.g. PID controller used in the operation of such a hybrid system can be improved by OC strategy in the current energy mix and electricity market environment. If this OC is implemented using MPC it could effectively counter error and future disturbance. The MPC as well alleviates the uncertainty concerning the input data and renewable energy generation. The MPC application has been recommended in chapter 8 for future research.

The next chapter compares the life cycle cost analysis of the existing (baseline) and the OC system for all the developed models in this thesis.

CHAPTER 7 COMPARISON OF LIFE CYCLE COST ANALYSIS

7.1 INTRODUCTION

This chapter looks at a detailed comparison of life cycle cost (LCC) analysis of pre-and-post implementation of these models. Several assumptions were made in the previous chapters, (e.g., the operation costs excluded the energy bills and other common equipment found in both baseline and OC scenarios) in calculating the payback period. However, for us to properly determine the feasibility of the project/system and alternative investment choices, a LCC over the project is necessary [122]. The main purpose of LCC is to assess the economic benefit of the proposed 24-h OC strategy, over the baseline yearly average system operation. In most cases, building owners and investors in RE and energy-efficient projects are interested only in the associated investment, to make a decision [123, 124].

The present value (PV_E) method is widely used to compute and compare the alternative investment choices, while keeping the same economic assumptions for pre-and-post implementation, project life and service period [125, 126, 127]. Several techniques in engineering are used to assess the project's environmental impact from production to its end of useful life such as; techno-economic analysis and life cycle assessment (LCA) [128]. These two techniques are not in the scope of this thesis. The LCC approach is adopted to compare the existing and the OC system (pre-and-post implementation) [129, 13]. The discounted cash flow (present worth) calculations are done to reflect the PV_E in future years. In this chapter assumptions are made on: maintenance costs, discounting rate, replacement cost and salvage value. LCC for pre-and-post implementation is calculated using cumulative present value over project's life for all the models developed in this thesis. The purpose of the chapter's LCC is

to compare the investment choices, whether to implement the OC or remain with existing baseline scenario.

The LCC approach first discounts the cash flows to determine the PV_E of money in the future time and summed to accumulative project life costing. The initial investment and any other cost incurred by the investor/end-users are presented as negative cash flow in the LCC financial statement (e.g., solar PV purchasing price = -*R*27 500.00) is represented in brackets as (27 500.00) in this chapter, in accordance to the international accounting standards board (IASB)[1]. The inflation rate, replacement cost, salvage value, running and maintenance cost over time are assumed constant over the project's life . Although, it is expected that there would be an increase in all these factors, it cannot be reliably estimated at this time. The LCC method adopted in this work, excludes most of the constant costs: the building construction, depreciation, water and sewerage costs, the end-user thermal energy benefits. The LCC is calculated as in [112]:

$$\mathrm{LCC} = \mathrm{CC} + \mathrm{OC} + \mathrm{MC} - \mathrm{SV}, \tag{7.1}$$

where CC,OC, MC and SV are; initial capital cost, running (operation) costs, maintenance cost and salvage value respectively.

The final LCC over the projects' life span is:

$$\mathrm{LLC} = \mathrm{CC} + \sum_{i=1}^{n} \frac{\mathrm{OC}_i + \mathrm{MC}_i}{(1+r)^i} - \mathrm{SV}, \tag{7.2}$$

where i and n are the number of years and project lifetime respectively and r is the discounting factor. The payback period has been done in the previous chapters, though several assumptions were considered (e.g., excluded the energy bills and the cost of the HPWHs). However, in this chapter all these factors are used to calculate a near-realistic LCC.

[1] http://www.accaglobal.com/ng/en/member/professional-standards/members-standards/international-standards.html (Date accessed 15.03.2016)

7.2 LCC OF CHAPTER 3 MODEL

Chapter 3 developed an optimal power dispatch of a grid-tied/battery/PV system supplying HPWH. The detailed LCC results of the four models developed in this thesis are shown in Appendix B. The baseline (existing) is the pre-implementation stage of these proposed OC models, while the post-implementation is the scenario obtaining after installation of OC. The equipment price, equipment useful life, energy tariffs, inflation rate and cost of services are based on local South African market rates[2] where applicable and some are taken from estimates found in literature [130].

7.2.1 LCC analysis of existing system

A $3 \times 15\ kW$ industrial HPWH with useful lifetime of 20 years with an initial total investment cost of R(143 274.00) is analyzed. The salvage value is approximated at R15 000 upon decommissioning. The baseline costs used in this chapter are presented in each respective previous chapter. The OC and baseline energy costs were as well tabulated in the previous chapters. These average daily baseline energy cost are averaged over the seasons and annualized to represent total operation costs in 365 days. The maintenance cost is held constant at R3 500 over the project life span. A discounting factor reflective of the 2014/2015 average inflation rate in South Africa is 4.4% and is kept constant throughout the project life. All amounts indicated in this chapter are in South African rand (ZAR) denoted as R. The daily baseline and the optimal costs are shown in chapter 3 Table 3.1. The LCC cumulative cash flows of baseline scenario are presented in Table B.1.

From Table B.1, it can be seen that the LCC of the pre-implementation scenario over 20 year period has an expense or in other words a negative cash flow. This means the existing system's operation costs are expenses only without income (revenue). This model has a LCC cumulative total R(17 403 132.51) at PV_E. This amount is huge when compared to the the LCC of the proposed OC mitigation discussed in subsection 7.2.2 below. Therefore, an alternative investment choice and new control strategy is necessary.

[2] http://www.sustainable.co.za/water-heating/heat-pumps/industrial.html (Date accessed: 23.03.2016)

7.2.2 LCC analysis of an optimal control system

In contrast to the LCC of the baseline operation strategy, the proposed OC strategy comes with an additional cost on equipment; PV, batteries, controllers and inverters. The LCC of the post implementation is shown in Table B.2. The battery life span is approximated to be 5 years, while the controller system is 10 years [130]. Therefore, a replacement cost in year 6 and year 11 is made and debited into the maintenance cost. The annual cost consists of the operations cost (annualized OC cost) and maintenance cost. The revenue consists of the PV energy sales and the OC benefits. The OC benefits are translated into income owing to the savings, that otherwise in baseline case would have been paid. The OC cumulative cash flows in Table B.2 shows that in year 7 the investor pays the last expense, amounting to R(29 414.82). Thereafter, from year 8, the revenue exceeds the expense. At this stage the system becomes positive NPVand the cumulative cost becomes positive.

This is clearly a positive cash benefit and by the end of the system's useful life, the investors would have received a total of R2 707 590.66. This is a major positive difference of the OC strategy presented in chapter 3. The investors will instead receive more revenue than expense by implementing this model. Otherwise if this model is not implemented as explained above in subsection 7.2.1, the investors will continue paying for this system over 20 years to the tune of R(17 403 132.51). Therefore, ultimately the OC stands out as the best option because after 7 years the revenue will off-set the expenditure.

7.3 LCC OF CHAPTER 4 MODEL

The model under LCC analysis is an optimal control of diesel generator/grid-tied/PV/battery system powering HPWH presented in chapter 4. The case study and operation constraints are similar to the model presented in chapter 3, except the difference in input data and load demand. The addition of the DG back-up is the major difference in this model.

7.3.1 LCC analysis of existing system chapter 4 model

Table B.3 shows the LCC has a negative cumulative cash cash flow of R(13 534 668.59). The existing system has no positive benefits only expenses.

7.3.2 LCC analysis of an optimal control system

The LCC is calculated based on the OC savings in chapter 4 and are shown in Table B.4. The battery has a lifespan of 5 years. The controllers are replaced in year 10. The DG fuel costs according to the OC operation consumed 10 liters/day at R11/liter. The fuel cost is added to the operation cost totaling R(68 251.35). The LCC cumulative cash flows is negative, presented in Table B.4 totaling R(4 432 506.88). There is no positive NPV benefit in this model, only an energy cost reduction is achieved owing to the OC intervention.

LCC analysis shows a negative cash flow in both pre-and post implementation stage. This entails that the expense will continue throughout the project's lifetime. The existing system cumulative cash flows equals to R(13 534 668.59) while the OC is R(4 432 506.88), showing a huge cost reduction. By implementing the OC model actual savings would be R9 102 161.71, which otherwise the investor would have spent in the existing operation scenario. Therefore, the LCC comparison shows a cost saving when OC is used , despite high operational costs due to the DG fuel cost.

7.4 LCC OF CHAPTER 5 MODEL

The model under LCC analysis is presented in chapter 5 an OC of a wind-PV-hybrid powered HPWH. In contrast to the previous LCC in sections 7.2 and 7.3 case study, a domestic 6 kW HPWH was considered. Like in the previous LCC analysis, some capital investment is required for the extra devices in the proposed OC models. The LCC cumulative cash flow of the pre-implementation is given in Table B.5 totaling to R(3 692 314.38) while an OC is R781 074.13 as presented in Table B.6. The LCC at pre-implementation has negative cumulative cash flow meaning the investor would continue incurring energy cost towards the system. On the other hand, the OC LCC cumulative totals are positive, showing that this system is instead earning revenue.

7.5 LCC OF CHAPTER 6 MODEL

The LCC shown in Table B.7 and Table B.8 are for pre-and-post implementation models respectively as was presented in chapter 6. This model is an OC of a fuel cell/wind/PV/grid hybrid system with thermal heat pump load. The fuel cell has a life span of 10 years [130]. The cumulative cash flow

under existing system is R(4 676 620.24), while for the OC is R(2 318 078.51). In both cases, the cumulative cash flows are negative, however the OC reduces the expenditure to about half the amount spent on the existing set-up.

7.6 LCC SUMMARY

The comparison of LCC analysis between the pre-and-post implementation has proved that the OC strategy reduces the lifetime cost and in certain instance gives a positive NPV benefit on cumulative cash flow. The decision whether to implement the OC or not should be thoroughly weighed, given that the OC shows huge cost savings over the project's lifetime. In this work, various combination of RE hybrid models with energy-efficient devices and grid interaction are developed to assess the possible variation on climatic and geographic availability of energy resources in different countries. Therefore, investors/building owners should carefully select which model best fits and has potential for lower operation cost based on the local situation.

Table 7.1. LCC summary table

Model	LCC of existing system	LCC of proposed optimal system	Cost benefits
Chapter 3 model	(17,403,132.51)	2,707,590.66	positive NPV
Chapter 4 model	(13,534,668.59)	(4,432,506.88)	negative NPV
Chapter 5 model	(3,692,314.38)	781,074.13	positive NPV
Chapter 6 model	(4,676,620.24)	(2,318,078.51)	negative NPV

Certain models in this work showed the potential of being positive NPV benefit from power feed-in and on-site DRE power generation. The models can as well attract rebates/incentives in certain countries for turning buildings into NZEB owing to the OC strategy. Therefore, the existing yearly operation though seems affordable at the beginning, will remain an expense for the rest of its project/system life. The LCC analysis is expected to be slightly much more than what has been shown in this chapter, if assumptions were not made on tariff and deprecation.

Finally, the next chapter is the conclusion that summarizes the thesis.

CHAPTER 8 CONCLUSION

This work developed four OC strategy models of the grid-tied renewable energy hybrid system in buildings supplying energy-efficient HPWHs and other household loads. The OC strategy formulation expresses each model component as a function of the control variable. The discrete objective/cost function is based on the TOU tariff and energy cost minimization. The case study is done for each proposed model in each chapter to validate its effectiveness; in many cases the economic analysis is performed to test the commercial viability. The heat pump is used as a DSM mitigation tool owing to its higher energy efficiency in thermal generation and space cooling.

The two most abundant renewable power sources found in South Africa; solar power and wind are modeled together with energy storage and a backup DG system. The high power deficit in various places and a quest to reduce greenhouse gas emissions require harvesting of all available renewable power sources and the use of energy-efficient equipment. Hence, this work strives to integrate various renewable power sources optimally and practically. A brief summary of each chapter's findings are presented below.

8.1 SUMMARY

In chapter 3, an OC strategy for a grid-tied PV system for a heat pump, yielded significant energy cost saving owing to the load-shifting strategy during peak TOU. The chapter presented a new battery usage model for energy storage. The HPWH's operational constraints were satisfied through the use of the actual performance index. This model has a positive NPV based on LCC as shown in Table 7.1 In certain countries incentives/rebates are offered for achieving and participating in renewable energy production and energy-efficiency maximization. There are several advantages of this model, since it is also suitable in regions with intermittent electrical power supply.

In chapter 4, an addition of a backup DG is added to the model develop in chapter 3. This model consisting of PV/grid/ battery/DG powering HPWH and domestic appliances. The DG is a backup power source to the HPWH in periods when the grid and solar power are not available, however the OC operated the DG in peak TOU period because it was much affordable to use diesel fuel than expensive grid energy. Though, this model increases the initial investment cost in comparison to chapter 3 and has a negative NPV. The security of power supply benefits outweighs the cost especially in the event of load shedding due to demand leveling on the supply side. The objective function minimizes energy and fuel cost while maximizing PV energy feed-in. The OC shows great potential to realize a practical NZEB and DSM. According to a case study the OC achieved huge savings both on energy and cost. The model showed the potential to save up to 114.06 kWh of energy daily, with a maximum cost saving of 68.09%. The higher cost saving is realized since the battery connection model is used only as storage of cheaper-to-buy grid energy. The TOU electricity tariff played an important part in the further reduction of energy cost because the battery could be charged in off-peak TOU. The chapter's model can enable end-user customers to trade off solar energy in return for incentives for participation in DSM. This contributes to the improvement of the utility's power reserves and security of supply through individual participation at building level.

In chapter 5, an OC model of a HPWH supplied by a wind generator-PV-grid system is presented. The objective function is energy cost minimization, taking into account the TOU electricity tariff. The model meets both the HPWH's technical and operational constraints in providing hot water at a desired temperature and achieving load shifting. The results show a 70.7% cost reduction upon implementation of this intervention. In the case study carried out, the OC shows significant potential for both energy and cost saving in comparison to the digital thermostat controller used in most of the HPWHs on the market. A maximum energy saving of 51.23% has been achieved and the system has the potential to be cost-effective on energy bills. This intervention provides practical optimal integration of wind and other DREs into homes, with the benefit of energy trade-off and the possibility of achieving a net zero-energy building.

The economic analysis shows a payback period of 3 years and 9 months and in addition this model has a positive NPV on LCC analysis. There are other incentives pertaining to rebates on HPWH, wind power and solar PV application that were not considered in this chapter, which are evident in the case study and could further reduce the payback period. This model is suitable for application in both peri-urban and rural areas, in the generation of hot water, space heating and renewable energy

integration.

Chapter 6 presented an optimal energy management strategy FC hybrid power supply system. The hybrid system meets the load demand consisting of an electrical load and a HPWH supplying thermal load. The objective was to minimize energy cost and maximize FC output, taking into account the TOU electricity tariff. The OC problem was solved using mixed binary and real linear programming. The supply switch to the HPWH and the power from the grid, power to/from the inverter, electrolyzer hydrogen power and FC power were the control variables. The temperature inside the water storage tank and the hydrogen in the storage tank were the state variables. The performance of the proposed control strategy was tested by simulating different operating scenarios, with and without renewable energy feed-in, and the results confirmed its effectiveness, as it increased the supply reliability of the system. The model had a daily optimal energy saving potential of 27.68% and a cost saving of 33.8%. Optimal operation of the FC and the required hot water temperature were achieved.

Finally, chapter 7 showed the comparison based on LCC analysis between pre-and-post implementation of the developed models. In all the models, the OC either reduced the energy or gave a positive NPV when compared to the existing system.

The Table 8.1 below shows the comparison based on the LCC analysis the positives/negatives of each of the four models. Several techniques are used to assess the advantages/disadvantages of each model such as: (a) general limitations of the model; (b) data requirements for the model (c) levels of difficulties in result interpretation; (d) the best model on LCC analysis. The advantages are depicted with a '+' and the disadvantages with a '-'.

Table 8.1. Summary comparison table of the positives and negatives of the models

Model	General limitations	Input data requirement	Results interpretation	LCC
Chapter 3 model	+	-	-	+
Chapter 4 model	+	-	-	-
Chapter 5 model	+	+	+	+
Chapter 6 model	-	-	+	-

Therefore, from the results model 5 has the highest positive benefits.

8.2 RECOMMENDATION AND FUTURE RESEARCH

1) Although this work developed open-loop OC strategies of a DREs-HPWH hybrid system, there is a need for future research into the application of closed-loop techniques such as MPC. This can minimize the uncertainty and unexpected disturbances resulting from hot water demand, solar radiation, water ambient temperature and wind velocity variations.

2) Developing an OC energy model incorporating other renewable sources, such as biomass, combine heat and power system powering HPWH could greatly save energy and increase the utility power reserves and security of supply.

3) This work did not look in the quantification on the climate benefit, carbon emission reduction, it would be of great help to quantify exactly these environmental benefits and savings on primary inputs of energy production.

4) The HPWHs might appear to have higher initial investment cost,but in the long run the benefits of energy saving, energy cost, and protection of the environment outweigh the initial costs. Such energy-efficient devices should be encouraged through incentives/rebates and rolled out by utilities firms/governments in every house.

5) Since the COP of HPWH is not a constant value as assumed in this thesis. It could be interesting in the future research to consider a variable COP.

6) The future work should look at developing the cost function model for commercial buildings where the hot water energy demand is primarily during the day

REFERENCES

[1] A. A. Bayod-Rújula, "Future development of the electricity systems with distributed generation," *Energy*, vol. 34, no. 3, pp. 377–383, 2009.

[2] J. Torriti, M. G. Hassan, and M. Leach, "Demand response experience in Europe: Policies, programmes and implementation," *Energy*, vol. 35, no. 4, pp. 1575–1583, 2010.

[3] P. Bradley, M. Leach, and J. Torriti, "A review of the costs and benefits of demand response for electricity in the UK," *Energy Policy*, vol. 52, pp. 312–327, 2013.

[4] J.-H. Kim and A. Shcherbakova, "Common failures of demand response," *Energy*, vol. 36, no. 2, pp. 873–880, 2011.

[5] P. Faria and Z. Vale, "Demand response in electrical energy supply: An optimal real time pricing approach," *Energy*, vol. 36, pp. 5374–5384, 2011.

[6] G. Strbac, "Demand side management: Benefits and challenges," *Energy Policy*, vol. 36, no. 12, pp. 4419–4426, 2008.

[7] P. Finn, C. Fitzpatrick, D. Connolly, M. Leahy, and L. Relihan, "Facilitation of renewable electricity using price based appliance control in Ireland's electricity market," *Energy*, vol. 36, no. 5, pp. 2952–2960, 2011.

[8] K. Chua, S. Chou, and W. Yang, "Advances in heat pump systems: A review," *Applied Energy*, vol. 87, no. 12, pp. 3611–3624, 2010.

[9] R. Rankin, P. G. Rousseau, and M. van Eldik, "Demand side management for commercial buildings using an inline heat pump water heating methodology," *Energy Conversion and Management*, vol. 45, no. 9, pp. 1553–1563, 2004.

[10] M. M. Rahman, M. Rasul, and M. M. K. Khan, "Energy conservation measures in an institutional building in sub-tropical climate in Australia," *Applied Energy*, vol. 87, no. 10, pp. 2994–3004, 2010.

[11] M. H. Albadi and E. El-Saadany, "A summary of demand response in electricity markets," *Electric Power Systems Research*, vol. 78, no. 11, pp. 1989–1996, 2008.

[12] A. J. Conejo, J. M. Morales, and L. Baringo, "Real-time demand response model," *Smart Grid, IEEE Transactions on*, vol. 1, no. 3, pp. 236–242, 2010.

[13] S. Sichilalu, T. Mathaba, and X. Xia, "Optimal control of a wind-PV-hybrid powered heat pump water heater," *Applied Energy*, vol. http://dx.doi.org/10.1016/j.apenergy.2015.10.072, 2015.

[14] A. Hepbasli and Y. Kalinci, "A review of heat pump water heating systems," *Renewable and Sustainable Energy Reviews*, vol. 13, no. 6, pp. 1211–1229, 2009.

[15] X. Sun, Y. Dai, V. Novakovic, J. Wu, and R. Wang, "Performance comparison of direct expansion solar-assisted heat pump and conventional air source heat pump for domestic hot water," *Energy Procedia*, vol. 70, pp. 394 – 401, 2015.

[16] M. Mehrpooya, H. Hemmatabady, and M. H. Ahmadi, "Optimization of performance of combined solar collector-geothermal heat pump systems to supply thermal load needed for heating greenhouses," *Energy Conversion and Management*, vol. 97, pp. 382 – 392, 2015.

[17] K. Kusakana, "Operation cost minimization of photovoltaic–diesel–battery hybrid systems," *Energy*, vol. 85, pp. 645–653, 2015.

[18] C. Fraga, F. Mermoud, P. Hollmuller, E. Pampaloni, and B. Lachal, "Large solar driven heat pump system for a multifamily building: Long term in-situ monitoring," *Solar Energy*, vol. 114,

pp. 427 – 439, 2015.

[19] C. Verhelst, D. Degrauwe, F. Logist, J. van Impe, and L. Helsen, "Multi-objective optimal control of an air-to-water heat pump for residential heating," *Building Simulation*, vol. 5, no. 3, pp. 281–291, 2012.

[20] L. Paull, H. Li, and L. Chang, "A novel domestic electric water heater model for a multi-objective demand side management program," *Electric Power Systems Research*, vol. 80, no. 12, pp. 1446–1451, 2010.

[21] M. Ranaboldo, B. Domenech, G. A. Reyes, L. Ferrer-Martí, R. P. Moreno, and A. García-Villoria, "Off-grid community electrification projects based on wind and solar energies: A case study in Nicaragua," *Solar Energy*, vol. 117, pp. 268–281, 2015.

[22] C. Verhelst, F. Logist, J. van Impe, and L. Helsen, "Study of the optimal control problem formulation for modulating air-to-water heat pumps connected to a residential floor heating system," *Energy and Buildings*, vol. 45, pp. 43–53, 2012.

[23] S. M. Sichilalu and X. Xia, "Optimal energy control of grid tied PV–diesel–battery hybrid system powering heat pump water heater," *Solar Energy*, vol. 115, pp. 243–254, 2015.

[24] M. Ellis, M. von Spakovsky, and D. Nelson, "Fuel cell systems: Efficient, flexible energy conversion for the 21st century," vol. 89, no. 12, Dec 2001, pp. 1808–1818.

[25] A. Mellit, M. Benghanem, and S. Kalogirou, "Modeling and simulation of a stand-alone photovoltaic system using an adaptive artificial neural network: Proposition for a new sizing procedure," *Renewable Energy*, vol. 32, no. 2, pp. 285 – 313, 2007.

[26] W. Kellogg, M. Nehrir, G. Venkataramanan, and V. Gerez, "Optimal unit sizing for a hybrid wind/photovoltaic generating system," *Electric Power Systems Research*, vol. 39, no. 1, pp. 35 – 38, 1996.

[27] T. Khatib, A. Mohamed, and K. Sopian, "Optimization of a PV/wind micro-grid for rural housing electrification using a hybrid iterative/genetic algorithm: Case study of Kuala Terengganu, Malaysia," *Energy and Buildings*, vol. 47, pp. 321–331, 2012.

[28] C. Nayar, S. Phillips, W. James, T. Pryor, and D. Remmer, "Novel wind/diesel/battery hybrid energy system," *Solar Energy*, vol. 51, no. 1, pp. 65 – 78, 1993.

[29] T. Mathaba, M. Mpholo, and M. Letuma, "Velocity and power density analysis of the wind at Letšeng-la-terae in Lesotho," *Renewable Energy*, vol. 46, pp. 210–217, 2012.

[30] M. Moghavvemi, M. Ismail, B. Murali, S. Yang, A. Attaran, and S. Moghavvemi, "Development and optimization of a PV/diesel hybrid supply system for remote controlled commercial large scale FM transmitters," *Energy Conversion and Management*, vol. 75, pp. 542–551, 2013.

[31] Y. Zhao, Y. Lu, C. Yan, and S. Wang, "MPC-based optimal scheduling of grid-connected low energy buildings with thermal energy storages," *Energy and Buildings*, vol. 86, pp. 415–426, 2015.

[32] H. Tazvinga, X. Xia, and J. Zhang, "Minimum cost solution of photovoltaics-diesel-battery hybrid power systems for remote consumers," *Solar Energy*, vol. 96, pp. 292–299, 2013.

[33] P. A. Torcellini and D. B. Crawley, "Understanding zero-energy buildings," *ASHRAE Journal*, vol. 48, no. 9, pp. 62–69, 2006.

[34] W. Zeiler and G. Boxem, "Net-zero energy building schools," *Renewable Energy*, vol. 49, pp. 282 – 286, 2013.

[35] A. Marszal, P. Heiselberg, J. Bourrelle, E. Musall, K. Voss, I. Sartori, and A. Napolitano, "Zero energy building - a review of definitions and calculation methodologies," *Energy and Buildings*, vol. 43, no. 4, pp. 971 – 979, 2011.

[36] A. Scognamiglio and H. N. Røstvik, "Photovoltaics and zero energy buildings: a new opportunity and challenge for design," *Progress in Photovoltaics: Research and Applications*, vol. 21,

no. 6, pp. 1319–1336, 2013.

[37] S. C. Bengea and R. A. Decarlo, "Optimal control of switching systems," *Automatica*, vol. 41, no. 1, pp. 11–27, 2005.

[38] S. Sichilalu, X. Xia, and J. Zhang, "Optimal scheduling strategy for a grid-connected photovoltaic system for heat pump water heaters," *Energy Procedia*, vol. 61, pp. 1511–1514, 2014.

[39] S. M. Sichilalu and X. Xia, "Optimal power dispatch of a grid tied-battery-photovoltaic system supplying heat pump water heaters," *Energy Conversion and Management*, vol. 102, pp. 81 – 91, 2015.

[40] M. Bouzerdoum, A. Mellit, and A. Massi Pavan, "A hybrid model (sarima–svm) for short-term power forecasting of a small-scale grid-connected photovoltaic plant," *Solar Energy*, vol. 98, pp. 226–235, 2013.

[41] N. Roonprasang, P. Namprakai, and N. Pratinthong, "Experimental studies of a new solar water heater system using a solar water pump," *Energy*, vol. 33, no. 4, pp. 639–646, 2008.

[42] I. M. Ross, *A primer on pontryagin's principle in optimal control*. Collegiate Publishers, 2015.

[43] J. Richalet, A. Rault, J. Testud, and J. Papon, "Model predictive heuristic control: Applications to industrial processes," *Automatica*, vol. 14, no. 5, pp. 413–428, 1978.

[44] A. J. Marszal, J. S. Bourrelle, E. Musall, P. Heiselberg, A. Gustavsen, and K. Voss, "Net zero energy buildings-calculation methodologies versus national building codes," *The Proceedings of EuroSun*, 2010.

[45] M. Stadler, A. Siddiqui, C. Marnay, H. Aki, and J. Lai, "Control of greenhouse gas emissions by optimal DER technology investment and energy management in zero-net-energy buildings," *European Transactions on Electrical Power*, vol. 21, no. 2, pp. 1291–1309, 2011.

[46] R. K. Mehra, R. Rouhani, J. Eterno, J. Richalet, and A. Rault, "Model algorithmic control: review and recent developments," in *Proceedings of the Eng. Foundation Conf. on Chemical Process Control II*, 1982, pp. 287–310.

[47] A. Li, "Comparison between Model Predictive Control and PID control for water-level maintenance in a two-tank system," Ph.D. dissertation, University of Pittsburgh, 2010.

[48] P. Rousseau and G. Greyvenstein, "Enhancing the impact of heat pump water heaters in the South African commercial sector," *Energy*, vol. 25, no. 1, pp. 51–70, 2000.

[49] A. Pegels, "Renewable energy in South Africa: Potentials, barriers and options for support," *Energy Policy*, vol. 38, no. 9, pp. 4945–4954, 2010.

[50] K. Menyah and Y. Wolde-Rufael, "Energy consumption, pollutant emissions and economic growth in South Africa," *Energy Economics*, vol. 32, no. 6, pp. 1374–1382, 2010.

[51] H. Winkler, "Renewable energy policy in South Africa: Policy options for renewable electricity," *Energy Policy*, vol. 33, no. 1, pp. 27–38, 2005.

[52] M. G. Patterson, "What is energy efficiency?: Concepts, indicators and methodological issues," *Energy Policy*, vol. 24, no. 5, pp. 377–390, 1996.

[53] R. Spalding-Fecher, A. Clark, M. Davis, and G. Simmonds, "The economics of energy efficiency for the poor: A South African case study," *Energy*, vol. 27, no. 12, pp. 1099–1117, 2002.

[54] T. Chow, Y. Bai, K. Fong, and Z. Lin, "Analysis of a solar assisted heat pump system for indoor swimming pool water and space heating," *Applied Energy*, vol. 100, pp. 309–317, 2012.

[55] H. Esen, M. Inalli, and M. Esen, "Technoeconomic appraisal of a ground source heat pump system for a heating season in Eastern Turkey," *Energy Conversion and Management*, vol. 47, no. 10, pp. 1281 – 1297, 2006.

[56] M. Esen and T. Yuksel, "Experimental evaluation of using various renewable energy sources for heating a greenhouse," *Energy and Buildings*, vol. 65, pp. 340 – 351, 2013.

[57] J. Tamasauskas, M. Poirier, R. Zmeureanu, and R. Sunyé, "Modeling and optimization of a solar assisted heat pump using ice slurry as a latent storage material," *Solar Energy*, vol. 86, no. 11, pp. 3316–3325, 2012.

[58] X. Zhang, X. Zhao, J. Xu, and X. Yu, "Characterization of a solar photovoltaic/loop-heat-pipe heat pump water heating system," *Applied Energy*, vol. 102, pp. 1229–1245, 2013.

[59] J. Ji, G. Pei, T.-t. Chow, W. He, A. Zhang, J. Dong, and H. Yi, "Performance of multi-functional domestic heat-pump system," *Applied Energy*, vol. 80, no. 3, pp. 307–326, 2005.

[60] I. Lane and N. Beute, "A model of the domestic hot water load," *Power Systems, IEEE Transactions on*, vol. 11, no. 4, pp. 1850–1855, 1996.

[61] Y. Tian and C.-Y. Zhao, "A review of solar collectors and thermal energy storage in solar thermal applications," *Applied Energy*, vol. 104, pp. 538–553, 2013.

[62] M. W. Ahmad, M. Eftekhari, T. Steffen, and A. M. Danjuma, "Investigating the performance of a combined solar system with heat pump for houses," *Energy and Buildings*, vol. 63, pp. 138–146, 2013.

[63] E. Kjellsson, G. Hellström, and B. Perers, "Optimization of systems with the combination of ground-source heat pump and solar collectors in dwellings," *Energy*, vol. 35, no. 6, pp. 2667–2673, 2010.

[64] J. Zhang, R. Wang, and J. Wu, "System optimization and experimental research on air source heat pump water heater," *Applied Thermal Engineering*, vol. 27, no. 5, pp. 1029–1035, 2007.

[65] H. Lund, "Renewable energy strategies for sustainable development," *Energy*, vol. 32, pp. 912 – 919, 2007.

[66] N. H. Afgan and M. G. Carvalho, "Multi-criteria assessment of new and renewable energy power plants," *Energy*, vol. 27, no. 8, pp. 739–755, 2002.

[67] Z. Abdmouleh, R. A. Alammari, and A. Gastli, "Review of policies encouraging renewable energy integration and best practices," *Renewable and Sustainable Energy Reviews*, vol. 45, pp. 249–262, 2015.

[68] P. Arul, V. K. Ramachandaramurthy, and R. Rajkumar, "Control strategies for a hybrid renewable energy system: A review," *Renewable and Sustainable Energy Reviews*, vol. 42, pp. 597–608, 2015.

[69] N. H. Afgan and M. G. Carvalho, "Sustainability assessment of hydrogen energy systems," *International Journal of Hydrogen Energy*, vol. 29, no. 13, pp. 1327–1342, 2004.

[70] X. Li, "Diversification and localization of energy systems for sustainable development and energy security," *Energy Policy*, vol. 33, no. 17, pp. 2237–2243, 2005.

[71] T. Hove and H. Tazvinga, "A techno-economic model for optimising component sizing and energy dispatch strategy for PV-diesel-battery hybrid power systems," *Journal of Energy in Southern Africa*, vol. 23, no. 4, pp. 18–28, 2012.

[72] R. Dufo-Lopez, J. L. Bernal-Agustin, J. M. Yusta-Loyo, J. Dominguez-Navarro, I. J. Ramirez-Rosado, J. Lujano, and I. Aso, "Multi-objective optimization minimizing cost and life cycle emissions of stand-alone PV–wind–diesel systems with batteries storage," *Applied Energy*, vol. 88, no. 11, pp. 4033–4041, 2011.

[73] A. Choudar, D. Boukhetala, S. Barkat, and J.-M. Brucker, "A local energy management of a hybrid PV-storage based distributed generation for microgrids," *Energy Conversion and Management*, vol. 90, pp. 21–33, 2015.

[74] M. Korpås and A. T. Holen, "Operation planning of hydrogen storage connected to wind power operating in a power market," *Energy Conversion, IEEE Transactions on*, vol. 21, no. 3, pp. 742–749, 2006.

[75] H. Tazvinga, B. Zhu, and X. Xia, "Energy dispatch strategy for a photovoltaic–wind–diesel–battery hybrid power system," *Solar Energy*, vol. 108, pp. 412–420, 2014.

[76] N. Bizon, M. Oproescu, and M. Raceanu, "Efficient energy control strategies for a stand-alone renewable/fuel cell hybrid power source," *Energy Conversion and Management*, vol. 90, pp. 93–110, 2015.

[77] S. Singh, M. Singh, S. Chanana, and S. Semwal, "Frequency regulation of isolated hybrid wind/diesel, power generation with fuel cell system," in *Power Electronics and Renewable Energy Systems*. Springer India, 2015, pp. 853–862.

[78] H. Lund, "Large-scale integration of optimal combinations of PV, wind and wave power into the electricity supply," *Renewable Energy*, vol. 31, no. 4, pp. 503–515, 2006.

[79] G. M. Montes, M. d. M. S. López, M. d. C. R. Gámez, and A. M. Ondina, "An overview of renewable energy in Spain: The small hydro-power case," *Renewable and Sustainable Energy Reviews*, vol. 9, no. 5, pp. 521–534, 2005.

[80] R. Baños, F. Manzano-Agugliaro, F. Montoya, C. Gil, A. Alcayde, and J. Gómez, "Optimization methods applied to renewable and sustainable energy: A review," *Renewable and Sustainable Energy Reviews*, vol. 15, no. 4, pp. 1753–1766, 2011.

[81] E. Oró, V. Depoorter, A. Garcia, and J. Salom, "Energy efficiency and renewable energy integration in data centres. Strategies and modelling review," *Renewable and Sustainable Energy Reviews*, vol. 42, pp. 429–445, 2015.

[82] D.-Z. Du and P. M. Pardalos, *Handbook of combinatorial optimization: Supplement*. Springer Science and Business Media, 2013, vol. 1.

[83] H. Panagopoulos, K. J. Åström, and T. Hägglund, "Design of PID controllers based on constrained optimisation," *IEE Proceedings-Control Theory and Applications*, vol. 149, no. 1, pp. 32–40, 2002.

[84] A. Voda and I. Landau, "A method for the auto-calibration of PID controllers," *Automatica*, vol. 31, no. 1, pp. 41–53, 1995.

[85] S.-Z. He, S. Tan, F.-L. Xu, and P.-Z. Wang, "Fuzzy self-tuning of PID controllers," *Fuzzy Sets and Systems*, vol. 56, no. 1, pp. 37–46, 1993.

[86] P. Hajela and C.-Y. Lin, "Genetic search strategies in multicriterion optimal design," *Structural Optimization*, vol. 4, no. 2, pp. 99–107, 1992.

[87] D. E. Goldberg and J. H. Holland, "Genetic algorithms and machine learning," *Machine Learning*, vol. 3, no. 2, pp. 95–99, 1988.

[88] C. Kahraman, İ. Kaya, and S. Cebi, "A comparative analysis for multiattribute selection among renewable energy alternatives using fuzzy axiomatic design and fuzzy analytic hierarchy process," *Energy*, vol. 34, no. 10, pp. 1603–1616, 2009.

[89] R. Baasos, F. Manzano-Agugliaro, F. Montoya, C. Gil, A. Alcayde, and J. Gaşmez, "Optimization methods applied to renewable and sustainable energy: A review," *Renewable and Sustainable Energy Reviews*, vol. 15, pp. 1753 – 1766, 2011.

[90] S. M. Sichilalu and X. Xia, "Optimal power dispatch of a grid tied-battery-photovoltaic system supplying heat pump water heaters," *Energy Conversion and Management*, vol. 102, pp. 81 – 91, 2015.

[91] N. Pardo, Á. Montero, J. Martos, and J. Urchueguía, "Optimization of hybrid–ground coupled and air source–heat pump systems in combination with thermal storage," *Applied Thermal Engineering*, vol. 30, no. 8, pp. 1073–1077, 2010.

[92] M. Hawlader, S. Chou, and M. Ullah, "The performance of a solar assisted heat pump water heating system," *Applied Thermal Engineering*, vol. 21, no. 10, pp. 1049–1065, 2001.

[93] P. Belotti, C. Kirches, S. Leyffer, J. Linderoth, J. Luedtke, and A. Mahajan, "Mixed-integer nonlinear optimization," *Acta Numerica*, vol. 22, pp. 1–131, 2013.

[94] J. L. B.-A. Rodolfo Dufo-Lopez, "Influence of mathematical models in design of PV-diesel systems," *Energy Conversion and Management*, vol. 49, no. 4, pp. 820 – 831, 2008.

[95] S.-K. Kim, J.-H. Jeon, C.-H. Cho, J.-B. Ahn, and S.-H. Kwon, "Dynamic modeling and control of a grid-connected hybrid generation system with versatile power transfer," *Industrial Electronics, IEEE Transactions on*, vol. 55, no. 4, pp. 1677–1688, April 2008.

[96] T. Ikegami, Y. Iwafune, and K. Ogimoto, "Optimum operation scheduling model of domestic electric appliances for balancing power supply and demand," in *IEEE International Conference on Power System Technology*, 2010.

[97] M. Ashari and C. Nayar, "An optimum dispatch strategy using set points for a photovoltaic (PV)–diesel–battery hybrid power system," *Solar Energy*, vol. 66, no. 1, pp. 1–9, 1999.

[98] S. Ashok, "Optimised model for community-based hybrid energy system," *Renewable Energy*, vol. 32, no. 7, pp. 1155–1164, 2007.

[99] R. Dufo-Lopez and J. L. Bernal-Agustin, "Multi-objective design of pv-wind-diesel-hydrogen-battery systems," *Renewable energy*, vol. 33, no. 12, pp. 2559–2572, 2008.

[100] R. Belfkira, L. Zhang, and G. Barakat, "Optimal sizing study of hybrid wind/PV/diesel power generation unit," *Solar Energy*, vol. 85, no. 1, pp. 100 – 110, 2011.

[101] D. Tungadio, B.P.Numbi, M. Siti, and A. Jimoh, "Particle swarm optimization for power system state estimation," *Neurocomputing*, vol. 148, pp. 175 –180, 2015.

[102] M. Kim, M. S. Kim, and J. D. Chung, "Transient thermal behavior of a water heater system driven by a heat pump," *International journal of refrigeration*, vol. 27, no. 4, pp. 415–421, 2004.

[103] J. Zhang and X. Xia, "Best switching time of hot water cylinder-switched optimal control approach," in *AFRICON 2007*. IEEE, 2007, pp. 1–7.

[104] K. Khan, M. Rasul, and M. M. K. Khan, "Energy conservation in buildings: Cogeneration and cogeneration coupled with thermal energy storage," *Applied Energy*, vol. 77, no. 1, pp. 15–34, 2004.

[105] M. Gustafson, J. Baylor, and G. Epstein, "Direct water heater load control-estimating program effectiveness using an engineering model," *Power Systems, IEEE Transactions on*, vol. 8, no. 1, pp. 137–143, 1993.

[106] P. Dolan, M. Nehrir, and V. Gerez, "Development of a Monte Carlo based aggregate model for residential electric water heater loads," *Electric Power Systems Research*, vol. 36, no. 1, pp. 29–35, 1996.

[107] H. Li, Z. Chen, and H. Polinder, "Optimization of multibrid permanent-magnet wind generator systems," *Energy Conversion, IEEE Transactions on*, vol. 24, no. 1, pp. 82–92, 2009.

[108] Department of Water Affairs and Forestry, South Africa, "Water conservation and demand management strategy for the water services sectors," August 2004.

[109] J. P. Meyer, "A review of domestic hot-water consumption in South Africa," *R&D Journal*, vol. 16, pp. p55–61, 2000.

[110] J. Meyer and M. Tshimankinda, "Domestic hot water consumption in South African townhouses," *Energy Conversion and Management*, vol. 39, no. 7, pp. 679–684, 1998.

[111] J. Jaffe, R. Randolph Westerfield *et al.*, *Corporate finance*. Tata McGraw-Hill Education, 2005.

[112] W. J. Fabrycky and B. Blanchard, *Life-cycle cost and economic analysis*. Prentice Hall, 1991.

[113] P. Rodatz, G. Paganelli, A. Sciarretta, and L. Guzzella, "Optimal power management of an experimental fuel cell/supercapacitor-powered hybrid vehicle," *Control Engineering Practice*, vol. 13, no. 1, pp. 41–53, 2005.

[114] J. T. Pukrushpan, A. G. Stefanopoulou, and H. Peng, *Control of fuel cell power systems: Principles, modeling, analysis and feedback design*. Springer Science & Business Media, 2004.

[115] S. Sichilalu, H. Tazvinga, and X. Xia, "Optimal control of a fuel cell/wind/pv/grid hybrid system with thermal heat pump load," *Solar Energy*, vol. 135, pp. 59–69, 2016.

[116] R. Belfkira, L. Zhang, and G. Barakat, "Optimal sizing study of hybrid wind/PV/diesel power generation unit," *Solar Energy*, vol. 85, no. 1, pp. 100–110, 2011.

[117] M. R. Patel, *Wind and Solar Power Systems: Design, Analysis, and Operation*. CRC Press, 2006, Boca Raton, FL.

[118] L. Lu, H. Yang, and J. Burnett, "Investigation on wind power potential on Hong Kong islands : An analysis of wind power and wind turbine characteristics," *Renewable Energy*, vol. 27, no. 1, pp. 1–12, 2002.

[119] C. Bueno and J. Carta, "Technical–economic analysis of wind-powered pumped hydrostorage systems. part i: model development," *Solar Energy*, vol. 78, no. 3, pp. 382–395, 2005.

[120] C. Wallmark and P. Alvfors, "Design of stationary PEFC system configurations to meet heat and power demands," *Journal of Power Sources*, vol. 106, no. 1, pp. 83–92, 2002.

[121] A. K. Kaviani, G. Riahy, and S. M. Kouhsari, "Optimal design of a reliable hydrogen-based stand-alone wind/PV generating system, considering component outages," *Renewable Energy*, vol. 34, no. 11, pp. 2380–2390, 2009.

[122] M. Leckner and R. Zmeureanu, "Life cycle cost and energy analysis of a Net Zero Energy House with solar combisystem," *Applied Energy*, vol. 88, no. 1, pp. 232–241, 2011.

[123] M. Ryghaug and K. H. Sørensen, "How energy efficiency fails in the building industry," *Energy Policy*, vol. 37, no. 3, pp. 984–991, 2009.

[124] M. Jakob, "Marginal costs and co-benefits of energy efficiency investments: The case of the Swiss residential sector," *Energy policy*, vol. 34, no. 2, pp. 172–187, 2006.

[125] A. Dell'Isola and S. J. Kirk, *Life cycle costing for facilities*. RSMeans, 2003, vol. 51.

[126] D. G. Cople and E. S. Brick, "A simulation framework for technical systems life cycle cost analysis," *Simulation Modelling Practice and Theory*, vol. 18, no. 1, pp. 9–34, 2010.

[127] A. J. Marszal, P. Heiselberg, R. L. Jensen, and J. NÃÿrgaard, "On-site or off-site renewable energy supply options? life cycle cost analysis of a Net Zero Energy Building in Denmark ," *Renewable Energy*, vol. 44, pp. 154 – 165, 2012.

[128] A. Sherwani, J. Usmani *et al.*, "Life cycle assessment of solar pv based electricity generation systems: A review," *Renewable and Sustainable Energy Reviews*, vol. 14, no. 1, pp. 540–544, 2010.

[129] L. Zhang, X. Xia, and J. Zhang, "Improving energy efficiency of cyclone circuits in coal beneficiation plants by pump-storage systems," *Applied Energy*, vol. 119, pp. 306–313, 2014.

[130] T. Mahlia and P. Chan, "Life cycle cost analysis of fuel cell based cogeneration system for residential application in Malaysia," *Renewable and Sustainable Energy Reviews*, vol. 15, no. 1, pp. 416–426, 2011.

APPENDIX A CHAPTER 5 ALGORITHM FORMULATION

The proposed model has a binary variable and real number control variables, solved using the *OPTI toolbox* SCIP algorithm in MATLAB.

A.0.0.1 Inequality matrices

The general formulation of the inequality constraint is shown in equation (A.1):

$$\mathbf{AX} \leq \mathbf{b}. \tag{A.1}$$

Vector $\mathbf{X}$ comprises all the control variables: switch u_k and grid power P_g written in equation (A.3). Let matrix $\mathbf{A}$ and vector $\mathbf{b}$ be:

$$\mathbf{A} = \begin{bmatrix} \mathbf{A_1} \\ -\mathbf{A_1} \end{bmatrix}, \qquad \mathbf{b} = \begin{bmatrix} \mathbf{b_1} \\ \mathbf{b_2} \end{bmatrix}, \tag{A.2}$$

and,

$$\mathbf{X} = \begin{bmatrix} u_0 \\ \vdots \\ u_{N-1} \\ P_{g,0} \\ \vdots \\ P_{g,N-1} \end{bmatrix}_{2N\times 1}. \tag{A.3}$$

Then matrix $\mathbf{A_1}$ is an $N \times 2N$ matrix given in equation (A.4):

$$\mathbf{A_1} = t_s\beta \begin{bmatrix} 1 & 0 & 0 & 0 & \dots & 0 & 0 & \dots & 0 \\ (1-t_s\alpha_1) & 1 & 0 & 0 & \dots & 0 & 0 & \dots & 0 \\ (1-t_s\alpha_2)(1-t_s\alpha_1) & (1-t_s\alpha_2) & 1 & 0 & \dots & 0 & 0 & \dots & 0 \\ \vdots & \vdots & \vdots & \ddots & \vdots & \vdots & 0 & \dots & 0 \\ (1-t_s\alpha_{N-2})\times\dots\times(1-t_s\alpha_1) & (1-t_s\alpha_{N-2})\times\dots\times(1-t_s\alpha_2) & \dots & \dots & 1 & 0 & 0 & \dots & 0 \\ (1-t_s\alpha_{N-1})(1-t_s\alpha_{N-2})\times\dots\times(1-t_s\alpha_1) & (1-t_s\alpha_{N-1})\times\dots\times(1-t_s\alpha_2) & \dots & \dots & (1-t_s\alpha_{N-1}) & 1 & 0 & \dots & 0 \end{bmatrix}, \tag{A.4}$$

inequality (5.21) is reformulated into inequality (A.5) and inequality (A.6):

$$t_s\beta \sum_{j=0}^{k} u_j \prod_{i=j+1}^{k} (1-t_s\alpha_i) \leq T_{up} - T_o \prod_{j=0}^{k} (1-t_s\alpha_j) - \sum_{j=0}^{k} t_s\gamma_j \prod_{i=j+1}^{k} (1-t_s\alpha_i), \tag{A.5}$$

$$-t_s\beta \sum_{j=0}^{k} u_j \prod_{i=j+1}^{k} (1-t_s\alpha_i) \leq -T_{low} + T_o \prod_{j=0}^{k} (1-t_s\alpha_j) + \sum_{j=0}^{k} t_s\gamma_j \prod_{i=j+1}^{k} (1-t_s\alpha_i). \tag{A.6}$$

According to inequality (A.5) and inequality (A.6), the element of vectors $\mathbf{b_1}$ and $\mathbf{b_2}$ is:

$$b_{1,k} = T_{up} - T_o \prod_{j=0}^{k} (1-t_s\alpha_j) - \sum_{j=0}^{k} t_s\gamma_j \prod_{i=j+1}^{k} (1-t_s\alpha_i), \tag{A.7}$$

$$b_{2,k} = -T_{low} + T_o \prod_{j=0}^{k} (1-t_s\alpha_j) + \sum_{j=0}^{k} t_s\gamma_j \prod_{i=j+1}^{k} (1-t_s\alpha_i). \tag{A.8}$$

Vector $\mathbf{b_1}$ in equation (A.7) is the difference in three vectors $\mathbf{b_3}$, $\mathbf{b_4}$ and $\mathbf{b_5}$, as shown in equation (A.9).

$$\mathbf{b_1} = \mathbf{b_3} - \mathbf{b_4} - \mathbf{b_5}, \tag{A.9}$$

where,

$$\mathbf{b_3} = \begin{bmatrix} T_{up} \\ \vdots \\ T_{up} \end{bmatrix}_{N\times 1}, \tag{A.10}$$

then vector $\mathbf{b_4}$ is given in equation (A.11),

$$\mathbf{b_4} = T_o \begin{bmatrix} (1-t_s\alpha_0) \\ (1-t_s\alpha_1)(1-t_s\alpha_0) \\ (1-t_s\alpha_2)(1-t_s\alpha_1)(1-t_s\alpha_0) \\ \vdots \\ (1-t_s\alpha_{N-2})(1-t_s\alpha_{N-3})\times\ldots\times(1-t_s\alpha_0) \\ (1-t_s\alpha_{N-1})(1-t_s\alpha_{N-2})(1-t_s\alpha_{N-3})\times\ldots\times(1-t_s\alpha_0) \end{bmatrix}_{N\times 1}, \tag{A.11}$$

and finally, $\mathbf{b_5}$ is given in equation (A.12) below,

$$\mathbf{b_5} = \begin{bmatrix} t_s\gamma_o \\ (1-t_s\alpha_1)t_s\gamma_o + t_s\gamma_1 \\ (1-t_s\alpha_2)(1-t_s\alpha_1)t_s\gamma_o + (1-t_s\alpha_2)t_s\gamma_1 + t_s\gamma_2 \\ \vdots \\ (1-t_s\alpha_{N-2})\times\ldots\times(1-t_s\alpha_1)t_s\gamma_o + (1-t_s\alpha_{N-2})\times\ldots\times(1-t_s\alpha_2)t_s\gamma_1 + \ldots + t_s\gamma_{N-2} \\ (1-t_s\alpha_{N-1})(1-t_s\alpha_{N-2})\times\ldots\times(1-t_s\alpha_1)t_s\gamma_o + (1-t_s\alpha_{N-1})\times\ldots\times(1-t_s\alpha_2)t_s\gamma_1 + \ldots(1-t_s\alpha_{N-1})t_s\gamma_{N-2} + t_s\gamma_{N-1} \end{bmatrix}. \tag{A.12}$$

The T_{low} vector is given in equation (A.13), the formulation of the $\mathbf{b_2}$ vector is analogous to $\mathbf{b_1}$ given in equation (A.14),

$$\mathbf{b_6} = \begin{bmatrix} T_{low} \\ \vdots \\ T_{low} \end{bmatrix}_{N\times 1}, \tag{A.13}$$

$$\mathbf{b_2} = -\mathbf{b_6} + \mathbf{b_4} + \mathbf{b_5}. \tag{A.14}$$

A.0.0.2 Equality matrices

The power balance equation (5.16) constitutes an equality constraint, a sparse matrix $\mathbf{A_{eq}}$, given in equation (A.15):

$$\mathbf{A_{eq}} = \begin{bmatrix} P_{hp} & 0 & \cdots & 0 & \vdots & -1 & 0 & \cdots & 0 \\ 0 & P_{hp} & 0 & \cdots & \vdots & 0 & \ddots & \cdots & 0 \\ \vdots & 0 & \ddots & 0 & \vdots & \vdots & 0 & -1 & \vdots \\ 0 & 0 & \cdots & P_{hp} & \vdots & 0 & 0 & \cdots & -1 \end{bmatrix}_{N\times 2N}. \tag{A.15}$$

The *k-th* total PV and wind power consisting of element of vector $\mathbf{b_{eq}}$ is shown in equation (A.16):

$$\mathbf{b_{eq}} = \begin{bmatrix} P_{w,1} + P_{pv,1} \\ \vdots \\ P_{w,N} + P_{pv,N} \end{bmatrix}_{N\times 1}. \tag{A.16}$$

Therefore, the canonical form is $\mathbf{A_{eq}X} = \mathbf{b_{eq}}$ where $\mathbf{A_{eq}}$ is given in equation (A.15) and $\mathbf{b_{eq}}$ in equation (A.16).

A.0.0.3 The objective function

The objective function is the total daily electrical energy cost under the TOU tariff given by,

$$f^T\mathbf{X} = \begin{bmatrix} 0 & \dots & 0_N, & p_1 & \dots & p_N \end{bmatrix} \begin{bmatrix} u_0 \\ \vdots \\ u_{N-1} \\ P_{g,0} \\ \vdots \\ P_{q,N-1} \end{bmatrix}_{2N\times 1} . \tag{A.17}$$

The limits of the control variables are restricted between the lower and upper bounds, given in equation (A.18) and equation (A.19).

lower bounds

$$lb^T = \begin{bmatrix} 0 & \dots & 0_N, & -\infty_1 & \dots & -\infty_N \end{bmatrix}, \tag{A.18}$$

upper bounds

$$ub^T = \begin{bmatrix} 1 & \dots & 1_N, & \infty_1 & \dots & \infty_N \end{bmatrix}. \tag{A.19}$$

APPENDIX B CHAPTER 7 TABLES FOR THE COMPARISON OF LIFE CYCLE COSTINGS

B.1 PRE-AND-POST IMPLEMENTATION OF LCC OF CHAPTER 3 MODEL

Tables (B.1) and (B.2) represent the full details of the LCC analysis calculated in Chapter (7).

B.1.1 Table of the LCC analysis of existing system

Table B.1. LCC of pre-implementation based on chapter 3 yearly average operation

Year	Initial investment/savage value		Annual costs		Total annual costs	Discounting factor	Discounted cash flows	Cumulative cash flows
			Operation costs	Maintainance cost				
0	Heat pump	(143 274.00)			(151 074.00)	1.00	(151 074.00)	
	Installation cost	(7 800.00)						
		15000						
1			(88 494.25)	(3 500.00)	(91 994.25)	0.96	(88 117.10)	(239 191.10)
2			(88 494.25)	(3 500.00)	(91 994.25)	0.92	(84 403.35)	(323 594.45)
3			(88 494.25)	(3 500.00)	(91 994.25)	0.88	(80 846.12)	(404 440.57)
4			(88 494.25)	(3 500.00)	(91 994.25)	0.84	(77 438.81)	(481 879.38)
5			(88 494.25)	(3 500.00)	(91 994.25)	0.81	(74 175.11)	(556 054.49)
6			(88 494.25)	(3 500.00)	(91 994.25)	0.77	(71 048.95)	(627 103.44)
7			(88 494.25)	(3 500.00)	(91 994.25)	0.74	(68 054.55)	(695 158.00)
8			(88 494.25)	(3 500.00)	(91 994.25)	0.71	(65 186.35)	(760 344.35)
9			(88 494.25)	(3 500.00)	(91 994.25)	0.68	(62 439.04)	(822 783.39)
10			(88 494.25)	(3 500.00)	(91 994.25)	0.65	(59 807.51)	(882 590.90)
11			(88 494.25)	(3 500.00)	(91 994.25)	0.62	(57 286.88)	(939 877.78)
12			(88 494.25)	(3 500.00)	(91 994.25)	0.60	(54 872.49)	(994 750.27)
13			(88 494.25)	(3 500.00)	(91 994.25)	0.57	(52 559.86)	(1 047 310.13)
14			(88 494.25)	(3 500.00)	(91 994.25)	0.55	(50 344.69)	(1 097 654.83)
15			(88 494.25)	(3 500.00)	(91 994.25)	0.52	(48 222.89)	(1 145 877.71)
16			(88 494.25)	(3 500.00)	(91 994.25)	0.50	(46 190.50)	(1 192 068.22)
17			(88 494.25)	(3 500.00)	(91 994.25)	0.48	(44 243.78)	(1 236 312.00)
18			(88 494.25)	(3 500.00)	(91 994.25)	0.46	(42 379.10)	(1 278 691.09)
19			(88 494.25)	(3 500.00)	(91 994.25)	0.44	(40 593.01)	(1 319 284.10)
20			(88 494.25)	(3 500.00)	(91 994.25)	0.42	(38 882.19)	(1 358 166.29)
Totals (R)		**(136 074.00)**		**(70 000.00)**				**(17 403 132.51)**

B.1.2 Post implementation LCC analysis

Table B.2. LCC of the post-implementation of the OC strategy of chapter 3 model

Year	Initial investment/savage value		Annual costs		Revenue						
			Operation costs	Maintainance cost	PV energy sales	OC benefits	Total annual costs	Discounting factor	Discounted cash flows	Cumulative cash flows
	Photovoltaics	(27 500.00)								
	Controllers	(22 900.00)								
	Inverters/accessories	(15 000.00)								
0	Heat pump	(143 274.00)	15000							
	Installation cost	(18 000.00)								
	Batteries	(30 500.00)					(242 174.00)	1.00	(242 174.00)	
1			(60 057.10)	(3 700.00)	94 419.11	28437.15	59099.16	0.96	56608.39	(298 782.39)
2			(60 057.10)	(3 700.00)	94 419.11	28437.15	59099.16	0.92	54222.60	(244 559.79)
3			(60 057.10)	(3 700.00)	94 419.11	28437.15	59099.16	0.88	51937.35	(192 622.44)
4			(60 057.10)	(3 700.00)	94 419.11	28437.15	59099.16	0.84	49748.42	(142 874.02)
5			(60 057.10)	(3 700.00)	94 419.11	28437.15	59099.16	0.81	47651.75	(95 222.27)
6			(60 057.10)	(34 200.00)	94 419.11	28437.15	28599.16	0.77	22087.69	(73 134.58)
7			(60 057.10)	(3 700.00)	94 419.11	28437.15	59099.16	0.74	43719.76	(29 414.82)
8			(60 057.10)	(3 700.00)	94 419.11	28437.15	59099.16	0.71	41877.17	12 462.35
9			(60 057.10)	(3 700.00)	94 419.11	28437.15	59099.16	0.68	40112.23	52 574.58
10			(60 057.10)	(3 700.00)	94 419.11	28437.15	59099.16	0.65	38421.68	90 996.26
11			(60 057.10)	(27 300.00)	94 419.11	28437.15	35499.16	0.62	22 106.12	113 102.38
12			(60 057.10)	(3 700.00)	94 419.11	28437.15	59099.16	0.60	35251.32	148 353.70
13			(60 057.10)	(3 700.00)	94 419.11	28437.15	59099.16	0.57	33765.63	182 119.33
14			(60 057.10)	(3 700.00)	94 419.11	28437.15	59099.16	0.55	32342.56	214 461.88
15			(60 057.10)	(3 700.00)	94 419.11	28437.15	59099.16	0.52	30979.46	245 441.34
16			(60 057.10)	(3 700.00)	94 419.11	28437.15	59099.16	0.50	29673.81	275 115.15
17			(60 057.10)	(3 700.00)	94 419.11	28437.15	59099.16	0.48	28423.19	303 538.34
18			(60 057.10)	(3 700.00)	94 419.11	28437.15	59099.16	0.46	27225.28	330 763.62
19			(60 057.10)	(3 700.00)	94 419.11	28437.15	59099.16	0.44	26077.85	356 841.47
20			(60 057.10)	(3 700.00)	94 419.11	28437.15	59099.16	0.42	24978.79	381 820.26
Totals (R)		**(242 174.00)**		**(128 100.00)**						**2 707 590.66**

B.2 LCC OF CHAPTER 4 MODEL

B.2.1 LCC analysis of existing system chapter 4 model

Table B.3. LCC of the baseline case for chapter 4 model

Year	Initial investment/savage value		Annual costs		Total annual costs	Discounting factor	Discounted cash flows	Cumulative cash flows
			Operation costs	Maintainance cost				
0	Heat pump	(143 274.00)			(151 074.00)	1.00	(151 074.00)	
	Installation cost	(7 800.00)						
		15000						
1			(63 749.08)	(3 500.00)	(67 249.08)	0.96	(64 414.83)	(215 488.83)
2			(63 749.08)	(3 500.00)	(67 249.08)	0.92	(61 700.03)	(277 188.85)
3			(63 749.08)	(3 500.00)	(67 249.08)	0.88	(59 099.64)	(336 288.50)
4			(63 749.08)	(3 500.00)	(67 249.08)	0.84	(56 608.85)	(392 897.35)
5			(63 749.08)	(3 500.00)	(67 249.08)	0.81	(54 223.04)	(447 120.39)
6			(63 749.08)	(3 500.00)	(67 249.08)	0.77	(51 937.78)	(499 058.16)
7			(63 749.08)	(3 500.00)	(67 249.08)	0.74	(49 748.83)	(548 806.99)
8			(63 749.08)	(3 500.00)	(67 249.08)	0.71	(47 652.13)	(596 459.13)
9			(63 749.08)	(3 500.00)	(67 249.08)	0.68	(45 643.81)	(642 102.93)
10			(63 749.08)	(3 500.00)	(67 249.08)	0.65	(43 720.12)	(685 823.06)
11			(63 749.08)	(3 500.00)	(67 249.08)	0.62	(41 877.51)	(727 700.57)
12			(63 749.08)	(3 500.00)	(67 249.08)	0.60	(40 112.56)	(767 813.13)
13			(63 749.08)	(3 500.00)	(67 249.08)	0.57	(38 421.99)	(806 235.12)
14			(63 749.08)	(3 500.00)	(67 249.08)	0.55	(36 802.67)	(843 037.79)
15			(63 749.08)	(3 500.00)	(67 249.08)	0.52	(35 251.60)	(878 289.39)
16			(63 749.08)	(3 500.00)	(67 249.08)	0.50	(33 765.90)	(912 055.30)
17			(63 749.08)	(3 500.00)	(67 249.08)	0.48	(32 342.82)	(944 398.11)
18			(63 749.08)	(3 500.00)	(67 249.08)	0.46	(30 979.71)	(975 377.83)
19			(63 749.08)	(3 500.00)	(67 249.08)	0.44	(29 674.05)	(1 005 051.88)
20			(63 749.08)	(3 500.00)	(67 249.08)	0.42	(28 423.42)	(1 033 475.30)
Totals (R)		**(136 074.00)**		**(70 000.00)**				**(13 534 668.59)**

B.2.2 LCC analysis of an optimal control system

Table B.4. LCC analysis of post-implementation of chapter 4 model

Year	Initial investment/savage value		Annual costs		Revenue		Total annual costs	Discounting factor	Discounted cash flows	Cumulative cash flows
			Operation costs	Maintainance cost	PV energy sales	OC benefits				
	Photovoltaics	(27 500.00)								
	Diesel generator	(64 500.00)	8700							
	Controllers	(22 900.00)								
	Inverters/accessories	(15 000.00)								
0	Heat pump	(143 274.00)	15000							
	Installation cost	(18 000.00)								
	Batteries	(30 500.00)					(306 674.00)	1.00	(306 674.00)	
1			(68 251.35)	(4 400.00)	55 618.70	35647.73	18615.08	0.96	17830.54	(324 504.54)
2			(68 251.35)	(4 400.00)	55 618.70	35647.73	18615.08	0.92	17079.06	(307 425.48)
3			(68 251.35)	(4 400.00)	55 618.70	35647.73	18615.08	0.88	16359.25	(291 066.23)
4			(68 251.35)	(4 400.00)	55 618.70	35647.73	18615.08	0.84	15669.78	(275 396.45)
5			(68 251.35)	(4 400.00)	55 618.70	35647.73	18615.08	0.81	15009.37	(260 387.08)
6			(68 251.35)	(34 900.00)	55 618.70	35647.73	-11884.92	0.77	-9178.96	(269 566.03)
7			(68 251.35)	(4 400.00)	55 618.70	35647.73	18615.08	0.74	13770.87	(255 795.16)
8			(68 251.35)	(4 400.00)	55 618.70	35647.73	18615.08	0.71	13190.49	(242 604.67)
9			(68 251.35)	(4 400.00)	55 618.70	35647.73	18615.08	0.68	12634.57	(229 970.11)
10			(68 251.35)	(4 400.00)	55 618.70	35647.73	18615.08	0.65	12102.08	(217 868.03)
11			(68 251.35)	(27 300.00)	55 618.70	35647.73	-4284.92	0.62	(2 668.32)	(220 536.34)
12			(68 251.35)	(4 400.00)	55 618.70	35647.73	18615.08	0.60	11103.48	(209 432.87)
13			(68 251.35)	(4 400.00)	55 618.70	35647.73	18615.08	0.57	10635.51	(198 797.36)
14			(68 251.35)	(4 400.00)	55 618.70	35647.73	18615.08	0.55	10187.27	(188 610.08)
15			(68 251.35)	(4 400.00)	55 618.70	35647.73	18615.08	0.52	9757.92	(178 852.16)
16			(68 251.35)	(4 400.00)	55 618.70	35647.73	18615.08	0.50	9346.67	(169 505.49)
17			(68 251.35)	(4 400.00)	55 618.70	35647.73	18615.08	0.48	8952.75	(160 552.74)
18			(68 251.35)	(4 400.00)	55 618.70	35647.73	18615.08	0.46	8575.43	(151 977.31)
19			(68 251.35)	(4 400.00)	55 618.70	35647.73	18615.08	0.44	8214.01	(143 763.30)
20			(68 251.35)	(4 400.00)	55 618.70	35647.73	18615.08	0.42	7867.83	(135 895.47)
Totals (R)		**(297 974.00)**		**(141 400.00)**						**(4 432 506.88)**

B.3 LCC OF CHAPTER 5 MODEL

B.3.1 LCC analysis of existing system chapter 5 model

Table B.5. LCC analysis of the existing system in chapter model 5

Year	Initial investment/savage value			Annual costs		Total annual costs	Discounting factor	Discounted cash flows	Cumulative cash flows
	Heat pump	(25 775.87)	2300	Operation costs	Maintainance cost				
0	Installation cost	(7 800.00)				(33 575.87)	1.00	(33 575.87)	
1				(17 822.95)	(1 500.00)	(19 322.95)	0.96	(18 508.57)	(52 084.44)
2				(17 822.95)	(1 500.00)	(19 322.95)	0.92	(17 728.52)	(69 812.96)
3				(17 822.95)	(1 500.00)	(19 322.95)	0.88	(16 981.34)	(86 794.30)
4				(17 822.95)	(1 500.00)	(19 322.95)	0.84	(16 265.65)	(103 059.95)
5				(17 822.95)	(1 500.00)	(19 322.95)	0.81	(15 580.12)	(118 640.08)
6				(17 822.95)	(1 500.00)	(19 322.95)	0.77	(14 923.49)	(133 563.57)
7				(17 822.95)	(1 500.00)	(19 322.95)	0.74	(14 294.53)	(147 858.10)
8				(17 822.95)	(1 500.00)	(19 322.95)	0.71	(13 692.08)	(161 550.18)
9				(17 822.95)	(1 500.00)	(19 322.95)	0.68	(13 115.02)	(174 665.20)
10				(17 822.95)	(1 500.00)	(19 322.95)	0.65	(12 562.28)	(187 227.48)
11				(17 822.95)	(1 500.00)	(19 322.95)	0.62	(12 032.83)	(199 260.31)
12				(17 822.95)	(1 500.00)	(19 322.95)	0.60	(11 525.70)	(210 786.02)
13				(17 822.95)	(1 500.00)	(19 322.95)	0.57	(11 039.95)	(221 825.96)
14				(17 822.95)	(1 500.00)	(19 322.95)	0.55	(10 574.66)	(232 400.62)
15				(17 822.95)	(1 500.00)	(19 322.95)	0.52	(10 128.99)	(242 529.61)
16				(17 822.95)	(1 500.00)	(19 322.95)	0.50	(9 702.09)	(252 231.70)
17				(17 822.95)	(1 500.00)	(19 322.95)	0.48	(9 293.19)	(261 524.89)
18				(17 822.95)	(1 500.00)	(19 322.95)	0.46	(8 901.53)	(270 426.42)
19				(17 822.95)	(1 500.00)	(19 322.95)	0.44	(8 526.37)	(278 952.79)
20				(17 822.95)	(1 500.00)	(19 322.95)	0.42	(8 167.02)	(287 119.80)
Totals (R)		**(31 275.87)**			**(30 000.00)**				**(3 692 314.38)**

B.3.2 Post implementation LCC analysis

Table B.6. LCC of post implementation of the chapter 5model

Year	Initial investment/savage value			Annual costs		Income						
	Photovoltaics	(27 500.00)		Operation costs	Maintenance cost	Wind energy sales	PV energy sales	OC benefits	Total annual costs	Discounting factor	Discounted cash flows	Cumulative cash flows
	Wind generator	(23 500.00)	1200									
	Controllers	(22 900.00)										
0	Inverters/accessories	(15 000.00)										
	Heat pump	(25 775.87)	2300									
	Installation cost	(14 000.00)										
									(128 675.87)	1.00	(128 675.87)	
1				(5 215.85)	(2 500.00)	6 638.66	13 568.47	12607.10	25098.39	0.96	24040.60	(152 716.47)
2				(5 215.85)	(2 500.00)	6 638.66	13 568.47	12607.10	25098.39	0.92	23027.40	(129 689.08)
3				(5 215.85)	(2 500.00)	6 638.66	13 568.47	12607.10	25098.39	0.88	22056.89	(107 632.18)
4				(5 215.85)	(2 500.00)	6 638.66	13 568.47	12607.10	25098.39	0.84	21127.29	(86 504.89)
5				(5 215.85)	(2 500.00)	6 638.66	13 568.47	12607.10	25098.39	0.81	20236.87	(66 268.02)
6				(5 215.85)	(2 500.00)	6 638.66	13 568.47	12607.10	25098.39	0.77	19383.97	(46 884.05)
7				(5 215.85)	(2 500.00)	6 638.66	13 568.47	12607.10	25098.39	0.74	18567.03	(28 317.02)
8				(5 215.85)	(2 500.00)	6 638.66	13 568.47	12607.10	25098.39	0.71	17784.51	(10 532.52)
9				(5 215.85)	(2 500.00)	6 638.66	13 568.47	12607.10	25098.39	0.68	17034.97	6 502.45
10				(5 215.85)	(2 500.00)	6 638.66	13 568.47	12607.10	25098.39	0.65	16317.02	22 819.47
11				(5 215.85)	(40 400.00)	6 638.66	13 568.47	12607.10	(12801.61)	0.62	(7971.85)	14 847.62
12				(5 215.85)	(2 500.00)	6 638.66	13 568.47	12607.10	25098.39	0.60	14970.62	29 818.24
13				(5 215.85)	(2 500.00)	6 638.66	13 568.47	12607.10	25098.39	0.57	14339.68	44 157.92
14				(5 215.85)	(2 500.00)	6 638.66	13 568.47	12607.10	25098.39	0.55	13735.32	57 893.24
15				(5 215.85)	(2 500.00)	6 638.66	13 568.47	12607.10	25098.39	0.52	13156.44	71 049.68
16				(5 215.85)	(2 500.00)	6 638.66	13 568.47	12607.10	25098.39	0.50	12601.95	83 651.63
17				(5 215.85)	(2 500.00)	6 638.66	13 568.47	12607.10	25098.39	0.48	12070.84	95 722.47
18				(5 215.85)	(2 500.00)	6 638.66	13 568.47	12607.10	25098.39	0.46	11562.10	107 284.57
19				(5 215.85)	(2 500.00)	6 638.66	13 568.47	12607.10	25098.39	0.44	11074.81	118 359.38
20				(5 215.85)	(2 500.00)	6 638.66	13 568.47	12607.10	25098.39	0.42	10608.06	128 967.44
Totals (R)			**(125 175.87)**		**(87 900.00)**							**781 074.13**

B.4 LCC OF CHAPTER 6 MODEL

B.4.1 LCC analysis of existing system chapter 6 model

Table B.7. Life cycle cost analysis pre-implementation for chapter 6 model

Year	Initial investment/savage value			Annual costs		Total annual costs	Discounting factor	Discounted cash flows	Cumulative cash flows
				Operation costs	Maintainance cost				
	Heat pump	(25 775.87)	2300						
0	Installation cost	(7 800.00)				(33 575.87)	1.00	(33 575.87)	
1				(24 119.20)	(1 500.00)	(25 619.20)	0.96	(24 539.46)	(58 115.33)
2				(24 119.20)	(1 500.00)	(25 619.20)	0.92	(23 505.23)	(81 620.57)
3				(24 119.20)	(1 500.00)	(25 619.20)	0.88	(22 514.59)	(104 135.16)
4				(24 119.20)	(1 500.00)	(25 619.20)	0.84	(21 565.70)	(125 700.86)
5				(24 119.20)	(1 500.00)	(25 619.20)	0.81	(20 656.80)	(146 357.66)
6				(24 119.20)	(1 500.00)	(25 619.20)	0.77	(19 786.21)	(166 143.87)
7				(24 119.20)	(1 500.00)	(25 619.20)	0.74	(18 952.31)	(185 096.17)
8				(24 119.20)	(1 500.00)	(25 619.20)	0.71	(18 153.55)	(203 249.73)
9				(24 119.20)	(1 500.00)	(25 619.20)	0.68	(17 388.46)	(220 638.18)
10				(24 119.20)	(1 500.00)	(25 619.20)	0.65	(16 655.61)	(237 293.79)
11				(24 119.20)	(1 500.00)	(25 619.20)	0.62	(15 953.65)	(253 247.45)
12				(24 119.20)	(1 500.00)	(25 619.20)	0.60	(15 281.27)	(268 528.72)
13				(24 119.20)	(1 500.00)	(25 619.20)	0.57	(14 637.24)	(283 165.96)
14				(24 119.20)	(1 500.00)	(25 619.20)	0.55	(14 020.34)	(297 186.30)
15				(24 119.20)	(1 500.00)	(25 619.20)	0.52	(13 429.45)	(310 615.74)
16				(24 119.20)	(1 500.00)	(25 619.20)	0.50	(12 863.45)	(323 479.20)
17				(24 119.20)	(1 500.00)	(25 619.20)	0.48	(12 321.32)	(335 800.51)
18				(24 119.20)	(1 500.00)	(25 619.20)	0.46	(11 802.03)	(347 602.54)
19				(24 119.20)	(1 500.00)	(25 619.20)	0.44	(11 304.62)	(358 907.16)
20				(24 119.20)	(1 500.00)	(25 619.20)	0.42	(10 828.18)	(369 735.35)
Totals (R)		**(31 275.87)**			**(30 000.00)**				**(4 676 620.24)**

B.4.2 Post implementation LCC analysis

Table B.8. Life cycle cost analysis of post-implementation of chapter 6 model

Year	Initial investment/savage value			Annual costs		Income						
	Photovoltaics	(27 500.00)		Operation costs	Maintainance cost	Wind energy sales	PV energy sales	OC benefits	Total annual costs	Discounting factor	Discounted cash flows	Cumulative cash flows
	Wind generator	(23 500.00)	1200									
	Controllers	(22 900.00)										
0	Inverters/accessories	(60 000.00)										
	Heat pump	(25 775.87)	2300									
	Installation cost	(32 000.00)										
	Fuel cell stucks	(47 400.08)							(179 075.95)	1.00	(179 075.95)	
1				(15 946.85)	(3 660.82)	6 638.66	13 568.47	12607.10	13206.57	0.96	12649.97	(191 725.92)
2				(15 946.85)	(3 660.82)	6 638.66	13 568.47	12607.10	13206.57	0.92	12116.83	(179 609.09)
3				(15 946.85)	(3 660.82)	6 638.66	13 568.47	12607.10	13206.57	0.88	11606.16	(168 002.93)
4				(15 946.85)	(3 660.82)	6 638.66	13 568.47	12607.10	13206.57	0.84	11117.01	(156 885.92)
5				(15 946.85)	(3 660.82)	6 638.66	13 568.47	12607.10	13206.57	0.81	10648.48	(146 237.45)
6				(15 946.85)	(3 660.82)	6 638.66	13 568.47	12607.10	13206.57	0.77	10199.69	(136 037.76)
7				(15 946.85)	(3 660.82)	6 638.66	13 568.47	12607.10	13206.57	0.74	9769.82	(126 267.94)
8				(15 946.85)	(3 660.82)	6 638.66	13 568.47	12607.10	13206.57	0.71	9358.06	(116 909.88)
9				(15 946.85)	(3 660.82)	6 638.66	13 568.47	12607.10	13206.57	0.68	8963.66	(107 946.21)
10				(15 946.85)	(3 660.82)	6 638.66	13 568.47	12607.10	13206.57	0.65	8585.88	(99 360.33)
11				(15 946.85)	(51 060.90)	6 638.66	13 568.47	12607.10	(34 193.51)	0.62	(21 293.07)	(120 653.40)
12				(15 946.85)	(3 660.82)	6 638.66	13 568.47	12607.10	13206.57	0.60	7877.42	(112 775.98)
13				(15 946.85)	(3 660.82)	6 638.66	13 568.47	12607.10	13206.57	0.57	7545.42	(105 230.56)
14				(15 946.85)	(3 660.82)	6 638.66	13 568.47	12607.10	13206.57	0.55	7227.41	(98 003.14)
15				(15 946.85)	(3 660.82)	6 638.66	13 568.47	12607.10	13206.57	0.52	6922.81	(91 080.33)
16				(15 946.85)	(3 660.82)	6 638.66	13 568.47	12607.10	13206.57	0.50	6631.05	(84 449.29)
17				(15 946.85)	(3 660.82)	6 638.66	13 568.47	12607.10	13206.57	0.48	6351.58	(78 097.71)
18				(15 946.85)	(3 660.82)	6 638.66	13 568.47	12607.10	13206.57	0.46	6083.88	(72 013.83)
19				(15 946.85)	(3 660.82)	6 638.66	13 568.47	12607.10	13206.57	0.44	5827.48	(66 186.35)
20				(15 946.85)	(3 660.82)	6 638.66	13 568.47	12607.10	13206.57	0.42	5581.87	(60 604.48)
Totals			**(235 575.95)**		**(120 616.48)**							**(2 318 078.51)**

APPENDIX C MODEL 6 MATLAB CODES

MATLAB CODE FOR MODEL 6

```
clear all
%%  TOU AND SAMPLING TIME
days=1;
hours=24*days;
ts=0.5;
N=hours/ts;
 off_peak=0.3656; std=0.6733; peak=2.2225; % Rand/Kwh
 p=[off_peak*ones(1,6/ts),std*ones(1,1/ts),peak*ones(1,3/ts),std*
    ones(1,8/ts),peak*ones(1,2/ts),std*ones(1,2/ts),off_peak*ones
    (1,2/ts)];
%% HOT WATER DEMAND FLOW RATE
%
%   Wd=[ 0 ;0;0;0;      0;      0;      0.5;    0;      0.1;
    1.7;    2.3     ;3.25;  4.2;    4.6;    5.6;    5;      4.4;...
%       4.15;   3.9;    3.325;  3;      2.75;   2.5;    2.3;
    2.1;    2.1;    2.1;    2.1;    2.1;    2.2;...
%       2.3;    2.35;   2.4;    2.4;    2.4;    3.3;    4.2;
    4.825;  5.3;    5.45;   5.6;    5.45;   1;...
%       0;      0;      0;      0;      0]; % SUMMER
%
% Wd=   [0;      0;      0;      0;      0;      0.9;    0.1;
    0.1;    0.1;    2.45;   3.6;    4.3;    5;      6;      7;
    6.45;   5.9;    4.95;   4;...
```

```
% 3.85; 3.7; 3.35; 3; 2.9; 2.8; 2.95;
    3.1; 3; 2.9; 3.05; 3.2; 3.6; 4; 5.5;
    7;...
% 6.7; 6.4; 5.7; 5; 6.2; 7.4; 6.2;
    0.2; 0; 0; 0; 0; 0];% AUTUMN

 Wd
    =[0;0;0;0;0;0;0;0;0;0;4;5.5;7;8.4;9.8;8.9;8;7.15;6.3;5.35;4.4;4.25;4.1;3.9

   3.9;3.95;4.05;4;4.15;4.1;6.1;4.2;8.05;8;8.7;8.1;8.85;9.3;7.7;8.4;0;0;0;0;0;0
      % WINTER

%
% Wd= [0; 0; 0; 0; 0; 0; 1;
    0.2; 0; 0; 2.2; 3.25; 4.3; 5.2; 6.1;
    5.55; 5; 4; 3; 3.3; 3.6;...
%  2.85; 2.1; 2.05; 2; 2.15; 2.3; 2.5;
    2.7; 2.85; 3; 3; 3; 4.15; 5.3; 5.15;
    5; 4.8;...
%  4.6; 4.8; 5; 4; 1; 0.2; 0; 0;
        0; 0]; % SPRING

 %% INLET WATER TEMPERATURES
 Tw=[16;16;16;16;16; 16.5; 17; 17; 17; 17; 17;
        17; 17; 17; 18; 17.5;19;18.5; 20;...
    19.5; 21; 21; 21; 21; 22; 21.5; 21;
            21; 21; 21; 21; 19; 20; 19;
            19; 18; 18.5;...
    18; 18; 18; 18; 18; 18; 17;
        17.5; 16; 16; 16]; % WINTER Ta=25
% Tw= [23.69; 23.20; 21.14; 22.17; 23.94; 22.86; 23.36;
    21.73; 21.88; 22.24; 21.08; 23.00;...
```

```
% 22.02; 22.59; 21.23; 20.55; 21.90; 21.45; 23.15; 23.12; 22.67; 20.53; 20.09; 22.24; 21.20;...
% 23.76; 23.92; 21.15; 23.20; 23.58; 22.39; 23.54; 23.77; 22.20; 22.91; 22.31; 20.10; 21.79;...
% 22.59; 22.08; 21.49; 23.75; 23.32; 23.40; 21.49; 22.37; 23.49; 23.73]; %SPRING Ta=25
%
% Tw=[24.00; 24.87; 23.25; 24.46; 24.29; 24.67; 23.80; 24.50; 24.67; 23.64; 24.10; 24.96; 24.10;...
% 23.66; 24.24; 23.72; 24.51; 23.83; 23.98; 24.39; 24.95; 23.66; 24.68; 24.48; 24.91; 23.06; 23.71;...
% 24.33; 23.56; 23.46; 24.42; 24.25; 24.18; 24.32; 23.10; 23.70; 23.90; 23.48; 24.43; 24.71; 23.56;...
% 24.46; 23.28; 24.67; 23.28; 24.18; 23.73; 24.61]; % SUMMER Ta=25

%
% Tw=[19.02; 18.94; 21.26; 18.12; 18.70; 21.78; 16.25; 21.84; 17.14; 20.00; 19.52; 20.05; 18.17; 19.72;...
% 20.87; 16.12; 16.50; 21.85; 19.91; 17.39; 18.42; 16.73; 17.61; 17.55; 17.99; 16.91; 18.09; 16.73;...
% 21.30; 16.57; 21.58; 18.39; 16.28; 18.05; 20.42; 20.77; 19.27; 20.12; 21.36; 16.33; 17.82; 16.28;...
% 17.17; 20.32; 20.33; 21.27; 19.49; 16.42];% AUTUMN Ta=25
%% HEAT PUMP WATER HEATER INPUT PARAMETERS ;
c1= 4180;
COP=3.8;
L=270;
S=2*3.142*0.33*1.41+ 2*3.142*0.33^2;
h=6.3;
dx=0.035;
k=0.055;
```

```
55 Php=7;
56 Ta=25;
57 To=55;
58 al= (S/(c1*L*(dx/k+1/h)))+Wd/L;
59 Hp=(Php*COP/c1*L);
60 c= (S*Ta/(c1*L*(dx/k+1/h)))+(Wd.*Tw/L);
61 Tup= 65;
62 Tlow=50;
63 %% PV AND FUEL CELL EFFICIENCY
64 nw=0.98;
65 npv=0.98;
66 nel=0.65;
67 nst=1;
68 nfc=0.5;
69 ninv=0.98;
70
71 %% HYDROGEN TANK STORAGE CAPACITY
72 E_Tmax=25;
73 E_T0=3;
74 E_Tmin=0;
75 %% WEIGHTING FACTORS
76 w1=0.5;
77 w2=0.5;
78 %% WIND MODEL INPUT DATA
79 vh=[4.17*ts*ones(1,1/ts), 3.75*ts*ones(1,1/ts), 3.47*ts*
    ones(1,1/ts), 3.06*ts*ones(1,1/ts), ...
80 3.06*ts*ones(1,1/ts), 3.47*ts*ones(1,1/ts), 3.75*ts*
    ones(1,1/ts), 3.75*ts*ones(1,1/ts), ...
81 3.75*ts*ones(1,1/ts), 3.89*ts*ones(1,1/ts), 4.31*ts*
    ones(1,1/ts), 5.00*ts*ones(1,1/ts), ...
82 8.06*ts*ones(1,1/ts), 10.97*ts*ones(1,1/ts), 11.11*ts*
    ones(1,1/ts), 10.97*ts*ones(1,1/ts),...
```

```
83      10.56*ts*ones(1,1/ts),      10.00*ts*ones(1,1/ts),   8.89*ts*
            ones(1,1/ts),    7.64*ts*ones(1,1/ts), ...
84      6.81*ts*ones(1,1/ts),       6.11*ts*ones(1,1/ts),    5.56*ts*
            ones(1,1/ts),    2.64*ts*ones(1,1/ts)]';
85
86  %v(t)-hourly wind speed at desired height (h)
87  %vh - Measured wind speed at anemometer height
88 alpha=1/7;% power law exponent ranging 1/7-1/4
89 h=30; % Mast height (m)
90 hh=10; %Anemometer height (m)
91 Pr=7;%Kw
92 % Pw=output power
93 vo=50;%cutout speed
94 vi=2.0;%cutin speed
95 vr=11;%rated speed
96 v=vh* (h/hh)^alpha;
97
98 for i=1:length(vh)
99
100 if vi >= v(i) <= vr
101
102 Pwind(i) = Pr.*((v(i)-vi)./(vr-vi)).^3;
103
104 elseif vr < v(i) <= vo
105
106 Pwind(i) = Pr;
107
108 elseif v(i) >= vo || v(i) < vi
109
110 Pwind(i)=0;
111
112 else
113
```

```
114 Pwind(i)=0;
115
116 end
117
118 index = find( Pwind <= 0);
119
120 for i = index
121
122 Pwind(i) = 0;
123
124 end
125
126 end
127 Pw=Pwind';
128
129 %% LOAD DEMAND
130 Pload=[1.5*ts*ones(1,1/ts), 1.5*ts*ones(1,1/ts),
        1.5*ts*ones(1,1/ts), 1.5*ts*ones(1,1/ts),...
131     1.5*ts*ones(1,1/ts), 1.95*ts*ones(1,1/ts),
        1.95*ts*ones(1,1/ts), 1.65*ts*ones(1,1/ts),...
132     1.35*ts*ones(1,1/ts), 3.25*ts*ones(1,1/ts),
        3.25*ts*ones(1,1/ts), 2.15*ts*ones(1,1/ts)
        ,...
133     2.15*ts*ones(1,1/ts), 2.15*ts*ones(1,1/ts),
        2.15*ts*ones(1,1/ts), 2.15*ts*ones(1,1/ts)
        ,...
134     2.15*ts*ones(1,1/ts), 1.8*ts*ones(1,1/ts),
        2.31*ts*ones(1,1/ts), 3.81*ts*ones(1,1/ts)
        ,...
135     2.31*ts*ones(1,1/ts), 2.31*ts*ones(1,1/ts),
        2.31*ts*ones(1,1/ts), 1.35*ts*ones(1,1/ts)
        ]';
136
```

```
137 %% SOLAR INPUT DATA
138 Ppv=[0.00*ts*ones(1,1/ts), 0.00*ts*ones(1,1/ts), 0.00*ts*
        ones(1,1/ts), 0.00*ts*ones(1,1/ts),...
139      0.00*ts*ones(1,1/ts), 0.00*ts*ones(1,1/ts), 0.01*ts*
           ones(1,1/ts), 0.28*ts*ones(1,1/ts),...
140      0.52*ts*ones(1,1/ts), 0.73*ts*ones(1,1/ts), 0.88*ts*
           ones(1,1/ts), 0.93*ts*ones(1,1/ts),...
141      0.91*ts*ones(1,1/ts), 0.81*ts*ones(1,1/ts), 0.66*ts*
           ones(1,1/ts), 0.46*ts*ones(1,1/ts),...
142      0.26*ts*ones(1,1/ts), 0.01*ts*ones(1,1/ts), 0.00*ts*
           ones(1,1/ts), 0.00*ts*ones(1,1/ts),...
143      0.00*ts*ones(1,1/ts), 0.00*ts*ones(1,1/ts), 0.00*ts*
           ones(1,1/ts), 0.00*ts*ones(1,1/ts)]'*5;
144
145 %% STATE VARIABLE MATRIX VECTORS HEAT PUMP
146 [A_mat,term_1] = GenerateABmatrixVector(To,al,Hp,c,N,ts);
147 A4= [ A_mat,zeros(N,N),zeros(N,N),zeros(N,N),zeros(N,N),zeros(N,N)
        ];
148 A5= [-A_mat,zeros(N,N),zeros(N,N),zeros(N,N),zeros(N,N),zeros(N,N)
        ];
149 b4=[Tup*ones(N,1)-term_1];
150 b5=[-Tlow*ones(N,1)+term_1];
151
152 %% EQUALITY CONSTRAINTS
153 P_re=nw*(Pw(1:N))+npv*Ppv(1:N);
154
155    Aeq1=[zeros(N,N),zeros(N,N),ninv*eye(N,N),nel*eye(N,N),zeros(N,N)
          ,zeros(N,N)];
156    beq1=P_re(1:N);
157
158    Aeq2=[-Php*eye(N,N),eye(N,N),eye(N,N),zeros(N,N),eye(N,N),zeros(N
          ,N)];
159    beq2=Pload;
```

```
160
161   Aeq3=[zeros(N,N),zeros(N,N),zeros(N,N),zeros(N,N),-eye(N,N),nfc*
          ninv*eye(N,N)];
162   beq3=zeros(N,1);
163
164      Aeq=[Aeq1;Aeq2;Aeq3];
165      beq=[beq1;beq2;beq3];
166
167  %% INQUALITY CONSTRAINTS
168   A1=[zeros(N,N),zeros(N,N),zeros(N,N),ts*eye(N,N),zeros(N,N),(-ts/
          nst)*tril(ones(N,N))];
169   b1=(E_Tmax-E_T0)*ones(N,1);
170   A2=[zeros(N,N),zeros(N,N),zeros(N,N),-ts*eye(N,N),zeros(N,N),(ts/
          nst)*tril(ones(N,N))];
171   b2=(-E_Tmin+ E_T0)*ones(N,1);
172   A=[A1;A2;A4;A5];
173   b=[b1;b2;b4;b5];
174   %% OBJECTIVE FUNCTION
175     f =@(x) w1*ts*sum(p(1:N)'.*(x(N+1:2*N)))/1000-w2*ts*sum(x(2*N
            +1:3*N));
176
177  %% BOUNDARIES
178  x0=zeros(6*N,1);
179
180  lb=[zeros(1,N),-Inf*ones(1,N),zeros(1,N), E_Tmin*ones(1,N),zeros(1,
       N),zeros(1,N)];
181
182  ub = [ones(1,N),Inf*ones(1,N),12*ones(1,N), E_Tmax*ones(1,N),2.5*
       ones(1,N),2.5*ones(1,N)]';
183
184  %% USE OPTI
185  % xtype = 'BCCCCCI';
186     xtype='';
```

```
187     for(each=1:N)
188         xtype=[xtype,'B'];
189     end
190     for(each=N+1:6*N)
191         xtype=[xtype,'C'];
192     end
193
194     MyOptions = optiset('solver','scip');
195 %
196     Opt = opti('fun',f,'nlmix',[],[],[],'ineq',A,b,'eq',Aeq,beq,'
            bounds',lb',ub','xtype',xtype,'options',MyOptions);
197     [x,fval,exitflag,info] = solve(Opt,x0');
198      info,x=x';
199 % %
200
201  %% ASSIGNING VARIABLES
202  U = x(1:N);
203  Pg = x(N+1:2*N);
204  PRE_IN = x(2*N+1:3*N);
205  PH2 = x(3*N+1:4*N);
206  PFC_IN= x(4*N+1:5*N);
207  PFC= x(5*N+1:6*N);
208
209
210   %% HYDROGEN
211
212  H2= E_T0*ones(N,1)+ ts*tril(ones(N,N))*x(3*N+1:4*N)'...
213 -(ts/nst)*tril(ones(N,N))*x(5*N+1:6*N)';
214
215   %% CONTROL VARIABLES
216      subplot(1,2,1)
217
218 set( 0, 'DefaultAxesFontName', 'times' );
```

```
219 set( 0, 'DefaultTextFontSize', 14 );
220 set( 0, 'DefaultAxesFontSize', 14);
221 set( 0, 'DefaultLineLineWidth', 3); % default is 1
222 set( 0, 'DefaultLineMarkerSize',2.5 ); % default is 6
223
224   hold on
225   peak=[0.95,0.87,0.73]; standard=[0.76,0.87,0.78]; offpeak
          =[0.93,0.93,0.93];
226
227       mydays=0;myTop=30;
228       hold on;
229       fill([0,0,7,7]+mydays*24,[-10,myTop,myTop,-10],offpeak,'
              HandleVisibility','off');
230       fill([23,23,24,24]+mydays*24,[-10,myTop,myTop,-10],offpeak,'
              HandleVisibility','off');
231       fill([7,7,8,8]+mydays*24,[-10,myTop,myTop,-10],standard,'
              HandleVisibility','off');
232       fill([11,11,19,19]+mydays*24,[-10,myTop,myTop,-10],standard,'
              HandleVisibility','off');
233       fill([21,21,23,23]+mydays*24,[-10,myTop,myTop,-10],standard,'
              HandleVisibility','off');
234       fill([8,8,11,11]+mydays*24,[-10,myTop,myTop,-10],peak,'
              HandleVisibility','off');
235       fill([19,19,21,21]+mydays*24,[-10,myTop,myTop,-10],peak,'
              HandleVisibility','off');
236       hold off;
237
238       hold on;
239
240       hold off;
241       axis([0,23,0,4]);
242       set(gca,'XTick',(0:1:1*23)');
243       set(gca,'XTickLabel',(0:1:1*23));
```

```
244         hold on
245
246     stairs(linspace(0,hours+ts,N), Pload(1:N),'b','linewidth',2.5,'
            HandleVisibility','on');
247     stairs(linspace(0,hours+ts,N),Pg(1:N),'k','linewidth',2.5,'
            HandleVisibility','on');
248     stairs(linspace(0,hours+ts,N),PRE_IN(1:N),'r','linewidth',2.5,'
            HandleVisibility','on');
249     stairs(linspace(0,hours+ts,N),PFC_IN(1:N),'g','linewidth',2.5,'
            HandleVisibility','on');
250     stairs(linspace(0,hours+ts,N),Php*U(1:N),'m','linewidth',2.5,'
            HandleVisibility','on');
251
252     hold on
253     ylabel('Power (kW)');xlabel('Hours');
254     hold on ;
255     legend( '{P_{load}}',...
256               '{P_{g}}',...
257             '{P_{RE_IN}}',...
258             '{P_{FC_IN}}',...
259             '{P_{hp}}');
260
261     subplot(1,2,2)
262
263   set( 0, 'DefaultAxesFontName', 'times' );
264   set( 0, 'DefaultTextFontSize', 14 );
265   set( 0, 'DefaultAxesFontSize', 14);
266   set( 0, 'DefaultLineLineWidth', 3); % default is 1
267   set( 0, 'DefaultLineMarkerSize',2.5 ); % default is 6
268
269     hold on
270         stairs(linspace(0,hours+ts,N),Ppv(1:N),'g','linewidth',3,'
              HandleVisibility','on');
```

```
271         stairs(linspace(0,hours+ts,N),Pw(1:N),'k','linewidth',3,'
                HandleVisibility','on');
272         hold on
273     ylabel('Power generation(kW)');xlabel('Hours');
274     hold on ;
275     legend( '{P_{pv}}',...
276               '{P_{w}}');
277
278     %% FUEL CELL PLOT
279    subplot(1,2,1)
280
281    set( 0, 'DefaultAxesFontName', 'times' );
282    set( 0, 'DefaultTextFontSize', 14 );
283    set( 0, 'DefaultAxesFontSize', 14);
284    set( 0, 'DefaultLineLineWidth', 3); % default is 1
285    set( 0, 'DefaultLineMarkerSize',2.5 ); % default is 6
286
287      hold on
288       peak=[0.95,0.87,0.73];standard=[0.76,0.87,0.78];offpeak
              =[0.93,0.93,0.93]
289          mydays=0;myTop=30;
290          hold on;
291          fill([0,0,7,7]+mydays*24,[-10,myTop,myTop,-10],offpeak,'
                HandleVisibility','off');
292          fill([23,23,24,24]+mydays*24,[-10,myTop,myTop,-10],offpeak,'
                HandleVisibility','off');
293          fill([7,7,8,8]+mydays*24,[-10,myTop,myTop,-10],standard,'
                HandleVisibility','off');
294          fill([11,11,19,19]+mydays*24,[-10,myTop,myTop,-10],standard,'
                HandleVisibility','off');
295          fill([21,21,23,23]+mydays*24,[-10,myTop,myTop,-10],standard,'
                HandleVisibility','off');
```

```
296         fill([8,8,11,11]+mydays*24,[-10,myTop,myTop,-10],peak,'
                HandleVisibility','off');
297         fill([19,19,21,21]+mydays*24,[-10,myTop,myTop,-10],peak,'
                HandleVisibility','off');
298         hold off;
299
300         hold on;
301
302         hold off;
303         axis([0,23,0,10]);
304         set(gca,'XTick',(0:1:1*23)');
305         set(gca,'XTickLabel',(0:1:1*23));
306         hold on
307     stairs(linspace(0,hours+ts,N), PH2(1:N),'r','linewidth',2.5,'
            HandleVisibility','on');
308     stairs(linspace(0,hours+ts,N),PFC_IN(1:N),'g','linewidth',2.5,'
            HandleVisibility','on');
309     stairs(linspace(0,hours+ts,N),PFC(1:N),'k','linewidth',2.5,'
            HandleVisibility','on');
310     stairs(linspace(0,hours+ts,N),H2(1:N),'m','linewidth',2.5,'
            HandleVisibility','on');
311      hold on
312     ylabel('Power (kW)');xlabel('Hours');
313     hold on ;
314     legend( '{P_{H2}}',...
315             '{P_{FC_IN}}',...
316             '{P_{FC}}',...
317             '{H_{2}}');
318
319
320         subplot(1,2,2)
321
322  set( 0, 'DefaultAxesFontName', 'times' );
```

```
323 set( 0, 'DefaultTextFontSize', 14 );
324 set( 0, 'DefaultAxesFontSize', 14);
325 set( 0, 'DefaultLineLineWidth', 3); % default is 1
326 set( 0, 'DefaultLineMarkerSize',2.5 ); % default is 6
327
328   hold on
329
330  % HYDROGEN MASS
331
332
333  Hmass= (H2./39.7);
334  stairs(linspace(0,hours+ts,N),Hmass(1:N),'m','linewidth',2.5,'
        HandleVisibility','on');
335
336  hold on
337  ylabel('H_{2} mass (Kg)^{-1}');xlabel('Hours');
338  hold on ;
339  legend('{Hydrogen}');
340
341  %% RENEWABLE FEEDIN AND POWER BALANCE PLOT
342  subplot(1,2,1)
343
344 set( 0, 'DefaultAxesFontName', 'times' );
345 set( 0, 'DefaultTextFontSize', 14 );
346 set( 0, 'DefaultAxesFontSize', 14);
347 set( 0, 'DefaultLineLineWidth', 3); % default is 1
348 set( 0, 'DefaultLineMarkerSize',2.5 ); % default is 6
349
350   hold on
351   peak=[0.95,0.87,0.73];standard=[0.76,0.87,0.78];offpeak
        =[0.93,0.93,0.93];
352
353       mydays=0;myTop=30;
```

```
354         hold on;
355         fill([0,0,7,7]+mydays*24,[-10,myTop,myTop,-10],offpeak,'
                HandleVisibility','off');
356         fill([23,23,24,24]+mydays*24,[-10,myTop,myTop,-10],offpeak,'
                HandleVisibility','off');
357         fill([7,7,8,8]+mydays*24,[-10,myTop,myTop,-10],standard,'
                HandleVisibility','off');
358         fill([11,11,19,19]+mydays*24,[-10,myTop,myTop,-10],standard,'
                HandleVisibility','off');
359         fill([21,21,23,23]+mydays*24,[-10,myTop,myTop,-10],standard,'
                HandleVisibility','off');
360         fill([8,8,11,11]+mydays*24,[-10,myTop,myTop,-10],peak,'
                HandleVisibility','off');
361         fill([19,19,21,21]+mydays*24,[-10,myTop,myTop,-10],peak,'
                HandleVisibility','off');
362         hold off;
363
364         hold on;
365
366         hold off;
367         axis([0,23,0,4]);
368         set(gca,'XTick',(0:1:1*23)');
369         set(gca,'XTickLabel',(0:1:1*23));
370         hold on
371
372     stairs(linspace(0,hours+ts,N), Pload(1:N),'b','linewidth',2.5,'
            HandleVisibility','on');
373     stairs(linspace(0,hours+ts,N),Pg(1:N),'k','linewidth',2.5,'
            HandleVisibility','on');
374     stairs(linspace(0,hours+ts,N),PRE_IN(1:N),'r','linewidth',2.5,'
            HandleVisibility','on');
375     stairs(linspace(0,hours+ts,N),PFC_IN(1:N),'g','linewidth',2.5,'
            HandleVisibility','on');
```

```
376   stairs(linspace(0,hours+ts,N),Php*U(1:N),'m','linewidth',2.5,'
          HandleVisibility','on');
377
378   hold on
379   ylabel('Power (kW)');xlabel('Hours');
380   hold on ;
381   legend( '{P_{load}}',...
382             '{P_{g}}',...
383           '{P_{RE_IN}}',...
384           '{P_{FC_IN}}',...
385           '{P_{hp}}');
386
387       subplot(1,2,2)
388
389  set( 0, 'DefaultAxesFontName', 'times' );
390  set( 0, 'DefaultTextFontSize', 14 );
391  set( 0, 'DefaultAxesFontSize', 14);
392  set( 0, 'DefaultLineLineWidth', 3); % default is 1
393  set( 0, 'DefaultLineMarkerSize',2.5 ); % default is 6
394
395    hold on
396  %    peak=[1,0.6,0.78];standard=[1,0.95,0.87];offpeak=[0.68,0.92,1];
397      peak=[0.95,0.87,0.73];standard=[0.76,0.87,0.78];offpeak
            =[0.93,0.93,0.93]
398        mydays=0;myTop=30;
399        hold on;
400        fill([0,0,7,7]+mydays*24,[-10,myTop,myTop,-10],offpeak,'
              HandleVisibility','off');
401        fill([23,23,24,24]+mydays*24,[-10,myTop,myTop,-10],offpeak,'
              HandleVisibility','off');
402        fill([7,7,8,8]+mydays*24,[-10,myTop,myTop,-10],standard,'
              HandleVisibility','off');
```

```
403         fill([11,11,19,19]+mydays*24,[-10,myTop,myTop,-10],standard,'
                HandleVisibility','off');
404         fill([21,21,23,23]+mydays*24,[-10,myTop,myTop,-10],standard,'
                HandleVisibility','off');
405         fill([8,8,11,11]+mydays*24,[-10,myTop,myTop,-10],peak,'
                HandleVisibility','off');
406         fill([19,19,21,21]+mydays*24,[-10,myTop,myTop,-10],peak,'
                HandleVisibility','off');
407         hold off;
408
409         hold on;
410
411         hold off;
412         axis([0,23,0,10]);
413         set(gca,'XTick',(0:1:1*23)');
414         set(gca,'XTickLabel',(0:1:1*23));
415         hold on
416     stairs(linspace(0,hours+ts,N), PH2(1:N),'r','linewidth',2.5,'
            HandleVisibility','on');
417     stairs(linspace(0,hours+ts,N),PFC_IN(1:N),'g','linewidth',2.5,'
            HandleVisibility','on');
418     stairs(linspace(0,hours+ts,N),PFC(1:N),'k','linewidth',2.5,'
            HandleVisibility','on');
419     stairs(linspace(0,hours+ts,N),H2(1:N),'m','linewidth',2.5,'
            HandleVisibility','on');
420      hold on
421     ylabel('Power (kW)');xlabel('Hours');
422     hold on ;
423     legend( '{P_{H2}}',...
424             '{P_{FC_IN}}',...
425             '{P_{FC}}',...
426             '{H_{2}}');
427
```

```
428
429  %% HEAT PUMP STATE AND SWITCHING
430
431   hold on
432    myTemps=nan(49,1);
433    myTemps(1) = To;
434    for k=1:48
435     myTemps(k+1) = (1-(al(k))*ts)*myTemps(k) + ts*Hp.*U(k)+ c(k)*ts
            ;
436
437     end
438 %       stairs(1:50,[myTemps;myTemps(end)]);grid on
439 %% WATER DEMAND
440 % subplot(3,1,1)
441
442  set( 0, 'DefaultAxesFontName', 'times' );
443  set( 0, 'DefaultTextFontSize', 14 );
444  set( 0, 'DefaultAxesFontSize', 14);
445  set( 0, 'DefaultLineLineWidth', 3); % default is 1
446  set( 0, 'DefaultLineMarkerSize',2.5 ); % default is 6
447
448    hold on
449
450    peak=[0.95,0.87,0.73];standard=[0.76,0.87,0.78];offpeak
          =[0.93,0.93,0.93]
451         mydays=0;myTop=30;
452         hold on;
453         fill([0,0,7,7]+mydays*24,[-10,myTop,myTop,-10],offpeak,'
              HandleVisibility','off');
454         fill([23,23,24,24]+mydays*24,[-10,myTop,myTop,-10],offpeak,'
              HandleVisibility','on');
455         fill([7,7,8,8]+mydays*24,[-10,myTop,myTop,-10],standard,'
              HandleVisibility','off');
```

```
456         fill([11,11,19,19]+mydays*24,[-10,myTop,myTop,-10],standard,'
                HandleVisibility','off');
457         fill([21,21,23,23]+mydays*24,[-10,myTop,myTop,-10],standard,'
                HandleVisibility','on');
458         fill([8,8,11,11]+mydays*24,[-10,myTop,myTop,-10],peak,'
                HandleVisibility','off');
459         fill([19,19,21,21]+mydays*24,[-10,myTop,myTop,-10],peak,'
                HandleVisibility','on');
460         hold on;
461
462         stairs(linspace(0,hours+ts,N),Wd(1:N),'k','linewidth',2.5,'
                HandleVisibility','on');
463         hold on
464          stairs(linspace(0,hours+ts,N),Tw(1:N),'k','linewidth',2.5,'
                 HandleVisibility','on');
465             hold on
466  ylabel('W_{D} (l/hr)/ T_{in} (^{o}C)');xlabel('Hours');
467 hold on ;
468  hold on
469
470 legend('off-peak','standard','peak','W_{D}','T_{in}');
471
472
473 %% HEAT PUMPS STATE PLOT
474 subplot(2,1,1)
475
476 set( 0, 'DefaultAxesFontName', 'times' );
477 set( 0, 'DefaultTextFontSize', 14 );
478 set( 0, 'DefaultAxesFontSize', 14);
479 set( 0, 'DefaultLineLineWidth', 3); % default is 1
480 set( 0, 'DefaultLineMarkerSize',2.5 ); % default is 6
481
482   hold on
```

```
483         stairs(linspace(0,hours+ts,N),Php*U(1:N),'k','linewidth',2.5,'
                HandleVisibility','on');
484         stairs(linspace(0,hours+ts,N),U(1:N),'k','linewidth',2.5,'
                HandleVisibility','on')
485         hold on
486  ylabel('Power(kW)/switch(0/1)');xlabel('Hours');
487 hold on ;
488 legend('{P_{hp}}',...
489           'u_{k}');
490
491 subplot(2,1,2)
492
493 set( 0, 'DefaultAxesFontName', 'times' );
494 set( 0, 'DefaultTextFontSize', 14 );
495 set( 0, 'DefaultAxesFontSize', 14);
496 set( 0, 'DefaultLineLineWidth', 3); % default is 1
497 set( 0, 'DefaultLineMarkerSize',2.5 ); % default is 6
498
499   hold on
500    stairs(linspace(0,hours+ts,N),myTemps(1:N),'r','linewidth',2.5,'
          HandleVisibility','on');
501          plot(0:23,ones(size(0:23))*Tup,':m');
502      plot(0:23,ones(size(0:23))*Tlow,':g');
503    hold on
504  ylabel('Hot water temperature (^{o}C) ');xlabel('Hours');
505 hold on ;
506 legend('{T_{k}}');
507  %% WIND SPEED PLOTTING
508
509   set( 0, 'DefaultAxesFontName', 'times' );
510 set( 0, 'DefaultTextFontSize', 14 );
511 set( 0, 'DefaultAxesFontSize', 14);
512 set( 0, 'DefaultLineLineWidth', 3); % default is 1
```

```
513 set( 0, 'DefaultLineMarkerSize',2.5 ); % default is 6
514   stairs(linspace(0,hours+ts,N),vh(1:N),'m','linewidth',2.5,'
        HandleVisibility','on');
515   stairs(linspace(0,hours+ts,N),v(1:N),'r','linewidth',2.5,'
        HandleVisibility','on');
516  hold on
517  ylabel('Wind speed (m/s)');xlabel('Hours');
518  hold on ;
519  legend('{V_{hub}}','{V_{ref}}' );
520 %
```

HEAT PUMP VECTOR MATRICES

```
1  function [A,term_1] = GenerateABmatrixVector(To,al,Hp,c,N,ts)
2
3  a_bar = al*ts;
4  c_bar = c*ts;
5  b_bar = Hp*ts;
6  % Term 1.1
7      t11 = To*ones(N,1);
8
9    for(jk=0:N-1)
10     t11(jk+1:N) = t11(jk+1:N)*(1-a_bar(jk+1));
11   end
12 % Term 1.2
13   % Create AA matrix
14    AA = tril(ones(N));
15    for(jk=1:N-1)
16     AA(jk+1:N,1:jk) = AA(jk+1:N,1:jk)*(1-a_bar(jk+1));
17    end
18   t12 = AA*c_bar;
19
20 term_1 = t11 + t12;
```

```
21 % A matrix for inequality constraints
22    A = b_bar*AA;
23 end
```